


2023

Ambient ammonia synthesis via microwave-catalytic materials and plasma chemistry

Sean Brown

West Virginia University, sbrown27@mix.wvu.edu

Follow this and additional works at: <https://researchrepository.wvu.edu/etd>

 Part of the [Catalysis and Reaction Engineering Commons](#), [Inorganic Chemistry Commons](#), and the [Other Materials Science and Engineering Commons](#)

Recommended Citation

Brown, Sean, "Ambient ammonia synthesis via microwave-catalytic materials and plasma chemistry" (2023). *Graduate Theses, Dissertations, and Problem Reports*. 11937.

<https://researchrepository.wvu.edu/etd/11937>

This Thesis is protected by copyright and/or related rights. It has been brought to you by the The Research Repository @ WVU with permission from the rights-holder(s). You are free to use this Thesis in any way that is permitted by the copyright and related rights legislation that applies to your use. For other uses you must obtain permission from the rights-holder(s) directly, unless additional rights are indicated by a Creative Commons license in the record and/ or on the work itself. This Thesis has been accepted for inclusion in WVU Graduate Theses, Dissertations, and Problem Reports collection by an authorized administrator of The Research Repository @ WVU. For more information, please contact researchrepository@mail.wvu.edu.

Ambient ammonia synthesis via microwave-catalytic materials and plasma chemistry

Sean Brown

A dissertation submitted to the Statler College of Engineering
at West Virginia University

In partial fulfillment of the requirements for the degree of
Doctor of Philosophy in
Chemical Engineering

Jianli Hu, Ph. D., Chair

Debangsu Battacharyya, Ph. D.

Charter Stinespring, Ph. D.

Xueyan Song, Ph. D.

Christina Wildfire, Ph. D.

Department of Chemical and Biomedical Engineering

Morgantown, West Virginia

2023

Keywords: Ammonia, Hydrogen, Nitrogen, Nitride, Plasma, Microwave, Catalysis,
Materials Science

Copyright 2023 Sean Brown

ABSTRACT

Ambient ammonia synthesis via microwave-catalytic materials and plasma chemistry

Sean Brown

Ammonia is critical to supporting human life on earth because of its use as fertilizer. The Haber-Bosch process to produce ammonia has been practiced for over 100 years. This process operates at high pressure and temperature to overcome the thermodynamic and kinetic limitations of the ammonia synthesis reaction thus researchers have tried to overcome it for decades. At present this process represents 1% of global energy usage and 2.5% of global CO₂ emissions. The proposed chemical looping ammonia synthesis approach seeks to reduce the environmental impact of this critical process and to elucidate microwave-catalytic principles.

This research aims to reduce the operating conditions of ammonia synthesis and, critically, to avoid the thermodynamic limitation on ammonia synthesis by operating in a cyclical manner. The cyclical nature of this process also lends itself to use with intermittent and geographically distant renewable energy sources. Ammonia is a promising energy storage vector for the hydrogen economy and the decentralized production of ammonia for agriculture and energy storage is an attractive prospect. Special materials must be developed and characterized to operate under these conditions and fundamentals of these systems are established.

Nitrogen storage materials were considered in model chemical looping cycles to study their productivity and deactivation. These materials included earth abundant transition metals such as Fe, CoMo, and Mn. Rapid thermal cycling achieved using microwave-active catalysts, and microwave-plasma is used to pre-activate the stable N₂ molecule. Microwave-matter interactions were analyzed to develop better catalysts, and well-established materials were characterized by kinetic and time on stream results are reported.

“I recognized my kinship with all living beings, and I made up my mind that I was not one bit better than the meanest on earth. I said then, and I say now, that while there is a lower class, I am in it, and while there is a criminal element, I am of it, and while there is a soul in prison, I am not free.”

-Eugene V. Debs, September 18th, 1918.

Dedication

To my father, my first scientific inspiration – the memory of your social conscience, curiosity and Appalachian laugh still guides me.

To my mother, my wife - Ashlee, my biological, and chosen families. I love and cherish you all. Without you, I'd never have taken the first of the many steps that led here. I am honored and lucky to be a part of your lives.

To my trans siblings – especially the trans women who have helped me to understand myself. I am grateful for the thankless task of answering my questions, and most importantly holding community for me.

To my constant companion, Bernie, from the day you showed up you kept my spirits high like only a Maine coon can.

Finally, to my sisters who come after me, I hope that you find a kinder, safer world.

Acknowledgements

I must first express my gratitude to my advisor, Dr. Jianli Hu. Dr. Hu recruited me from industry and took a chance on me, I hope that it has paid off. He provided the necessary guidance, advice, and direction throughout my project. I am also thankful for the committee's careful consideration of my work, methods, and writing throughout.

I would like to thank my lab mates and my cohort, both socially and scientifically I benefited from your company. I felt welcomed the first moment I set foot in the lab, even when it was a single room with two microwave reactors in the basement.

Finally, I would like to extend a thank you to the faculty and staff of the Chemical and Biomedical Engineering department who provided me a supportive and safe place that taught me engineering as both an undergraduate and graduate student. The staff of the WVU shared resources facilities, Dr. Marcela Redigolo and Dr. Qiang Wang, were essential to my success in publications.

Table of Contents

ABSTRACT	ii
Dedication	iv
Acknowledgements	v
List of Equations	x
1. Introduction	1
1.1 Background	2
1.1.0 Historical Development.....	2
1.1.1 Haber-Bosch Ammonia Synthesis.....	4
1.1.2 Chemical Looping Ammonia Synthesis.....	5
1.2 Current State of Alternative Catalysis Technologies	9
1.2.1 Industrial Microwave.....	9
1.2.2 Microwave Plasma	12
1.3 Conclusions and Outlook	13
1.4 References	16
2. Nitrogen Storage Materials Review	22
2.1 Introduction	22
2.2 Nitride Bonding	22
2.3 Thermodynamics	23
2.5 Methodology of the Literature Review	26
2.6 Classes of Materials	27
2.6.1 Single Metal Nitrides.....	27
2.6.2 Transition Metal Systems	28
2.6.3 Ternary Nitrides.....	32
2.6.4 $A_2B_{17}N$ Compounds	35
2.6.5 Perovskite, and Anti-Perovskite Systems.....	36
2.6.6 Semimetals.....	36
2.6.7 TM-Nitride Mediated Materials	36
2.7 Conclusions	37
2.8 References	40
3. Microwave and Thermal Catalysis Reactions	46
3.1 Introduction	46

3.2 Experimental Methods	48
3.2.1 Materials	48
3.2.2 Chemical Looping Reactors	49
3.2.4 Particle Characterization.....	52
3.3 Results and Discussion	53
3.3.1 CLAS Performance Comparison between Microwave and Thermal Heating	55
3.3.2 Material Characterization	61
3.3.3 Deactivation.....	71
3.4 Conclusions	75
3.5 References	77
4. Thermal Kinetics and Thermal Phenomena	80
4.1 Introduction	80
4.2 Experimental Methods	81
4.3 Thermal Kinetic Results and Discussion	84
4.4 Nitridation of CoMo Alloys	90
4.4.1 Time on Stream Nitridation Experiments.....	91
4.4.2 Characterization of CoMo Particles	92
4.5 Conclusions	98
4.6 References	101
5. Plasma-Catalysis and Pretreatment	103
5.1 Introduction	103
5.2 Methods	103
5.2.1 Catalyst Materials	103
5.2.2 Thermal Fixed Bed Reactor Experiments	103
5.2.3 Plasma Fixed Bed Reactor Experiment	104
5.3 Results and Discussion	107
5.3.1 Plasma Characterization	111
5.3.2 Proposed Mechanism.....	115
5.3.3 Kinetic Parameter Determination	118
5.4 Conclusions	121
5.5 References	122
6. General Conclusions	123

6.1 Conclusions	123
6.2 Future Work	124
6.3 Contributions to the Field	125
6.3.1 Publications	126
6.3.2 Oral Presentations.....	128
6.3.3 Poster Presentations.....	129
6.4 References	131

List of Figures and Tables

Figure	Title	Page
Figure 1.	A simplified reaction schematic of the chemical looping ammonia synthesis process.	6.
Figure 2.	Microwave heating in metallic powders with uniform heating versus the "skin effect."	11.
Figure 3.	Flow chart of the dissertation project.	14.
Figure 4.	The proposed reaction mechanisms for (a) nitridation and (b) hydrogenation reactions.	26.
Figure 5.	Metal particles heating under microwave.	50.
Figure 6.	The microwave catalytic reactor.	51.
Figure 7.	The CLAS loop visualized.	55.
Figure 8.	Microwave and thermal reactor results for a three cycle CLAS process.	56.
Figure 9.	. The temperature distribution for MWFB conditions under both N ₂ and H ₂ flow at 50 sccm was acquired with thermal imaging.	58.
Figure 10.	CoMoO ₄ X-ray diffraction patterns as the sample are reacted under CLAS conditions.	61.
Figure 11.	X-ray diffraction patterns of spent MW and regenerated samples.	63.
Figure 12.	Electron micrography of CLAS Samples.	65.
Figure 13.	TGA-DSC results of CoMo samples.	69.
Figure 14.	TGA nitridation of Fe under N ₂ .	70.
Figure 15.	The dielectric properties for both CoMo and Fe samples.	73.
Figure 16.	The effect of 10:1 addition of Fe ₂ O ₃ , MnO ₂ , MgO, and Al ₂ O ₃ to Mn in a 10:1 Mn to oxide weight ratio.	81.

Figure 17.	Shrinking core model activation energy.	85.
Figure 18.	Shrinking core best fit models.	86.
Figure 19.	CoMo nitridation time on stream.	91.
Figure 20.	Micrography of CoMo particles.	92.
Figure 21.	XPS results for CoMo samples.	93.
Figure 22.	Raman spectroscopy of CoMo.	95.
Figure 23.	Proposed $\text{Co}_3\text{Mo}_3\text{N}$ mechanism.	97.
Figure 24.	. Plasma reactor schematic and reactor outlet.	105.
Figure 25.	Plasma time on stream results for time of treatment and temperature.	106.
Figure 26.	Time on stream MWP ammonia synthesis.	107.
Figure 27.	Representative kinetics of the ammonia synthesis process over plasma nitrided Fe particles, a.) 300 °C, b.) 250 °C, c.) 200 °C, and d.) 150 °C.	108.
Figure 28.	Optical emission spectra and Boltzmann plot.	111.
Figure 29.	Stepwise plasma-enhanced chemical looping ammonia synthesis reaction with idealized catalyst bed and gaseous species.	113.
Figure 30.	Representative kinetics of the ammonia synthesis process over plasma nitrided Fe particles.	117.
Figure 31	Apparent activation energy of ammonia synthesis over plasma nitrided Fe by the Arrhenius plot method.	119.

Figure	Title	Page
Table 1.	The time on stream experimental notes for nitrogen chemical looping catalysts.	53.
Table 2.	ICP-OES results were collected from the metal films coated on quartz tubes used in CoMo experiments.	68.
Table 3.	BET surface areas collected for Fe and CoMo for both thermal and MW heating.	71.
Table 4.	Results from pulse N_2 chemisorption tests for both Fe and CoMo samples.	72.
Table 5.	Thermal-only fixed bed kinetics determined by the shrinking core reaction model for spheres of constant volume*.	89.
Table 6.	SCM to obtain initial rates of ammonia synthesis on plasma treated Fe particles.	109.

List of Equations

Equation	Title	Page
Equation 1.	Calcium cyanide synthesis.	2..
Equation 2.	Barium cyanide synthesis.	2..
Equation 3.	Ammonia synthesis.	4..
Equation 4.	Nitrogen fixation step 1.	8.
Equation 5.	Nitrogen fixation step 2.	8.
Equation 6.	Dielectric loss tangent.	10.
Equation 7.	Complex dielectric constant.	10.
Equation 8.	Complex magnetic constant.	10.
Equation 9.	Electron temperature for NTP.	13.
Equation 10.	Nitrogen dissociation.	25.
Equation 11.	Nitrogen storage kinetics.	25.
Equation 12.	Microwave penetration depth.	47.
Equation 13.	Landau Lifshits Loonyenga equation.	53.
Equation 14.	SCM gas model.	88.
Equation 15.	SCM bulk model.	88.
Equation 16.	SCM surface model.	88.
Equation 17.	Plasma reaction 1.	114.
Equation 18.	Plasma reaction 2.	114.
Equation 19.	Plasma reaction 3.	114.
Equation 20.	Boltzmann plot.	115.
Equation 21.	Number of atomic nitrogen species.	115.
Equation 22.	Deactivation of vibrationally active nitrogen.	115.
Equation 23.	Average velocity.	115.
Equation 24.	Definition of conversion.	118.
Equation 25.	Integration of concentration.	118.
Equation 26.	Power rate law.	118.
Equation 27.	Power law kinetics.	119.

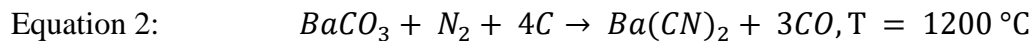
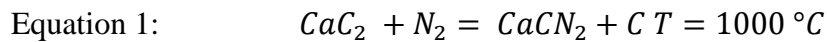
1. Introduction

Global climate change is the most pressing issue of modern times. Reports detailing the specific environmental and social impacts due to the excess of greenhouse gases in the atmosphere, specifically that of CO₂ are published regularly indicating the need for a reduction in human emissions. Alternative processes for energy generation, transportation and chemical manufacturing are urgently needed to avoid the 2 °C heating threshold developed by the IPCC ¹. Industrial ammonia synthesis as currently practiced is performed by the Haber-Bosch process ². This highly centralized process operates at high temperature, 300-550 °C, and high pressures. This process has been the industrial standard for ammonia production since its inception over 100 years ago ³. Ammonia is the second most produced chemical per year globally, the synthesis of ammonia accounts for 1-2% of energy usage per year ⁴. Advances in ammonia synthesis are still sought to overcome the high energy costs and chemical looping using microwave or plasma-enhanced catalysis may provide one such means. This corresponds to 2.5 % of the global CO₂ emissions with 90% of production from natural gas and the remainder using coal ^{2,4}.

1.1 Background

1.1.0 Historical Development

Humans have known of derivatives of ammonia since ancient times, the name itself derives from “*sal ammoniacum*,” originally found in Egypt². Fixed nitrogen compounds occur naturally by various processes such as lightning, volcanic activity, and the *Rhizobium* bacteria^{2,5}. In 1840, it was discovered that fixed nitrogen fertilizers increased crop yields². This discovery led to the development of organized fixed nitrogen collection from coal combustion and saltpeter mining². The Margueritte & de Sourdeval reaction is shown in Equation 1, and the Frank-Caro reaction is shown in Equation 2^{5,6}. The Frank-Caro process was developed in 1898 and relied on high temperatures, ~1000 °C⁶.



The works of Alwin Mittasch provide a fascinating insight into the early work leading up to the current HB process, as well as a repository of periodic trends for nitrogen activation^{7,8}. The extensive search process screened many of the transition metals currently being revisited by nitrogen chemical looping researchers at present⁷. The search for a suitable nitrogen fixation catalyst eventually shifted from a nitride stepwise model towards the now traditional surface catalytic model, ultimately yielding the multi-promoted iron system that won Fritz Haber the Nobel prize in 1919^{7,9}. The high-pressure engineering and scale up of the process won Carl Bosch the Nobel prize in 1931¹⁰.

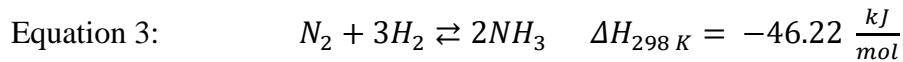
These early studies by Mittasch et. al. also included hydrides, nitrides, amides, carbides, and bimetallic systems ⁷. These methods of stepwise ammonia synthesis would be continued sporadically until present day: nitride reactivity and synthesis were extensively review by Glasson et. al. in 1968 ¹¹, Takeshita et. al. studied a considerable number of rare-earth intermetallics as traditional HB catalysts and found nitride formation in 1976 ¹², Ertl and his coworkers investigated the surface reaction on iron and the HB ammonia synthesis mechanism that ultimately culminated in the Nobel prize in 2007 ¹³.

Ammonia synthesis by chemical looping methods was pioneered by Soliman in 1951, but not much exists in the publishing record afterward ¹⁴. Volpe and Boudart reported synthesizing ammonia directly from molybdenum nitride in 1986 ¹⁵, Uchida et. al. reported the diffusion behavior of nitrogen in rare-earth intermetallics in 1993 ¹⁶, that led to Itoh et. al. reporting a reversible nitrogen storing ruthenium promoted cerium-iron alloy that was chemical looping of nitrogen in all but name ^{17,18}, Kojima and Aika identified cobalt molybdenum nitride as an efficient ammonia synthesis catalyst in 2001 ¹⁹⁻²¹,

In more recent times, investigators have picked up this thread of breaking the HB ammonia synthesis reaction into separated steps again. The resurgence of interest in nitrogen chemical looping started in 2007 with four papers: McKay et. al. published a study of cobalt molybdenum nitride as a reversible nitrogen store for the purpose of ammonia synthesis and Gálvez et. al. published a three-part study on the environmental, economic, thermodynamic and kinetics of using aluminum as a solar powered recyclable nitride for ammonia synthesis ²²⁻²⁴.

1.1.1 Haber-Bosch Ammonia Synthesis

Today, industrial ammonia synthesis proceeds by the HB process. This is a high temperature and high-pressure which operates industrially in the range of 300-500 °C and between 20-100 MPa which relies on a multi-promoted iron or ruthenium-based catalyst systems ². The industrial process is highly integrated relying on efficient heat transfer, air separation to obtain pure dinitrogen gas, multistage reactors, and steam methane reforming to obtain a hydrogen gas supply ². The reaction to form ammonia from its elements is thermodynamically favorable at room temperature, $\Delta G^f_{298 K} = -16.45 \text{ kJmol}^{-1}$ ²⁵, and is exothermic, the stoichiometry and heat of reaction at room temperature can be seen in Equation 2:



Typically, reactions involving negative Gibbs free energy proceed spontaneously, obviously this is not the case for ammonia from its elements at STP. Even at elevated temperatures and pressures ammonia synthesis is not favorable, and the vessel walls used to determine activation energy of the homogeneous reaction are thought to catalyze ammonia synthesis ². Even with a catalytic surface to limit the diatomic molecules vibrational modes, the process is kinetically limited at low temperatures ². Ammonia decomposition proceeds to 99.1% at 400°C ²⁶. Thus, a trade-off exists between the kinetic requirements of temperature and the enthalpy of formation, this typically translates to high pressure, recycle of unreacted gases, separation of ammonia product and extensive heat removal ².

Ammonia is the world's second most produced chemical, with over 100 Tg produced per year ^{3,4}. An estimated 4 million people (or 27% of the world population) since the last century owe their

nutritional balance to fertilizer manufactured from the HB process ²⁶. 80-87% of ammonia produced is used in agriculture as fertilizer and only around 3% of ammonia produced is used directly, with the remainder being used for various chemical manufacturing: explosives, plastics, fibers, organic compounds, other ammonia nitrogen containing compounds ^{2,27}.

The most efficient modern plants utilize 600 kg of natural gas to produce 1000 kg of ammonia ⁴. Considering global climate change there is an urgent need to reduce both CO₂ and methane emissions, as well as the energy required to form ammonia, these interests drive the current study in alternative ammonia synthesis technologies ^{4,28}.

1.1.2 Chemical Looping Ammonia Synthesis

Chemical looping is a field of research and reaction concept that originated in the field of fossil fuel combustion ²⁹. Oxygen carrying metal particles allow isolation of the fuel source from air, this makes treatment of flue gases such as NO_x and SO_x much easier, in addition CO₂ is the only major product making carbon capture much easier ²⁹. Presently chemical looping as a concept is being extended beyond combustion, sometimes termed CLBC in the literature ³⁰.

The basic principle behind nitrogen chemical looping is illustrated in Figure 1. Energy is supplied to the material under an atmosphere of N₂ forming fixed nitrogen compounds. Then the material may wait until ammonia is needed, H₂ or H₂O and energy can then be supplied to produce ammonia, and the process may be repeated. Aside from the basic science yielded, this process may prove to be a modular and renewable friendly system similar to the small-scale HB process designed by the University of Minnesota which operates at atmospheric pressure and relies on a wind turbine to provide ammonia for nearby farms ³¹.

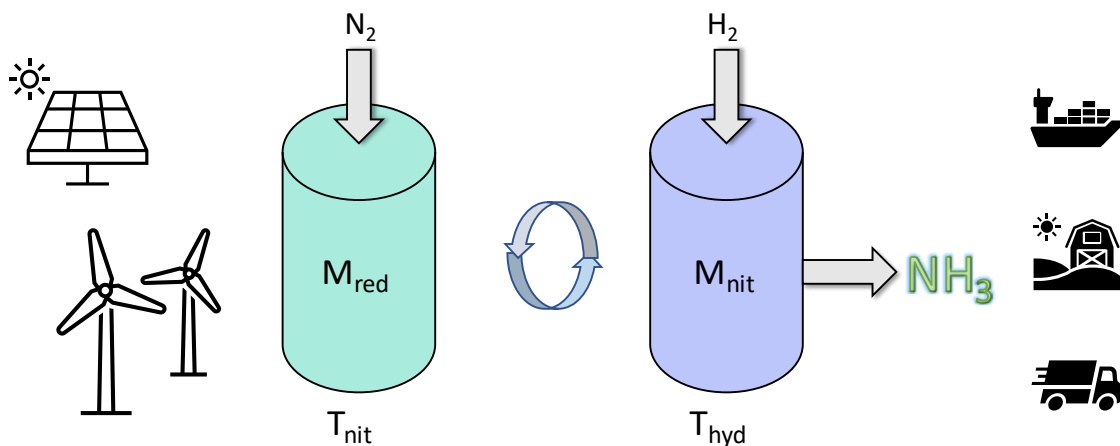


Figure 1. A simplified reaction schematic of the chemical looping ammonia synthesis process. The process converts renewable energy into ammonia in a looped atmospheric process that reacts nitrogen stepwise, first to a reduced metal (M_{red}), then as a metal nitride (M_{nit}) to gaseous ammonia. Both processes occur at different temperatures of nitridation (T_{nit}) and hydrogenation (T_{hyd}), respectively.

Ammonia energy is a closely related concept to CLBC ammonia synthesis, in this perspective nitrogen itself is the energy carrier wherein hydrogen is the energy source^{32–35}. Ammonia conversion can be performed by combustion as in the AmVeh gas/ammonia powered car or by catalytic decomposition, electrolyzed or used in fuel cells^{32,36,37}. Theoretically this process can be performed to release only H_2O and N_2 back into the environment^{32,36,37}. An additional benefit of ammonia as an energy vector is its storage versus hydrogen, ammonia is soluble in water, and is chemically absorbed on metal chloride materials which solves the safety issues inherent in liquid or gaseous storage³².

Metal nitrides have seen renewed interest in the form of both ongoing wideband gap semiconductors, optoelectronic, and as highly active catalyst supports. The nitrides themselves

are also often active catalysts and electrocatalysts, especially under ammonia synthesis conditions³⁸. This attention has extended to the concept of nitrogen chemical looping, or chemical looping ammonia synthesis (CLAS), chemical looping ammonia production (CLAP), or chemical looping ammonia generation (CLAG) systems^{39,40}.

Chemical looping ammonia synthesis decouples the ammonia synthesis reaction as commonly understood in Haber-Bosch (HB). Nitrogen is first dissociated and stored in a material, then later in time, the reaction to form ammonia is completed with a hydrogen source, typically water or dihydrogen. Notably, metal hydrides enhance CLAS systems and the ammonia synthesis reaction by assisting with nitrogen reduction⁴¹.

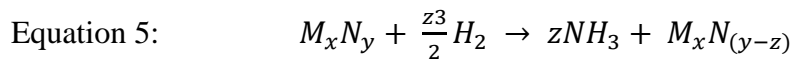
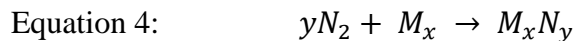
The ammonia synthesis reaction from its elements is shown in Equation 1. While the reaction is spontaneous, it rarely occurs without a catalyst due to the high dissociation energy of the $\text{N}\equiv\text{N}$ bond. The HB process requires high pressures and temperatures to enhance the reaction kinetics of the inherent process.

Many of these chemistries are based on long studied periodic trends for single metals under thermal conditions^{7,42}. However, the solid state, bonding, diffusion, and surface chemistry of these compounds under CLAS conditions is not well studied or understood. Additionally, ternary nitride systems are also not well characterized. Unfortunately, this knowledge gap limits material development and the realization of competitive CLAS systems.

Decarbonization of HB is a major target, ammonia is the second most produced chemical globally, and represents a possible energy vector due to its high hydrogen content³⁴. The transportation of ammonia from centralized production sites to use as fertilizer is not included in

this the figure for CO₂ generation ⁴³. Although pipeline transportation is highly efficient, not all geographies offer these distribution systems.

The typical reactions then are of the form in Equation 4, the nitridation step, and Equation 5, the hydrogenation, or ammonia synthesis step, sometimes referred to as the ammonia harvesting step ⁴⁴. All these reaction steps would rely on some form of an air separation unit to provide a relatively pure N₂ for nitridation, and on electrolysis to provide gaseous H₂ or, water vapor, H₂O, streams for ammonia synthesis. Where H₂ and N₂ are provided in excess. These reactions are highly simplified, but in most cases, nitrogen is dissociated and stored and is later reacted to form gaseous ammonia – even if the specific chemistries differ, as in imide, hydride, or oxide systems.



Additional varieties of the basic CLAS loop exist, they may require an intermediate oxide if water vapor is used as the hydrogen source. Many different possibilities exist but the fundamental feature, cleaving dinitrogen and storing the atomic nitrogen for later is a key feature.

One of the major barriers to nitride synthesis is the nitrogen triple bond, the energy of formation of O₂ is -498.458 kJmol⁻¹ while for N₂ it is -944.87 kJmol⁻¹ ⁴⁵. This means the nitride system requires much more energy input to form than an oxide. Historically, therefore the ammonia synthesis via catalysis route has taken precedence over the nitride-hydrogenation-nitride CLAS route. However, with advances in both understanding of surface catalytic principles and

understanding of materials science these materials can be designed specifically for the ready storage of nitrogen in mind.

1.2 Current State of Alternative Catalysis Technologies

1.2.1 Industrial Microwave

Microwave frequencies are defined as those between 300 MHz and 300 GHz⁴⁶. Microwave technology offers a variety of potential benefits over conventional thermal heating owing to the difference in the physical processes by which heating occurs. Uniform and non-uniform heating modes exist and depend upon the dielectric properties, to a lesser so the magnetic permeability, the size, and the geometry of the particle^{47,48}. Reactor design and arrangement also play a role in the microwave reaction engineering system. Microwave standards exist to avoid interference with various microwave-based communication technologies; therefore, the most common frequency of industrial microwave generator is 2.45 GHz, with 915 MHz also available⁴⁷.

Microwave heating occurs by several physical processes, assumptions are made about the scale or and nature of the interaction given the type of material^{46,48}. The basic interaction of microwaves with matter are governed by Maxwell's equations⁴⁶. The interaction for dielectric "lossy materials" i.e., those that heat best in the microwave are governed by Equations 6 and 7. Dielectric heating occurs via two processes: polarization (electronic, dipolar, atomic and interfacial) and ionic conduction, essentially polarized materials cannot reorient quickly enough before the E field changes^{46,49}. The term ϵ^* is the complex permittivity, it includes the permittivity ϵ' and the loss factor ϵ'' , that described the penetration of microwaves and the ability of the material to store energy, respectively⁴⁶. The loss tangent or, $\tan(\delta)$, describes the ability of

the material to convert absorbed energy into heat and is useful in characterizing supported catalysts for microwave reaction engineering ^{46,50}.

Equation 6:
$$\tan (\delta) = \frac{\varepsilon''}{\varepsilon'}$$

Equation 7:
$$\varepsilon^* = \varepsilon' - j\varepsilon''$$

Magnetic heating is assumed to apply to materials such as iron, nickel, cobalt, some semiconductors, and other strongly magnetic samples, frequently excluding their oxides ^{48,51}.

Equation 8 presents how the magnetic field interacts with matter. The complex permeability, μ^* , the permeability is given by μ' , and the magnetic loss factor is given by μ'' ⁴⁶. These variables explain the penetration depth and the magnetic loss in the material, respectively ⁴⁶. The physical processes by which most magnetic heating occurs are hysteresis losses and eddy current formation ^{46,48}.

Equation 8:
$$\mu^* = \mu' - j\mu''$$

Finally, materials can couple weakly with microwaves resulting in transmission of microwaves, meaning these materials have very low loss and are effectively transparent ⁴⁶. Although this may change during a reaction as both dielectric and magnetic permeability properties are temperature dependent and can drastically alter reaction conditions resulting in thermal runaway ^{46,48}.

Bulk metals typically reflect microwaves, therefore microwave ovens and waveguides are constructed from them ⁴⁶. Eddy current generation depends on skin depth and is a function of the magnetic field pushing the conduction electrons to the surface ⁴⁶. Conductive metal particles however can be uniformly heated by induction, this effect depends on the penetration depth of

the microwave energy^{46,48,51}. Figure 2 illustrates the concept of uniform heating of metallic particles as a function of the penetration depth, typically this effect is on the order of $\sim 100 \mu\text{m}$ ⁴⁸.

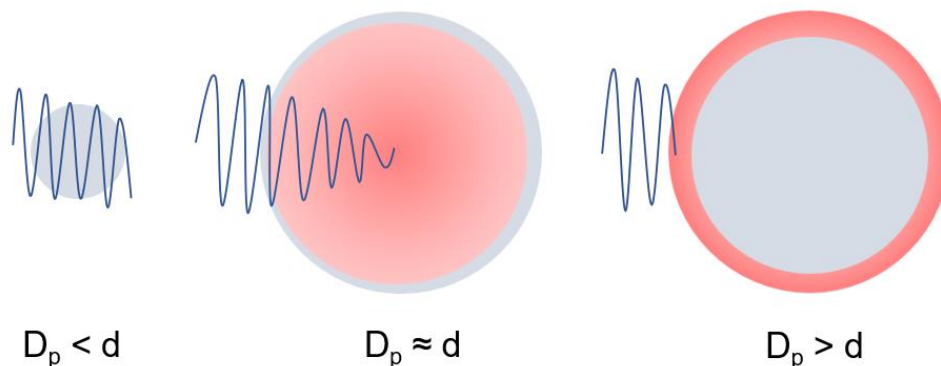


Figure 2. Microwave heating in metallic powders with uniform heating versus the "skin effect."

Supported catalysts can effectively exploit the various heating modes of microwave energy for "selective heating"^{48,50,52,53}. It is possible to generate high temperature localized "hot spots," on metallic or metallic oxide particles on a catalyst support that can significantly increase reaction rates⁵³⁻⁵⁵. This heating process has been demonstrated in the Hu group to increase productivity in dehydroaromatization and ammonia synthesis reactions^{50,50}. Ammonia synthesis based on HB type reactors has also occurred with just E or H fields but has thus-far not elucidated ammonia specific electromagnetic effects on reaction mechanism, but the surface mobility of reactants appears to play a role^{56,57}.

Microwaves have also been studied for catalytic reaction and for catalytic material synthesis, many of these applications are well outside the research presented here^{48,58}. Despite the limitations in heating metal particles, microwaves have also been employed in metal nitride synthesis^{59,60}. Although the reports are limited, most of the surveyed powders were found to be

difficult to heat but in some cases did result in lowered maximum temperature or reaction time^{59,60}. These effects motivate the current study of microwave enhanced CLAS nitride synthesis.

Finally, a few additional purported microwave induced effects include electronic enhancement or “microwave photoelectric effect” in semiconductor materials and microwave induced ionic pondermotive diffusion in solids^{61–63}. Microwave pondermotive forces can cause diffusion into crystal structures or across grain boundaries, unfortunately only two studies exist that explore these phenomena^{62,63}. Microwave induced electron – hole pairs may also be useful to activate stable chemical bonds⁶¹. These are attractive phenomena that could theoretically enhance ammonia synthesis.

1.2.2 Microwave Plasma

One of the early nitrogen fixation processes competing with HB, named for its coinventors utilized plasma; the Birkeland-Eyde process was developed in 1904 utilizing an electric arc in air⁶⁴. The high temperature plasma generated NO, which was oxidized in air to NO₂ and then separated by absorption in water^{64,65}. Much work on plasma nitridation and plasma catalysis has continued since that time⁶⁵.

Specifically, most plasma enhanced catalysts for ammonia synthesis target activation of the dinitrogen triple bond, with a dissociation energy of 911 kJmol⁻¹⁶⁶. A multitude of different plasma generation techniques and reactor designs have been explored the most popular being the dielectric barrier discharge^{67–73}, microwave^{74–76}, and radio-frequency plasma enhanced catalysis reactors^{77–81}. Plasma can excite gaseous products and to affect their absorption and reaction on catalyst surfaces⁸². Plasma enhanced catalysis also operates by many additional physical effects; electric field enhancement, micro-discharges in pores, adsorption probability changes, oxidation

state changes on the surface, hot spot formation, work function changes, activation by photon irradiation, and the presence of alternate chemical species, and reaction pathway changes ⁶⁶.

Microwave plasma is a non-thermal plasma, defined by the electron temperature being much greater than the gas and ion temperature, shown in Equation 9 ⁸³. Therefore, they are sometimes called non-equilibrium plasmas because the thermal energy is not in equilibrium between the various constituents of the plasma stream ⁸³. Atmospheric plasmas may be either thermal or non-thermal and can be ignited by microwaves ⁸³.

Equation 9: $T_{\text{electron}} \gg T_{\text{ion}} \approx T_{\text{gas}}$

Plasma nitridation also has an extensive representation in the literature, specifically microwave plasma and metal nitride synthesis ⁸³. Plasma reactors have been utilized in various configurations to synthesize metal nitrides from oxides and from their metallic forms, typically allowing for lower temperature nitridation reactions for the formation of energy intensive nitrides and exotic nanostructures ⁸⁴⁻⁸⁶. Much of the literature on CLAS processes has involved materials development, and proof of concept work ^{87,88}. Only more recently have researchers considered the thermodynamics and scalability of typical CLAS type-processes ⁸⁹. As such, the CLAS approach is in the material development and reproducibility stage, with much work remaining. However, the combination of a plasma enhanced nitridation with a CLAS system has not yet been reported.

1.3 Conclusions and Outlook

In this body of work activation of nitrogen and storage of the activated nitrogen atom is considered from thermal, microwave and plasma sources. This is of importance due to reduction

of emissions, ammonia as energy vector and the difficulty in shipping ammonia. Many countries do not have the same pipeline infrastructure as the US. Thus, ambient condition decentralized systems may be preferable in situations where they can be paired with passive and intermittent renewable electricity sources. Figure 3 describes the basic flow of this work from materials identification to the various processes and problems associated with each.

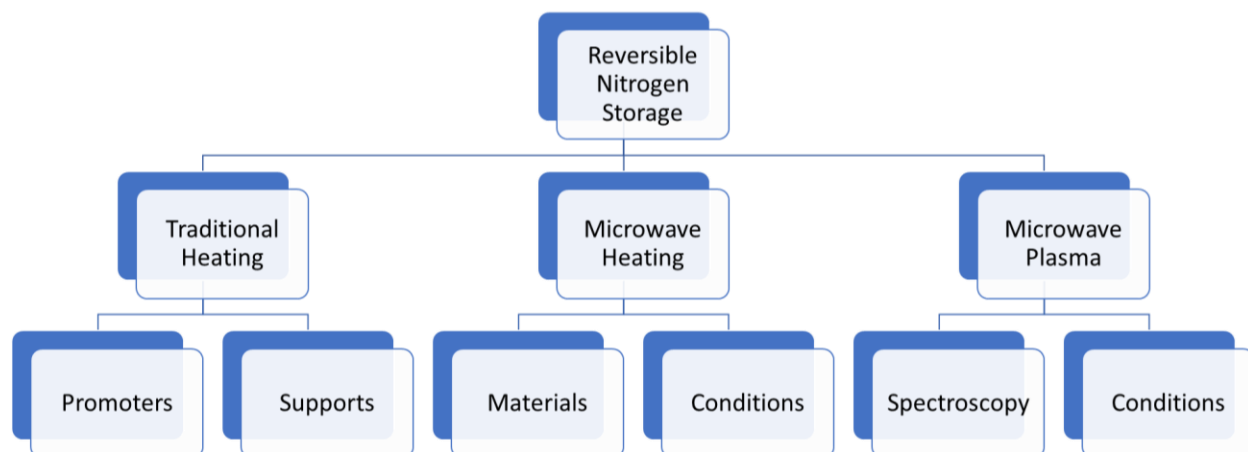


Figure 3. Flow chart of the dissertation project.

The chapters of this dissertation are as follows:

In the first chapter of the work, the topic is introduced, then context and background information are provided. The historical development of ammonia synthesis is reviewed because the field is quite well developed this background knowledge is essential to understanding the context of the work.

In the second chapter, a review of the relevant nitrogen storage materials and systems considered in the work. The chapter also describes the thermodynamics of the CLAS process. The materials science and chemistries are discussed. Much of the work that could fall under the concept

“nitrogen storage” or “chemical looping ammonia synthesis” was not developed as such, thus, this work aims to synthesize previous disparate work towards this aim. The results here are used in the experimental sections which comprise the remaining chapters, three through five.

In the third chapter, the conventional thermal and microwave fixed bed time-on-stream results are presented. In addition to the comparison of the reactors, the temperature of the beds is considered. From there the surface and bulk structure is considered using a variety of methods. Strategies for effective microwave heating of CLAS particles are considered such as, particle size, and dielectric properties.

In the fourth chapter, unique features of thermally heated reactions and thermal kinetics are presented, this chapter is a direct continuation of the work performed in chapter three. The fixed bed thermal kinetics of these nitridation – hydrogenation reactions are largely unknown or described phenomenologically in the literature. Activation energy, observed kinetics, and rate limiting steps are developed. Finally, a unique feature of the thermally heated CoMo system is described, the synthesis of ammonia on nitridation, which is best described by a shrinking core model with hydroxyl counter-diffusion.

In the fifth chapter the use of plasma-enhanced CLAS processes are presented. This chapter continues to build on the thermal fixed bed results of chapters three and four. Plasma-nitridation is used to lower the bulk temperature of the thermal fixed bed reactors during the nitridation step of the reaction by pre-activating the stable nitrogen molecule. Optical emission spectroscopy, time-on-stream measurements and micro-kinetic modelling are used to describe these reactions.

1.4 References

- (1) Ipcc. Global Warming of 1.5°C: IPCC Special Report on Impacts of Global Warming of 1.5°C above Pre-Industrial Levels in Context of Strengthening Response to Climate Change, Sustainable Development, and Efforts to Eradicate Poverty, 1st ed.; Cambridge University Press, 2022. <https://doi.org/10.1017/9781009157940>.
- (2) Appl, M. Ammonia. In Ullmann's Encyclopedia of Industrial Chemistry; Wiley-VCH Verlag GmbH & Co. KGaA: Weinheim, 2006.
- (3) Erisman, J. W.; Sutton, M. A.; Galloway, J.; Kilmont, Z.; Winiwarter, W. How a Century of Ammonia Synthesis Changed the World. *Nature Geoscience* **2008**, 1, 636–639. <https://doi.org/10.1038/ngeo325>.
- (4) Pfromm, P. H. Towards Sustainable Agriculture: Fossil-Free Ammonia. *Journal of Renewable and Sustainable Energy* **2017**, 9 (3), 034702. <https://doi.org/10.1063/1.4985090>.
- (5) Smil, V. Detonator of the Population Explosion. *Nature* **1999**, 400 (6743), 415–415. <https://doi.org/10.1038/22672>.
- (6) Eschenmoser, W. 100 Years of Progress with Lonza. *Chimia* **1997**, 51, 259–269.
- (7) Mittasch, A.; Frankenburg, W. Early Studies of Multicomponent Catalysts. In *Advances in Catalysis*; Elsevier, 1950; Vol. 2, pp 81–104. [https://doi.org/10.1016/S0360-0564\(08\)60375-2](https://doi.org/10.1016/S0360-0564(08)60375-2).
- (8) Mittasch, A.; Frankenburg, W. The Historical Development and Theory of Ammonia Synthesis. *Journal of Chemical Education* **1929**, 6 (12), 2097–2103.
- (9) Haber, F. The synthesis of ammonia from its elements. NobelPrize.org. <https://www.nobelprize.org/prizes/chemistry/1918/summary/>.
- (10) Bosch, C. The Development of the Chemical High Pressure Method During the Establishment of the New Ammonia Industry, 1932. <https://www.nobelprize.org/prizes/chemistry/1931/bosch/lecture/> (accessed 2020-11-09).
- (11) Glasson, D. R.; Jayaweera, S. A. A. Formation and Reactivity of Nitrides II. Calcium and Magnesium Nitrides and Calcium Cyanamide. *J. Appl. Chem.* **2007**, 18 (3), 77–83. <https://doi.org/10.1002/jctb.5010180302>.
- (12) Takeshita, T.; Wallace, W. E.; Craig, R. S. Rare Earth Intermetallics as Synthetic Ammonia Catalysts. *Journal of Catalysis* **1976**, No. 44, 236–243.
- (13) Ertl, G. Reactions at Surfaces: From Atoms to Complexity (Nobel Lecture). *Angew. Chem. Int. Ed.* **2008**, 47 (19), 3524–3535. <https://doi.org/10.1002/anie.200800480>.
- (14) Soliman, A. Formation of Metallic Hydrides and Nitrides and Their Significance in the Synthesis of Ammonia. *J. Appl. Chem.* **2007**, 1 (3), 98–104. <https://doi.org/10.1002/jctb.5010010303>.
- (15) Volpe, L.; Boudart, M. Ammonia Synthesis on Molybdenum Nitride. *J. Phys. Chem.* **1986**, 90 (20), 4874–4877. <https://doi.org/10.1021/j100411a031>.
- (16) Uchida, H.-H.; Uchida, H.; Yanagisawa, T.; Kise, S.; Suzuki, T.; Matsumura, Y.; Koike, U.; Kamada, K.; Kurino, T.; Kaneko, H. Reaction Kinetics of N₂ Absorption by Sm₂Fe₁₇. *Journal of Alloys and Compounds* **1993**, 196 (1–2), 71–74. [https://doi.org/10.1016/0925-8388\(93\)90572-5](https://doi.org/10.1016/0925-8388(93)90572-5).
- (17) Itoh, M.; Machida, K.; Nakajima, H.; Hirose, K.; Adachi, G. Nitrogen Storage Properties Based on Nitrogenation and Hydrogenation of Rare Earth–Iron Intermetallic Compounds R₂Fe₁₇ (R=Y, Ce, Sm). *Journal of Alloys and Compounds* **1999**, 288 (1–2), 141–146. [https://doi.org/10.1016/S0925-8388\(99\)00105-X](https://doi.org/10.1016/S0925-8388(99)00105-X).

- (18) Itoh, M.; Machida, K.; Hirose, K.; Sakata, T.; Mori, H.; Adachi, G. Nitrogenation and Hydrogenation Characteristics of Transition Metal–Iron Intermetallic Compounds. *J. Phys. Chem. B* **1999**, 103 (44), 9498–9504. <https://doi.org/10.1021/jp9916182>.
- (19) Kojima, R.; Aika, K. Cobalt Molybdenum Bimetallic Nitride Catalysts for Ammonia Synthesis Part 1. Preparation and Characterization. *Applied Catalysis A: General* **2001**, 215 (1–2), 149–160.
- (20) Kojima, R.; Aika, K. Cobalt Molybdenum Bimetallic Nitride Catalysts for Ammonia Synthesis Part 2. Kinetic Study. *Applied Catalysis A: General* **2001**, 218 (121–128), 8.
- (21) Kojima, R.; Aika, K. Cobalt Molybdenum Bimetallic Nitride Catalysts for Ammonia Synthesis Part 3. Reactant Gas Treatment. *Applied Catalysis A: General* **2001**, 219 (1–2), 157–170.
- (22) McKay, D.; Gregory, D. H.; Hargreaves, J. S. J.; Hunter, S. M.; Sun, X. Towards Nitrogen Transfer Catalysis: Reactive Lattice Nitrogen in Cobalt Molybdenum Nitride. *Chem. Commun.* **2007**, No. 29, 3051. <https://doi.org/10.1039/b707913c>.
- (23) Gálvez, M. E.; Halmann, M.; Steinfeld, A. Ammonia Production via a Two-Step $\text{Al}_2\text{O}_3/\text{AlN}$ Thermochemical Cycle. 1. Thermodynamic, Environmental, and Economic Analyses. *Ind. Eng. Chem. Res.* **2007**, 46 (7), 2042–2046. <https://doi.org/10.1021/ie061550u>.
- (24) Gálvez, M. E.; Hischer, I.; Frei, A.; Steinfeld, A. Ammonia Production via a Two-Step $\text{Al}_2\text{O}_3/\text{AlN}$ Thermochemical Cycle. 3. Influence of the Carbon Reducing Agent and Cyclability. *Ind. Eng. Chem. Res.* **2008**, 47 (7), 2231–2237. <https://doi.org/10.1021/ie071244w>.
- (25) Atkins, P. W.; De Paula, J. *Physical Chemistry*, 7th ed.; W.H. Freeman: New York, 2002.
- (26) Nagaoka, K.; Eboshi, T.; Takeishi, Y.; Tasaki, R.; Honda, K.; Imamura, K.; Sato, K. Carbon-Free H_2 Production from Ammonia Triggered at Room Temperature with an Acidic $\text{RuO}_2/\text{g-Al}_2\text{O}_3$ Catalyst. *SCIENCE ADVANCES* **2017**, 9.
- (27) Erisman, J. W.; Sutton, M. A.; Galloway, J.; Kilmont, Z.; Winiwarter, W. How a Century of Ammonia Synthesis Changed the World. *Nature Geoscience* **2008**, 1, 636–639. <https://doi.org/10.1038/ngeo325>.
- (28) Alvarez, R. A.; Pacala, S. W.; Winebrake, J. J.; Chameides, W. L.; Hamburg, S. P. Greater Focus Needed on Methane Leakage from Natural Gas Infrastructure. *Proceedings of the National Academy of Sciences* **2012**, 109 (17), 6435–6440. <https://doi.org/10.1073/pnas.1202407109>.
- (29) Fan, L.-S. *Chemical Looping Systems for Fossil Energy Conversions*; John Wiley & Sons, Incorporated & AIChE: Hoboken, NJ, USA, 2010.
- (30) Zhu, X.; Imtiaz, Q.; Donat, F.; Müller, C. R.; Li, F. Chemical Looping beyond Combustion – a Perspective. *Energy Environ. Sci.* **2020**, 13 (3), 772–804. <https://doi.org/10.1039/C9EE03793D>.
- (31) Reese, M.; Marquart, C.; Malmali, M.; Wagner, K.; Buchanan, E.; McCormick, A.; Cussler, E. L. Performance of a Small-Scale Haber Process. *Ind. Eng. Chem. Res.* **2016**, 55 (13), 3742–3750. <https://doi.org/10.1021/acs.iecr.5b04909>.
- (32) Klerke, A.; Christensen, C. H.; Nørskov, J. K.; Vegge, T. Ammonia for Hydrogen Storage: Challenges and Opportunities. *J. Mater. Chem.* **2008**, 18 (20), 2304. <https://doi.org/10.1039/b720020j>.
- (33) Lan, R.; Irvine, J. T. S.; Tao, S. Ammonia and Related Chemicals as Potential Indirect Hydrogen Storage Materials. *International Journal of Hydrogen Energy* **2012**, 37 (2), 1482–1494. <https://doi.org/10.1016/j.ijhydene.2011.10.004>.
- (34) Guo, J.; Chen, P. Catalyst: NH_3 as an Energy Carrier. *Chem* **2017**, 3 (5), 709–712. <https://doi.org/10.1016/j.chempr.2017.10.004>.
- (35) Green, Jr., L. An Ammonia Energy Vector for the Hydrogen Economy. *International Journal of Hydrogen Energy* **1982**, 7 (4), 355–359. [https://doi.org/10.1016/0360-3199\(82\)90128-8](https://doi.org/10.1016/0360-3199(82)90128-8).

- (36) Brown, T. The AmVeh – an ammonia fueled car from South Korea. NH3 Fuel Association. <https://nh3fuelassociation.org/2013/06/20/the-amveh-an-ammonia-fueled-car-from-south-korea/> (accessed 2013-11-09).
- (37) Zamfirescu, C.; Dincer, I. Using Ammonia as a Sustainable Fuel. *Journal of Power Sources* **2008**, 185 (1), 459–465. <https://doi.org/10.1016/j.jpowsour.2008.02.097>.
- (38) Ye, T.-N.; Park, S.-W.; Lu, Y.; Li, J.; Sasase, M.; Kitano, M.; Hosono, H. Contribution of Nitrogen Vacancies to Ammonia Synthesis over Metal Nitride Catalysts. *J. Am. Chem. Soc.* **2020**, 142 (33), 14374–14383. <https://doi.org/10.1021/jacs.0c06624>.
- (39) Hua, J.; Wang, K.; Wang, Q.; Peng, R. Feasibility of Fe-Based Nitrogen Carrier for Chemical Looping Ammonia Synthesis: Thermodynamics. *J Therm Anal Calorim* **2021**, 146 (2), 673–680. <https://doi.org/10.1007/s10973-020-10029-x>.
- (40) Zhang, Q.; Wu, Y.; Gao, Y.; Chen, X.; Liu, D.; Fan, M. High-Performance Mesoporous (AlN/Al₂O₃) for Enhanced NH₃ Yield during Chemical Looping Ammonia Generation Technology. *International Journal of Hydrogen Energy* **2020**, 45 (16), 9903–9913. <https://doi.org/10.1016/j.ijhydene.2020.01.172>.
- (41) Chang, F.; Guan, Y.; Chang, X.; Guo, J.; Wang, P.; Gao, W.; Wu, G.; Zheng, J.; Li, X.; Chen, P. Alkali and Alkaline Earth Hydrides-Driven N₂ Activation and Transformation over Mn Nitride Catalyst. *J. Am. Chem. Soc.* **2018**, 140 (44), 14799–14806. <https://doi.org/10.1021/jacs.8b08334>.
- (42) Maxted, E. B. *Ammonia and the Nitrides*; J. & A. Churchill: London, 1921.
- (43) McArthur, J. W.; McCord, G. C. Fertilizing Growth: Agricultural Inputs and Their Effects in Economic Development. *Journal of Development Economics* **2017**, 127, 133–152. <https://doi.org/10.1016/j.jdeveco.2017.02.007>.
- (44) Aframehr, W. M.; Huang, C.; Pfromm, P. H. Chemical Looping of Manganese to Synthesize Ammonia at Atmospheric Pressure: Sodium as Promoter. *Chem. Eng. Technol.* **2020**, 43 (10), 2126–2133. <https://doi.org/10.1002/ceat.202000154>.
- (45) CRC Handbook of Chemistry and Physics, 102nd edition 2021-2022.; Rumble, J. R., Ed.; CRC Press: Boca Raton London New York, 2021.
- (46) *Microwaves - Theory*. In *Microwaves and Metals*; John Wiley & Sons (Asia) Pte Ltd: Singapore, 2011; pp 25–41. <https://doi.org/10.1002/9780470822746.ch2>.
- (47) Will, H.; Scholz, P.; Ondruschka, B. Microwave-Assisted Heterogeneous Gas-Phase Catalysis. *Chem. Eng. Technol.* **2004**, 27 (2), 113–122. <https://doi.org/10.1002/ceat.200401865>.
- (48) Mishra, R. R.; Sharma, A. K. *Microwave–Material Interaction Phenomena: Heating Mechanisms, Challenges and Opportunities in Material Processing*. *Composites Part A: Applied Science and Manufacturing* **2016**, 81, 78–97. <https://doi.org/10.1016/j.compositesa.2015.10.035>.
- (49) Sun, J.; Wang, W.; Yue, Q. Review on Microwave-Matter Interaction Fundamentals and Efficient Microwave-Associated Heating Strategies. *Materials* **2016**, 9 (4), 231. <https://doi.org/10.3390/ma9040231>.
- (50) Hu, J.; Wildfire, C.; Stiegman, A. E.; Dagle, R. A.; Shekhawat, D.; Abdelsayed, V.; Bai, X.; Tian, H.; Bogle, M. B.; Hsu, C.; Luo, Y.; Davidson, S. D.; Wang, Y. Microwave-Driven Heterogeneous Catalysis for Activation of Dinitrogen to Ammonia under Atmospheric Pressure. *Chemical Engineering Journal* **2020**, 397, 125388. <https://doi.org/10.1016/j.cej.2020.125388>.
- (51) *Microwave Heating of Metal-Based Materials*. In *Microwaves and Metals*; John Wiley & Sons (Asia) Pte Ltd: Singapore, 2011; pp 65–157. <https://doi.org/10.1002/9780470822746.ch4>.

- (52) Wildfire, C.; Abdelsayed, V.; Shekhawat, D.; Spencer, M. J. Ambient Pressure Synthesis of Ammonia Using a Microwave Reactor. *Catalysis Communications* **2018**, 115, 64–67. <https://doi.org/10.1016/j.catcom.2018.07.010>.
- (53) Zhang, X.; Hayward, D. O.; Mingos, D. M. P. Effects of Microwave Dielectric Heating on Heterogeneous Catalysis. *Catalysis Letters* **2003**, 88, 33–38. <https://doi.org/10.1023/A:1023530715368>.
- (54) Bai, X.; Robinson, B.; Killmer, C.; Wang, Y.; Li, L.; Hu, J. Microwave Catalytic Reactor for Upgrading Stranded Shale Gas to Aromatics. *Fuel* **2019**, 243, 485–492. <https://doi.org/10.1016/j.fuel.2019.01.147>.
- (55) Perry, W. L.; Cooke, D. W.; Katz, J. D.; Datye, A. K. On the Possibility of a Significant Temperature Gradient in Supported Metal Catalysts Subjected to Microwave Heating. *Catalysis Letters* **1997**, 47 (1), 1–4. <https://doi.org/10.1023/A:1019020013544>.
- (56) Murakami, K.; Manabe, R.; Nakatsubo, H.; Yabe, T.; Ogo, S.; Sekine, Y. Elucidation of the Role of Electric Field on Low Temperature Ammonia Synthesis Using Isotopes. *Catalysis Today* **2018**, 303, 271–275. <https://doi.org/10.1016/j.cattod.2017.08.008>.
- (57) Yahya, N.; Puspitasari, P.; Koziol, K.; Pavia, G. New Approach to Ammonia Synthesis by Catalysis in Magnetic Field. *JNanoR* **2012**, 16, 119–130. <https://doi.org/10.4028/www.scientific.net/JNanoR.16.119>.
- (58) Kokel, A.; Schäfer, C.; Török, B. Application of Microwave-Assisted Heterogeneous Catalysis in Sustainable Synthesis Design. *Green Chem.* **2017**, 19 (16), 3729–3751. <https://doi.org/10.1039/C7GC01393K>.
- (59) Houmes, J. D.; zur Loye, H.-C. Microwave Synthesis of Ternary Nitride Materials. *Journal of Solid State Chemistry* **1997**, 130 (2), 266–271. <https://doi.org/10.1006/jssc.1997.7303>.
- (60) Huang, J.-W.; Li, J.; Peng, H. Microwave Synthesis of Manganese Nitride. *Powder Metallurgy* **2007**, 50 (2), 137–141. <https://doi.org/10.1179/174329007X153323>.
- (61) Zhou, J.; You, Z.; Xu, W.; Su, Z.; Qiu, Y.; Gao, L.; Yin, C.; Lan, L. Microwave Irradiation Directly Excites Semiconductor Catalyst to Produce Electric Current or Electron-Holes Pairs. *Sci Rep* **2019**, 9 (1), 5470. <https://doi.org/10.1038/s41598-019-41002-w>.
- (62) Freeman, S. A.; Booske, J. H.; Cooper, R. F. Modeling and Numerical Simulations of Microwave-Induced Ionic Transport. *Journal of Applied Physics* **1998**, 83 (11), 5761–5772. <https://doi.org/10.1063/1.367432>.
- (63) Booske, J. H.; Cooper, R. F.; Freeman, S. A.; Rybakov, K. I.; Semenov, V. E. Microwave Ponderomotive Forces in Solid-State Ionic Plasmas. *Physics of Plasmas* **1998**, 5 (5), 1664–1670. <https://doi.org/10.1063/1.872835>.
- (64) Appl, M. Ammonia. In *Ullmann's Encyclopedia of Industrial Chemistry*; Wiley-VCH Verlag GmbH & Co. KGaA: Weinheim, 2006.
- (65) Patil, B. S.; Wang, Q.; Hessel, V.; Lang, J. Plasma N₂-Fixation: 1900–2014. *Catalysis Today* **2015**, 256, 49–66. <https://doi.org/10.1016/j.cattod.2015.05.005>.
- (66) Neyts, E. C.; Bogaerts, A. Understanding Plasma Catalysis through Modelling and Simulation—a Review. *J. Phys. D: Appl. Phys.* **2014**, 47 (22), 224010. <https://doi.org/10.1088/0022-3727/47/22/224010>.
- (67) Wang, Y.; Craven, M.; Yu, X.; Ding, J.; Bryant, P.; Huang, J.; Tu, X. Plasma-Enhanced Catalytic Synthesis of Ammonia over a Ni/Al₂O₃ Catalyst at Near-Room Temperature: Insights into the Importance of the Catalyst Surface on the Reaction Mechanism. *ACS Catal.* **2019**, 9 (12), 10780–10793. <https://doi.org/10.1021/acscatal.9b02538>.

- (68) Srinath, N. V. Plasma Catalytic Ammonia Synthesis at Atmospheric Pressure in a Dielectric Barrier Discharge Reactor. 90.
- (69) Rouwenhorst, K. H. R.; Burbach, H. G. B.; Vogel, D. W.; Núñez Paulí, J.; Geerdink, B.; Lefferts, L. Plasma-Catalytic Ammonia Synthesis beyond Thermal Equilibrium on Ru-Based Catalysts in Non-Thermal Plasma. *Catal. Sci. Technol.* **2021**, 10.1039/D0CY02189J. <https://doi.org/10.1039/D0CY02189J>.
- (70) Rouwenhorst, K. H. R.; Kim, H.-H.; Lefferts, L. Vibrationally Excited Activation of N₂ in Plasma-Enhanced Catalytic Ammonia Synthesis: A Kinetic Analysis. *ACS Sustainable Chem. Eng.* **2019**, 7 (20), 17515–17522. <https://doi.org/10.1021/acssuschemeng.9b04997>.
- (71) Akay, G.; Zhang, K. Process Intensification in Ammonia Synthesis Using Novel Coassembled Supported Microporous Catalysts Promoted by Nonthermal Plasma. *Ind. Eng. Chem. Res.* **2017**, 56 (2), 457–468. <https://doi.org/10.1021/acs.iecr.6b02053>.
- (72) Gómez-Ramírez, A.; Cotrino, J.; Lambert, R. M.; González-Elipe, A. R. Efficient Synthesis of Ammonia from N₂ and H₂ Alone in a Ferroelectric Packed-Bed DBD Reactor. *Plasma Sources Sci. Technol.* **2015**, 24 (6), 065011. <https://doi.org/10.1088/0963-0252/24/6/065011>.
- (73) Gorky, F.; Best, A.; Jasinski, J.; Allen, B. J.; Alba-Rubio, A. C.; Carreon, M. L. Plasma Catalytic Ammonia Synthesis on Ni Nanoparticles: The Size Effect. *Journal of Catalysis* **2021**, 393, 369–380. <https://doi.org/10.1016/j.jcat.2020.11.030>.
- (74) Uyama, H.; Matsumoto, O. Synthesis of Ammonia in High-Frequency Discharges. II. Synthesis of Ammonia in a Microwave Discharge under Various Conditions. *Plasma Chem Plasma Process* **1989**, 9 (3), 421–432. <https://doi.org/10.1007/BF01083676>.
- (75) Nakajima, J.; Sekiguchi, H. Synthesis of Ammonia Using Microwave Discharge at Atmospheric Pressure. *Thin Solid Films* **2008**, 516, 4446–4451.
- (76) Tiwari, S.; Khan, T. S.; Tavadze, P.; Hu, J. Activation of Two Highly Stable Molecules – Nitrogen and Methane to Co-Produce Ammonia and Ethylene. *Chemical Engineering Journal* **2020**, 127501. <https://doi.org/10.1016/j.cej.2020.127501>.
- (77) Shah, J.; Wu, T.; Lucero, J.; Carreon, M. A.; Carreon, M. L. Nonthermal Plasma Synthesis of Ammonia over Ni-MOF-74. *ACS Sustainable Chem. Eng.* **2019**, 7 (1), 377–383. <https://doi.org/10.1021/acssuschemeng.8b03705>.
- (78) Shah, J.; Harrison, J.; Carreon, M. Ammonia Plasma-Catalytic Synthesis Using Low Melting Point Alloys. *Catalysts* **2018**, 8 (10), 437. <https://doi.org/10.3390/catal8100437>.
- (79) Shah, J.; Wang, W.; Bogaerts, A.; Carreon, M. L. Ammonia Synthesis by Radio Frequency Plasma Catalysis: Revealing the Underlying Mechanisms. *ACS Appl. Energy Mater.* **2018**, 1 (9), 4824–4839. <https://doi.org/10.1021/acsaem.8b00898>.
- (80) Antunes, R.; Steiner, R.; Romero Muñoz, C.; Soni, K.; Marot, L.; Meyer, E. Plasma-Assisted Catalysis of Ammonia Using Tungsten at Low Pressures: A Parametric Study. *ACS Appl. Energy Mater.* **2021**, acsaem.0c03217. <https://doi.org/10.1021/acsaem.0c03217>.
- (81) Ben Yaala, M.; Saeedi, A.; Scherrer, D.-F.; Moser, L.; Steiner, R.; Zutter, M.; Oberkofler, M.; De Temmerman, G.; Marot, L.; Meyer, E. Plasma-Assisted Catalytic Formation of Ammonia in N₂–H₂ Plasma on a Tungsten Surface. *Phys. Chem. Chem. Phys.* **2019**, 21 (30), 16623–16633. <https://doi.org/10.1039/C9CP01139K>.
- (82) Mehta, P.; Barboun, P.; Herrera, F. A.; Kim, J.; Rumbach, P.; Go, D. B.; Hicks, J. C.; Schneider, W. F. Overcoming Ammonia Synthesis Scaling Relations with Plasma-Enabled Catalysis. *Nat Catal* **2018**, 1 (4), 269–275. <https://doi.org/10.1038/s41929-018-0045-1>.

- (83) Szabó, D.; Schlabach, S. Microwave Plasma Synthesis of Materials—From Physics and Chemistry to Nanoparticles: A Materials Scientist’s Viewpoint. *Inorganics* **2014**, 2 (3), 468–507. <https://doi.org/10.3390/inorganics2030468>.
- (84) Li, S. L.; Ma, C. Y.; Zhang, Q. Y.; Ren, C. S.; Lu, W. Q. Ion Nitriding of Pure Iron Using High-Density Plasma Beam Generated by a Tubular Plasma Source. *Surface and Coatings Technology* **2017**, 309, 47–53. <https://doi.org/10.1016/j.surfcoat.2016.11.040>.
- (85) Houmes, J. D.; zur Loye, H.-C. Plasma Nitridation of Metal Oxides. *Chem. Mater.* **1996**, 8 (11), 2551–2553. <https://doi.org/10.1021/cm960384l>.
- (86) Ouyang, B.; Zhang, Y.; Zhang, Z.; Fan, H. J.; Rawat, R. S. Nitrogen-Plasma-Activated Hierarchical Nickel Nitride Nanocorals for Energy Applications. *Small* **2017**, 13 (34), 1604265. <https://doi.org/10.1002/sml.201604265>.
- (87) Gao, W.; Wang, P.; Guo, J.; Chang, F.; He, T.; Wang, Q.; Wu, G.; Chen, P. Barium Hydride-Mediated Nitrogen Transfer and Hydrogenation for Ammonia Synthesis: A Case Study of Cobalt. *ACS Catal.* **2017**, 7 (5), 3654–3661. <https://doi.org/10.1021/acscatal.7b00284>.
- (88) Gao, W.; Guo, J.; Wang, P.; Wang, Q.; Chang, F.; Pei, Q.; Zhang, W.; Liu, L.; Chen, P. Production of Ammonia via a Chemical Looping Process Based on Metal Imides as Nitrogen Carriers. *Nat Energy* **2018**, 3 (12), 1067–1075. <https://doi.org/10.1038/s41560-018-0268-z>.
- (89) Burrows, L.; Gao, P.-X.; Bollas, G. M. Thermodynamic Feasibility Analysis of Distributed Chemical Looping Ammonia Synthesis. *Chemical Engineering Journal* **2021**, 426, 131421. <https://doi.org/10.1016/j.cej.2021.131421>.

2. Nitrogen Storage Materials Review

2.1 Introduction

While the use of refractory nitrides has long been of interest to the scientific community, and the use of nitrides in electronic materials has seen significant interest, a systematic understanding of metal nitrides is lacking. This is especially true when considering these systems in a reactive state to produce ammonia. Nitride formation and hydrogenation processes are not well understood in the literature, and the material space is only recently being systematically explored.

The purpose of this review then is to collate current research on CLAS systems. There is an abundance of nitride research, much of it relevant to this work, but this review will focus on that work which has been completed towards the goal of ammonia synthesis or nitrogen storage. The goal is to assimilate these strategies and approaches which exist in the literature under a variety of different names for the same concept and provide the depth and breadth of that work to future researchers.

This literature survey was carried out by searching the following phrases “nitrogen storage” “chemical looping ammonia” “CLAS” “chemical looping nitrogen” or combinations thereof. Articles about ammonia synthesis by heterogeneous metal nitride catalysts were also included because of the contribution of nitrogen vacancies and nitrogen exchange.

2.2 Nitride Bonding

The nitride bond forms due to the N^{-3} interstitial in a parent metal. This results in a different set of crystal structures than usually found in mineral oxides. The nitride family is then categorized

in several ways, but the most common are the so called “refractory” nitrides, which have high melting points, are brittle, stable, and wear resistant. The bonds of metal nitride compounds are often characterized as either having covalent or ionic behaviors thus leading to the common names: “salt-like” and “covalent-like” to describe the ligand.

While the most familiar nitrides tend to be those in semiconductors (Si_3N_4 , InN , GaN) and those in refractory coatings (AlN , BN , TiN) the application of nitrides as supports, and active phases for both thermal and electrochemical catalysts have gained much attention in recent years. Materials such as CeN , Mo_2N , VN , and Li_3N have seen wide application in the literature.

The unique features of the metal nitride bond and band structure lead to the continued interest in these kinds of materials. As catalysts nitrides catalysts are known to enhance hydrogenation reactions. The electronic structures formed by nitrides are of great interest in electronic materials applications, but also in both gas phase and electrochemical catalysis.

The most common nitride bond is of a metallic or covalent character, and typically sub-nitride composition with nitrogen in interstitial locations, transition metals and semimetals make up the majority of the studied nitride compounds¹⁻³. Ionic nitride bonding is rarer and exists only in Li , Be , Mg , and to some degree Ca , the more electropositive an element, the more likely an ionic nitride bond is to form, a trend that was identified early in HB work^{2,4}.

2.3 Thermodynamics

Comprehensive data on the formation energies for metal-nitrides in the form of Ellingham diagrams are not available for all but the most common nitride compounds. This is likely due to the lack of research on the field as a whole and due to the inherent instability of the compounds.

Simulated data exists for a larger number of CLAS materials and nitrides, this data is essential for developing and modelling CLAS systems ^{5,6}. Burrows, Gao and Bollas recently published a paper on these reaction systems and enumerated the various possible approaches ⁵. The major reactions are described as the following: (1) nitride – hydride reaction, (2) the partially reduced nitride loop, (3) the alkali imide – alkali hydride (AH), (4) the nitric oxide loop, and (5) the cyanide loop.

Here the focus shall be on the first three types of reactions, with special interest on the active phase of the nitrogen carrier. The thermodynamics of formation of all the compounds reviewed in this article are not all reported. Many of the nitride synthesis steps are not well developed, or the nitridation process is not well understood. However, the basic binary formation energies for metal-nitride compounds are typically well developed in the literature. Ellingham diagrams can provide the Gibbs free energy of formation of nitrogen containing compounds at different temperatures. While the data collected may not be complete it can help to guide simulations and experimental design.

2.4 Kinetics

The kinetics of specific nitridation processes under CLAS conditions are not well established. Typically, the process would rely on small particle sized catalyst powders. At times these powders may be included with oxide supports, or other structural promoters to improve cyclability and surface area ⁷.

A more generalized kinetic development of nitridation kinetics can be drawn from research on steel corrosion and from the synthesis of electronic nitride materials. Many different processes for the nitridation of materials exist, the most common being nitridation by dinitrogen (either

performed by a pure N₂ flow or a mixture of N₂ and H₂ gas), or ammonolysis by gaseous NH₃.

Nitridation of metals can be modelled on the macro view by the relationship in Equations 10 and 11⁸.

Equation 10: $\frac{1}{2}N_2 = [N_{dissolved}]$

Equation 11: $[\%N] = k[P_{N_2}]^{\frac{1}{2}}$

The kinetics of particular CLAS materials are not well developed outside of a very small handful of loosely controlled bench-scale studies and industrial surface coating modification. Effects of gas composition, internal and external diffusion have not been well defined. The effectiveness of specific promoters of the electronic or the structural variety have not been systematically investigated either, although the literature on traditional HB processes may be of use.

Most CLAS processes are intended to operate at atmospheric pressure, thus the effect of pressure on nitridation processes is of less interest. The goal to overcome the HB thermodynamic equilibrium limit thus relies on the cyclability and separability of reactions, not on high pressures to drive Le Chatelier equilibrium.

With some exceptions (CLAS materials that are closer akin to heterogeneous catalysts), CLAS reactions follow the shrinking unreacted core model (SCM). Originally developed by C. Y. Wen to describe the combustion of coal particles, the SCM describes the reaction with three reaction constants⁹. These constants combine various resistances to chemical reactions into the fluid film diffusion regime, the internal diffusion regime, and the surface reaction constant regime^{9,10}. The basic reactions mechanism of both nitridation and reduction may be seen in Figure 4.

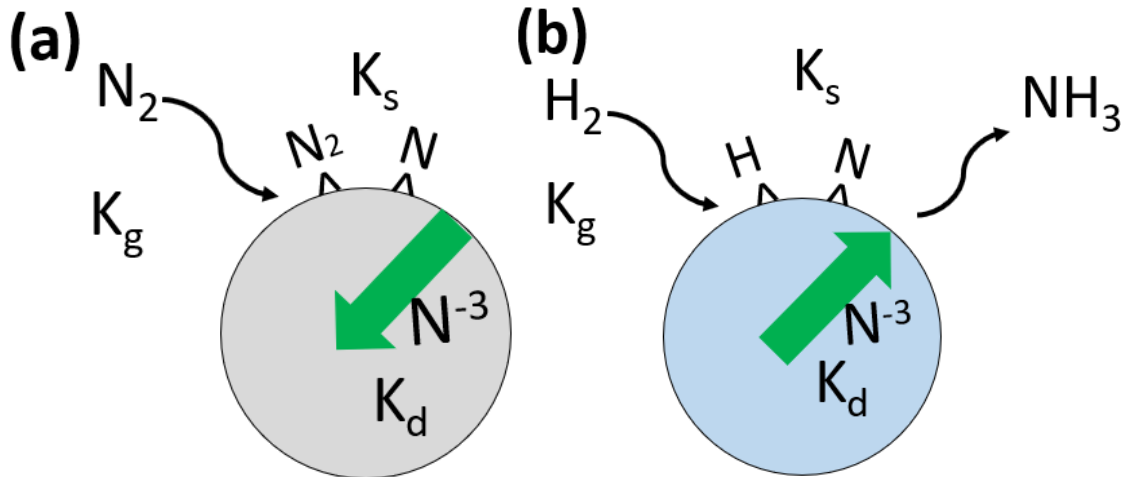


Figure 4. The proposed reaction mechanisms for (a) nitridation and (b) hydrogenation reactions. Where K_g represents the gas diffusion coefficient to the particle surface, K_s represents the surface reaction coefficient, and K_d represents the internal diffusion coefficient.

Standard reaction engineering methods are useful to determine the various rate limiting steps of nitrogen-surface, diffusion, and hydrogen-source-surface reactions. These phenomenological results can provide data for more detailed simulation and mechanism investigation, which in turn drives more advanced catalyst design.

2.5 Methodology of the Literature Review

The purpose of this review then is to collate current research on CLAS systems. There is an abundance of nitride research, much of it relevant to this work, but this review will focus on that work which has been completed towards the goal of ammonia synthesis or nitrogen storage. The goal is to assimilate these strategies and approaches which exist in the literature under a variety of different names for the same concept and provide the depth and breadth of that work to future researchers.

This literature survey was carried out by searching the following phrases “nitrogen storage” “chemical looping ammonia” “CLAS” “chemical looping nitrogen” or combinations thereof. Articles about ammonia synthesis by heterogeneous metal nitride catalysts were also included because of the contribution of nitrogen vacancies and nitrogen exchange.

2.6 Classes of Materials

A recent publication extensively reviewed the thermodynamics of single metal CLAS candidates⁵. This kind of work is extremely important for the development and for directing future work in the field. This work is aimed at reviewing the material systems which have been the subject of nitrogen fixation research in the past and presenting them in a unified way under the heading of chemical looping ammonia synthesis.

2.6.1 Single Metal Nitrides

Single metal nitrides have been studied since the early 1900s by many workers Juza, Mittasch and others^{4,11-13}. These systems were of considerable interest for their use as refractory materials and later, as catalysts, electronic materials, and nitrogen transfer reagents.

Transition metal nitrides have been the subject of interest over the years but not in a significant and sustained way. Many systems described are only of the single transition metal-nitrogen composition.

2.6.1.1 Alkali and Alkaline Earth Systems

The group I and II metals are known to be reactive towards gaseous N_2 . Many of these elements form nitrides spontaneously upon reaction with gaseous N_2 . Some of the metals do not form nitrides easily, or at all, they include Na, and K (nitridation under $Ar:N_2$ discharge), Rb, and Cs

which can be synthesized from their hydride forms ¹⁴. The use of Li as a potent activator of nitrogen has been long reported in the literature ¹⁵. The thermodynamics of formation of these systems in general under N₂ tend to be favorable at pressure ¹⁴.

Many of these metals are instead used as “electronic” promoters to enhance catalysis reaction rates. Some examples include the industrial standard HB catalyst, K promoted Fe, Cs promoted Ru ^{12,16}. Co-active bimetallic catalysts such as Li₂NH or BaNH-transition metal materials will be discussed in later sections ¹⁷.

The magnesium oxide to magnesium nitride MgO-Mg₂N₃, system has been studied by two groups, the proposed CLAS loops would use methane to reduce MgO and water to hydrolyze ammonia ^{18,19}. Converting MgO to its reduced metallic form before nitridation with N₂ likely will encounter surface area limitations caused by the low melting point of Mg metal. Literature exists suggesting that unconverted MgO and Al₂O₃ promoters may provide surface sites for adsorbed species to diffuse over, increasing the conversion of the nitride phase ²⁰. Thus far though, only promotion by NaOH, TM dopants, and hydride-imide systems has been investigated in depth for any CLAS applications.

2.6.2 Transition Metal Systems

Transition metal nitrides may be synthesized in the following ways, by reaction with gaseous ammonia, or nitrogen in their pure form or as forming gas. Solid state reaction methods utilizing amides, or urea. Sometimes solvent, CVD or plasma methods are also utilized for more advanced materials. A thorough review of synthesis methods has been prepared by Yin at al. ²¹.

Specific thermodynamic modelling of chemical looping ammonia synthesis systems was performed by Burrows, et al.⁵ which described several single transition metal nitrides. The study considers many different formulations of the CLAS loop.

Bond ionicity is proposed as a useful metric for considering the nature of bonds in a potential CLAS nitride. The concept has been existent for a long period of time but, Michalsky et al. contextualized it in terms of the nitrogen transfer reaction in transition metals to judge the relative ionic character of the metal-nitrogen bonding^{6,22}. The general bonding character in nitride materials is still not fully understood, but some general conclusions can be drawn⁶. Ionicity is defined as, the properties of ionicity, metallicity, and covalency are relevant from a theoretic standpoint to select. Metal nitrides tend to favor the covalent bond due to the large amount of energy required to sever the dinitrogen triple bond. The covalent bond is undesirable despite the lower bond energy of the system, in a more ionic system it is easier to store and retrieve the nitride ion under these conditions.

For the reaction scheme proposed in Michalsky et al.'s work, using H₂O as the hydrogen source, there exists an “optimum” where too dense d-level electrons result in too weak bonds and too few d-level electrons result in too strong of bonds²². This general principle of nitrogen storage – similar in principle to the Sabatier principle for catalytic reactions, specifically ammonia synthesis in this case – requires that not too strong or weak bonding exists to successfully cycle nitrogen storage^{22,23}. Strong nitrogen-metal bonds would require excess heat which can degrade carrier at a fast rate relative to weaker bonds. Too weak nitrogen bonds may not be stable enough to cycle in a way to produce ammonia at all.

Nitrogen vacancy formation energy is an important consideration for all CLAS nitride systems²⁴⁻²⁶. The ability to form a nitride at favorable conditions may be offset by extremely long internal

diffusion times. This consideration has been discussed by Pfromm and co-workers, but for the most part has not entered the larger CLAS materials literature ²². Rates of diffusion may be calculated for binary materials or determined by experiment to guide the development of materials. Some diffusion rates calculated by Pfromm for binary nitride systems varied from seconds to days depending on the transition metal system ²².

Single metal nitrides may also be promoted or synthesized with stable oxides which can improve nitrogen transport properties. Additionally, oxides with Brønsted acidity can be incorporated with single nitrides to enhance -H addition and promote ammonia formation ²⁷. This phenomenon has been observed in other processes but attributed to surface area increase and to possible structural and electronic promotion, both of which likely do play a part in enhanced rates.

Among the single transition metal nitrides, those composed of Fe₄N, Mo₂N, Ni₃N, Mn₄N, Mn₂N, Mn₃N₂, AlN, ZrN, TiN, Cr₂N, CrN, Re₃N, and Co₄N have received the most interest for the CLAS type reaction ²⁸⁻³⁰. However, only the Al₂O₃ to AlN loop system was extensively studied in a series of papers by Gálvez et al ³¹⁻³³. The thermodynamics, kinetics, economics and cyclability of the material was investigated.

Early solar-thermal work by Pfromm utilized chromium as a nitrogen carrier under a variety of conditions ²⁹. The conditions that the Cr nitrogen carrier was tested under gas flows containing N₂, H₂, and CO to simulate bio-gas ²⁹. The Cr₂N and CrN phases were both present in the reactions, and CaO/Ca(OH)₂ was used as a promoter ²⁹. The maximum rate found for this approach at 1000 °C is 4.1 (± 0.5) x10⁻² mol_{NH₃}mol_{metal}⁻¹min⁻¹ ²⁹.

Manganese has been well studied for nitrogen storage and CLAS by many different groups, conceivably because of favorable thermodynamics and relative availability of the material. The material was studied in several publications on the material under CLAS reaction conditions, extensive characterization, simulation and through the use of promoters such as Fe, Ni, and NaOH ^{22,34-41}.

Manganese is known to form several stable nitride phases on heating under an N₂ atmosphere. From the most nitrogen rich to the least: MnN, Mn₆N₅, Mn₃N₂, Mn₂N, Mn₄N ⁴². The typical temperature where the reaction begins is 500-600 °C ^{22,38}. The typical rate achieved with this material is $9.7 (\pm 0.9) \times 10^{-6} \text{ mol}_{\text{NH}_3} \text{mol}_{\text{metal}}^{-1} \text{s}^{-1}$ ^{36 22,38}. The typical reaction condition in literature is run at 700 °C nitridation and between 400 and 500 °C hydrogenation ^{22,38}.

Cu and Zn have received considerably less experimental attention ⁴³. Zn is thermodynamically feasible, but kinetics often require that it reaches its melting point to be successfully nitrided.

Tantalum nitride (Ta₃N₅) represents another nitrogen rich material for nitrogen storage and transfer ^{43,44}. The oxide form (Ta₂O₅) is difficult to reduce under hydrogen, but Ta₂O₅ can be ammonolyzed to the nitride form under ammonia at 900 °C, with partial nitridation possible at 800 °C ⁴⁴. This material has been found to yield as much as 81% of its lattice nitrogen in the form of gaseous ammonia when doped with Co to form the structure Ta_{2.5}Co_{0.5}N₅ ⁴⁴. Other dopants were tested, Fe, Re, Co but only the composition of the cobalt included system was analyzed by changing the Ta:Co ratio ⁴⁴. Surface mechanism and promotion DFT was performed by Zeinalipour-Yazdi, et al. ⁴⁵.

Supported transition metal on oxide material systems show great promise for future CLAS materials as demonstrated by many studies which indicate their effectiveness ^{7,46}. TiO₂/AlN and

Fe, and Mn on Al_2O_3 ⁴⁶. The Mn and Fe on Al_2O_3 systems were studied in detailed compositions of Fe/Mn by thermogravimetric methods ⁷.

Aluminum oxide requires a temperature of 1500 °C under flowing N_2 to form the desired AlN product, and aluminum nitride also requiring high reaction temperatures, between 800-1000 °C under water vapor ⁴⁶. Extensive kinetic analysis was performed by Gao et al., to identify activity of the TiO_2 promoter and to describe ammonia synthesis versus decomposition rate in a stationary bed ⁴⁶.

2.6.3 Ternary Nitrides

Ternary metal nitride systems of the form $(\text{A}_x\text{B}_y\text{N}_z)$, represent an enormous materials space, many of which are uncharacterized by experiment. Recent work by Sun et al., made a significant effort in mapping and describing the energies of formation of this materials space ⁶. An interactive map exists which describes the thermodynamics.

The work by Sun et al. also describes metal nitride bonding in ternary systems by building on the concept of the inductive effect with a reductive effect ⁶. These two effects can be used to describe both nitrogen rich and nitrogen poor nitride systems. In the inductive effect, the electrons are withdrawn leading to higher nitrogen containing species, while in the reductive case the electrons are donated to the metal bonds ⁶. These results point towards the hard soft acid base theory to aid understanding the metal – metal nitrogen bonding in metals ⁴⁷.

Only a small subset of the predicted ternary nitrides has been studied experimentally. The most successful of those candidates have been described below.

2.6.3.1 Co₃Mo₃N Type Systems

The cobalt molybdenum nitride system for ammonia synthesis was developed by Kojima and Aika as an alternative HB catalyst for atmospheric pressure reactions⁴⁸⁻⁵⁰. This work built on previous explorations of Mo₂N systems for alternative HB catalysts and previous work with the supported CoMo catalyst in hydrodesulfurization reactions⁵¹. The material was characterized by reaction engineering, crystallography, and surface chemistry. The material was first synthesized as bulk for its application as an ammonia synthesis material, then was used sparingly as a supported material.

The bimetallic CoMo system was simulated by Nørskov, et al. and identified as a good catalyst by the volcano plot⁵². Other researchers from the Hargreaves group have modeled the Co₃Mo₃N surface and bulk slice in much more detail. The proposed mechanisms of ammonia synthesis are well supported by their findings. A proposed Mars van-Krevelen type mechanism is supported by both experiment and simulation^{26,44}. A dynamic reaction is proposed by Hunter, et al., where N exchange occurs between the saturated Co₃Mo₃N system and the reduced Co₆Mo₆N system⁵³.

The rates determined for ammonia production under Ar/H₂ flow in a CLAS-type reaction over unpromoted Co₃Mo₃N are given by Sun, et al. at 400 °C, 158 μmolg⁻¹h⁻¹ and at 500 °C, 369 μmolg⁻¹h⁻¹⁵⁴. The system begins as a CoMoO₄ oxide, is typically ammonolyzed at 700-750 °C to form the Co₃Mo₃N phase. Nitrogen alone is also sometimes used to nitride the reduced surface, and combinations of H₂:N₂ are also used to synthesize the nitride phase.

The crystal structure for the hydrated oxide precursor has been well established and has been studied with in-situ diffraction techniques during the ammonolysis process⁵⁵⁻⁵⁷. The role of the preparation step for synthesis of the nitride is a critical one and can impact the reactivity of the

final product. The effect of initial reduction on CoMoO_4 was first identified by cyclic TPR/TPO, with the first cycle being significantly different ⁵⁸. The effect of reaction pretreatment gases was reported on by Aslan et al. and Brown et al., for the HB reaction and the CLAS-type reaction, respectively ^{59,60}. The author's previous work suggested a dynamic surface-bulk exchange between hydroxyl and nitride groups with surface rearrangement to ammonia ⁶⁰.

The CLAS utilization of this material has been demonstrated by Hargreaves et al. and Brown, et al ^{54,61}. The rates found for this process vary, but the overall stoichiometry indicates that 2.93% of the compound is nitrogen. Under microwave fixed bed heating the rate is found to be $56 \mu\text{molg}^{-1}$ on a 15 min ammonia synthesis cycle ⁶¹.

2.6.3.2 $\text{Fe}_3\text{Mo}_3\text{N}$, $\text{Ni}_2\text{Mo}_3\text{N}$, and $\text{Mn}_2\text{Mo}_2\text{N}$, and others

Additional bimetallic oxides have been synthesized, typically starting from the metal salt solution route. These materials are then calcined, and ammonolyzed at relatively high temperatures ($750 \text{ }^\circ\text{C}$) to achieve the desired nitride phase. Unlike the case of the CoMo bimetallic, there is not substantial DFT modeling available for these materials and their reactive surfaces.

Materials considered are: $\text{Fe}_3\text{Mo}_3\text{N}$, $\text{Ni}_2\text{Mo}_3\text{N}$, $\text{Mn}_2\text{Mo}_2\text{N}$ ^{41,62,63}. Some of these materials have been extensively characterized by the Al Sohbi et al., and few others, mostly for their material properties ⁶². The relative rates of ammonia productivity of these materials are considered in other publications under HB conditions, but $\text{Ni}_2\text{Mo}_3\text{N}$ was found to be higher, but comparable to $\text{Co}_3\text{Mo}_3\text{N}$, between 383 and $395 \text{ molg}^{-1}\text{h}^{-1}$, under differing synthesis conditions ^{63,64}. Less interest has been expressed in these materials as purely CLAS catalysts.

Doped manganese nitrides are considered by Hargreaves, et al., K-Mn, Li-Mn, Fe-Mn, and Co-Mn along with Mn_3N_2 as baseline³⁸. The characterization of these materials generally consists of crystallographic phase identification, surface area measurement and in some cases conductivity.

Another class of bimetallics of the Co_xRe_y composition was studied extensively by McAulay, et al^{65,66}. The CoRe_4 system was found to perform best after pretreatment step of 2 h at 600 °C with H_2/N_2 co-feed with a rate $\mu\text{molg}^{-1}\text{h}^{-1}$ ⁶⁶. A potential Re nitride phase is suggested by experiment and previous authors but remains unconfirmed⁶⁶.

2.6.4 $\text{A}_2\text{B}_{17}\text{N}$ Compounds

Early reversible nitrogen storage work was published by Machida and Itoh, et al. in the 1990s following earlier work by Uchida on nitridation of $\text{Sm}_2\text{Fe}_{17}$ ⁶⁷⁻⁷⁰. Compounds of the form $\text{A}_2\text{B}_{17}\text{N}$ where A = Y, Ce, Sm, and Nd and B = Fe, Ti, Zr, Nb, Mo, and V were synthesized by arc furnace under Ar blanket^{67,70,71}. A variety of products were synthesized CeFe_2 , CeFe_7 , and $\text{Ce}_2\text{Fe}_{17}$ ^{67,71}. The materials were well characterized by XRD and time on stream reaction testing, yielding rates, nitrogen content, and apparent activation energies^{67,71}.

More advanced materials were developed which utilized other intermetallic chemistries and Ru as promoter. Additionally, supported catalysts like $\text{Ru}/\text{Al}_2\text{O}_3$ were used as co-catalysts with the TiFe_2N materials^{67,71}. Hydrogen generation/nitride regenerations studies were also performed with these material systems with $\text{Ru}/\text{La}_2\text{O}_3$ as catalyst⁷².

Other AB_2 compound intermetallics have also seen interest in HB reactions⁷³. The HB rates reported with this proposed catalyst were quite high $3318 \mu\text{molh}^{-1}\text{g}^{-1}$ (laser ablated) and $486 \mu\text{molh}^{-1}\text{g}^{-1}$ (bulk)⁷³.

2.6.5 Perovskite, and Anti-Perovskite Systems

The potential of perovskite, ABO_3 , and anti-perovskite, A_3BN , nitrogen storage materials is an attractive research goal due to the high H and O diffusion rates found in these materials in various other applications. The antiperovskite structure where N is present at the four corners of the unit cell. These systems may or may not contain oxygen ^{74,75}. Some have notably been exploited as active, or dynamic supports for HB ammonia synthesis ⁷⁴.

The $BaCeO_{3-x}N_yH_z$ perovskite support is considered “active” in that it exchanges O and N vacancies with surface absorbed species ⁷⁴. Materials of this type have most served as supports for more active traditional HB type catalysts. Surface reactions encourage O/N vacancy interchange which forms the active catalyst support.

2.6.6 Semimetals

Semimetals tend to form more covalent nitrides and thus are not particularly interesting from the perspective of CLAS systems. The field of semimetal nitrides is however vast, and under much research at present and in the past for electronic materials and refractory coatings.

2.6.7 TM-Nitride Mediated Materials

Another class of materials which has gained interest are those of nitride-transition metal mediated systems, typically with dynamic nitride phases as supports for more catalytically active metal islands on the surface. The most well known of these for CLAS are probably the hydride-imide systems; $LiNH$ and $BaNH$ systems published by Gao et al. ^{17,76}. These materials are enhanced by the inclusion of TMs such as Co, Ni and Fe ^{17,76}. The productivity of the Co- BaH_2 system was further enhanced by including a CNT supports which increased the dispersion of the

Co cocatalyst ⁷⁶. Rates of up to 3125 $\mu\text{molg}^{-1}\text{h}^{-1}$ were detected for the CLAS system with 50% Ni–BaH₂ ¹⁷.

The HB-type reaction synthesis catalyst LaN is shown to be able to synthesize ammonia from both gas-surface nitrogen and from lattice nitrogen ⁷⁷. This catalyst was found to be highly effective with 5% wt. Ni/LaN having a rate of 2400 $\mu\text{molg}^{-1}\text{h}^{-1}$, and when using nanoparticle 12.5% wt. Ni/LaN 5543 $\mu\text{molg}^{-1}\text{h}^{-1}$ at 400 °C ⁷⁷. The potential of lattice nitrogen involvement in this reaction and other similar catalysts can provide useful insights for CLAS material development.

Alloys containing lithium (Li₁₇Sn₄) have also been developed that allow a “pseudo-catalytic” ammonia synthesis process to proceed, this process is essentially identical to other CLAS processes, except that the alloy is first prepared under H₂ gas before nitridation ⁷⁸.

2.7 Conclusions

The materials space of metal nitrides is poorly defined. Although recent work has made huge progress in defining and understanding nitride materials. Most understanding of nitrides comes from the understanding of oxide minerals, the difference being that N₂ dissociation requires a large amount of energy comparatively to O₂. With computational methods exploration of this space is more

Examples of ternary nitrides include both nitrophilic and nitrophobic elements, The examples of hydrides and electrides provide an interesting example of how materials design can be utilized to augment HB type reaction catalysts. This same broad approach to materials synthesis could be harnessed to design nitride containing materials.

Material spaces which may hold promise for the future of CLAS research are those similar to mixed TM-catalyst systems. Covalent type metal nitrides appear to require much higher temperatures than metal-type bonds.

Additional material development which is of interest for functional catalyst supports include electrides (mayenite, LaRuSi, CaCN₂) which have a reservoir of e⁻ available for N₂ reduction, some having dynamic lattice structures⁷⁹⁻⁸². Other materials of interest may be oxynitrides, or oxyhydrides which may facilitate N⁻³ exchange without lattice collapse. Finally, new materials which may be heated non-uniformly such as microwave catalysts may be synthesized by high-entropy alloy tuning of electronic and material properties.

Future work in this space can be augmented by novel methods in catalysis preparation and reaction conditions. Microwave catalysis and plasma-enhanced catalysis can provide new reaction intermediates and pre-activate stable molecules such as CO₂, CH₄, and N₂. Another set of possible consideration is atom economy, material synthesis, cyclability, and environmental impact of extraction.

Most CLAS candidates are evaluated on the productivity, and the temperature of operation. These are important metrics for the consideration of a new catalytic system, but more considerations are required to develop the technology. CLAS systems typically have very high selectivity, theoretically 100%, sometimes with small concentrations of H₂O or NO_x produced as side products. Metrics like cyclability, material cost and the environmental impact should also be considered. The rates of reaction for the gas-particle interactions should be considered for the development of reaction cycle times. Finally, typical concerns in reaction engineer, such as surface area, temperature distribution and attrition should also be considered. A few select

candidates will need to experience longer-term testing and development to reach this stage and gather this data, this will require concentrated study on the best candidates.

2.8 References

- (1) Brese, N. E.; O’Keeffe, M. Crystal Chemistry of Inorganic Nitrides. In *Complexes, Clusters and Crystal Chemistry*; Structure and Bonding; Springer-Verlag: Berlin/Heidelberg, 1992; Vol. 79, pp 307–378. <https://doi.org/10.1007/BFb0036504>.
- (2) Gregory, D. H. Structural Families in Nitride Chemistry. *J. Chem. Soc., Dalton Trans.* **1999**, No. 3, 259–270. <https://doi.org/10.1039/a807732k>.
- (3) Salamat, A.; Hector, A. L.; Kroll, P.; McMillan, P. F. Nitrogen-Rich Transition Metal Nitrides. *Coordination Chemistry Reviews* **2013**, 257 (13–14), 2063–2072. <https://doi.org/10.1016/j.ccr.2013.01.010>.
- (4) Mittasch, A.; Frankenburg, W. Early Studies of Multicomponent Catalysts. In *Advances in Catalysis*; Elsevier, 1950; Vol. 2, pp 81–104. [https://doi.org/10.1016/S0360-0564\(08\)60375-2](https://doi.org/10.1016/S0360-0564(08)60375-2).
- (5) Burrows, L.; Gao, P.-X.; Bollas, G. M. Thermodynamic Feasibility Analysis of Distributed Chemical Looping Ammonia Synthesis. *Chemical Engineering Journal* **2021**, 426, 131421. <https://doi.org/10.1016/j.cej.2021.131421>.
- (6) Sun, W.; Bartel, C. J.; Arca, E.; Bauers, S. R.; Matthews, B.; Orvañanos, B.; Chen, B.-R.; Toney, M. F.; Schelhas, L. T.; Tumas, W.; Tate, J.; Zakutayev, A.; Lany, S.; Holder, A. M.; Ceder, G. A Map of the Inorganic Ternary Metal Nitrides. *Nat. Mater.* **2019**, 18 (7), 732–739. <https://doi.org/10.1038/s41563-019-0396-2>.
- (7) Wang, B.; Guo, H.; Yin, X.; Shen, L. N-Sorption Capability of Al₂O₃-Supported Mn-/Fe-Based Nitrogen Carriers during Chemical Looping Ammonia Synthesis Technology. *Energy Fuels* **2020**, 34 (8), 10247–10255. <https://doi.org/10.1021/acs.energyfuels.0c01000>.
- (8) Lai, G. Y. Nitridation. In *High-temperature corrosion and materials applications*; ASM International: Materials Park, Ohio, 2007.
- (9) Wen, C. Y. NONCATALYTIC HETEROGENEOUS SOLID-FLUID REACTION MODELS. 21.
- (10) Levenspiel, O. *Chemical Reaction Engineering*, 3rd ed.; Wiley: New York, 1999.
- (11) Maxted, E. B. *Ammonia and the Nitrides*; J. & A. Churchill: London, 1921.
- (12) Appl, M. Ammonia. In *Ullmann’s Encyclopedia of Industrial Chemistry*; Wiley-VCH Verlag GmbH & Co. KGaA: Weinheim, 2006.
- (13) Juza, R.; Hahn, H. Über die Kristallstrukturen von Zn₃N₂, Cd₃N₂ und Ge₃N₄. Metallamide und Metallnitride. IX. Mitteilung. *Z. Anorg. Allg. Chem.* **1940**, 244 (2), 125–132. <https://doi.org/10.1002/zaac.19402440204>.
- (14) Moody, G. J.; Thomas, J. D. R. Alkali Metal Nitrides. *J. Chem. Educ.* **1966**, 43 (4), 205. <https://doi.org/10.1021/ed043p205>.
- (15) Dafert, F. W.; Miklauz, R. Über einige neue Verbindungen von Stickstoff und Wasserstoff mit Lithium. *Monatshefte für Chemie* **1910**, 31 (9), 981–996. <https://doi.org/10.1007/BF01518423>.
- (16) Wang, Y.; Wildfire, C.; Khan, T. S.; Shekhawat, D.; Hu, J.; Tavadze, P.; Quiñones-Fernández, R.; Moreno, S. Effects of Support and Promoter on Ru Catalyst Activity in Microwave-Assisted Ammonia Synthesis. *Chemical Engineering Journal* **2021**, 425, 130546. <https://doi.org/10.1016/j.cej.2021.130546>.
- (17) Gao, W.; Guo, J.; Wang, P.; Wang, Q.; Chang, F.; Pei, Q.; Zhang, W.; Liu, L.; Chen, P. Production of Ammonia via a Chemical Looping Process Based on Metal Imides as Nitrogen Carriers. *Nat Energy* **2018**, 3 (12), 1067–1075. <https://doi.org/10.1038/s41560-018-0268-z>.

- (18) Swearer, D. F.; Knowles, N. R.; Everitt, H. O.; Halas, N. J. Light-Driven Chemical Looping for Ammonia Synthesis. *ACS Energy Lett.* **2019**, *4* (7), 1505–1512. <https://doi.org/10.1021/acsenergylett.9b00860>.
- (19) Michalsky, R.; Pfromm, P. H. Thermodynamics of Metal Reactants for Ammonia Synthesis from Steam, Nitrogen and Biomass at Atmospheric Pressure. *AIChE Journal* **2012**, *58* (10), 3203–3213. <https://doi.org/10.1002/aic.13717>.
- (20) Szabó, Z. G.; Perczel, S.; Gábor, M.; Zsolt, G.; Galwey, A. K. The Role of Magnesia and Alumina in Promoting the Nitridation of Magnesium and Aluminium. *Thermochimica Acta* **1983**, *64* (1–2), 167–178. [https://doi.org/10.1016/0040-6031\(83\)80140-3](https://doi.org/10.1016/0040-6031(83)80140-3).
- (21) Ma, Y.; Xiong, L.; Lu, Y.; Zhu, W.; Zhao, H.; Yang, Y.; Mao, L.; Yang, L. Advanced Inorganic Nitride Nanomaterials for Renewable Energy: A Mini Review of Synthesis Methods. *Front. Chem.* **2021**, *9*, 638216. <https://doi.org/10.3389/fchem.2021.638216>.
- (22) Michalsky, R.; Pfromm, P. H. An Ionicity Rationale to Design Solid Phase Metal Nitride Reactants for Solar Ammonia Production. *J. Phys. Chem. C* **2012**, *116* (44), 23243–23251. <https://doi.org/10.1021/jp307382r>.
- (23) Nørskov, J. K.; Bligaard, T.; Rossmeisl, J.; Christensen, C. H. Towards the Computational Design of Solid Catalysts. *Nature Chem* **2009**, *1* (1), 37–46. <https://doi.org/10.1038/nchem.121>.
- (24) Ye, T.-N.; Park, S.-W.; Lu, Y.; Li, J.; Sasase, M.; Kitano, M.; Hosono, H. Contribution of Nitrogen Vacancies to Ammonia Synthesis over Metal Nitride Catalysts. *J. Am. Chem. Soc.* **2020**, *142* (33), 14374–14383. <https://doi.org/10.1021/jacs.0c06624>.
- (25) Liu, B.; Manavi, N.; Deng, H.; Huang, C.; Shan, N.; Chikan, V.; Pfromm, P. The Activation of N₂ on Manganese Nitride-Supported Ni₃ and Fe₃ Clusters and Relevance to Ammonia Formation. *12*.
- (26) Zeinalipour-Yazdi, C. D.; Hargreaves, J. S. J.; Catlow, C. R. A. Nitrogen Activation in a Mars–van Krevelen Mechanism for Ammonia Synthesis on Co₃Mo₃N. *J. Phys. Chem. C* **2015**, *119* (51), 28368–28376. <https://doi.org/10.1021/acs.jpcc.5b06811>.
- (27) Heyns, A. M.; Prinsloo, L. C. The Vibrational Spectra and Decomposition of -Calcium Nitride (-Ca₃N₂) and Magnesium Nitride (Mg₃N₂). *9*.
- (28) Alexander, A.-M.; Hargreaves, J. S. J.; Mitchell, C. The Denitridation of Nitrides of Iron, Cobalt and Rhenium Under Hydrogen. *Top Catal* **2013**, *56* (18–20), 1963–1969. <https://doi.org/10.1007/s11244-013-0133-z>.
- (29) Michalsky, R.; Pfromm, P. H. Chromium as Reactant for Solar Thermochemical Synthesis of Ammonia from Steam, Nitrogen, and Biomass at Atmospheric Pressure. *Solar Energy* **2011**, *85* (11), 2642–2654. <https://doi.org/10.1016/j.solener.2011.08.005>.
- (30) Tricker, A. W.; Hebisch, K. L.; Buchmann, M.; Liu, Y.-H.; Rose, M.; Stavitski, E.; Medford, A. J.; Hatzell, M. C.; Sievers, C. Mechanocatalytic Ammonia Synthesis over TiN in Transient Microenvironments. *ACS Energy Lett.* **2020**, *5* (11), 3362–3367. <https://doi.org/10.1021/acsenergylett.0c01895>.
- (31) Gálvez, M. E.; Hischer, I.; Frei, A.; Steinfeld, A. Ammonia Production via a Two-Step Al₂O₃/AlN Thermochemical Cycle. 3. Influence of the Carbon Reducing Agent and Cyclability. *Ind. Eng. Chem. Res.* **2008**, *47* (7), 2231–2237. <https://doi.org/10.1021/ie071244w>.
- (32) Gálvez, M. E.; Frei, A.; Halmann, M.; Steinfeld, A. Ammonia Production via a Two-Step Al₂O₃/AlN Thermochemical Cycle. 2. Kinetic Analysis. *Ind. Eng. Chem. Res.* **2007**, *46* (7), 2047–2053. <https://doi.org/10.1021/ie061551m>.

- (33) Gálvez, M. E.; Halmann, M.; Steinfeld, A. Ammonia Production via a Two-Step $\text{Al}_2\text{O}_3/\text{AlN}$ Thermochemical Cycle. 1. Thermodynamic, Environmental, and Economic Analyses. *Ind. Eng. Chem. Res.* **2007**, *46* (7), 2042–2046. <https://doi.org/10.1021/ie061550u>.
- (34) Aframehr, W. M.; Huang, C.; Pfromm, P. H. Chemical Looping of Manganese to Synthesize Ammonia at Atmospheric Pressure: Sodium as Promoter. *Chem. Eng. Technol.* **2020**, *43* (10), 2126–2133. <https://doi.org/10.1002/ceat.202000154>.
- (35) Kim, S.; Zhong, H.; Park, Y.; Loose, F.; Chirik, P. J. Catalytic Hydrogenation of a Manganese(V) Nitride to Ammonia. *J. Am. Chem. Soc.* **2020**, *142* (20), 9518–9524. <https://doi.org/10.1021/jacs.0c03346>.
- (36) Liu, B.; Manavi, N.; Deng, H.; Huang, C.; Shan, N.; Chikan, V.; Pfromm, P. Activation of N_2 on Manganese Nitride-Supported Ni_3 and Fe_3 Clusters and Relevance to Ammonia Formation. *J. Phys. Chem. Lett.* **2021**, *12* (28), 6535–6542. <https://doi.org/10.1021/acs.jpcclett.1c01752>.
- (37) Liu, B.; Shan, N.; Lee, R. T.; Pfromm, P. Predicting the Behavior of Manganese Nitrides for Atmospheric Ammonia Synthesis. 1.
- (38) Laassiri, S.; Zeinalipour-Yazdi, C. D.; Catlow, C. R. A.; Hargreaves, J. S. J. The Potential of Manganese Nitride Based Materials as Nitrogen Transfer Reagents for Nitrogen Chemical Looping. *Applied Catalysis B: Environmental* **2018**, *223*, 60–66. <https://doi.org/10.1016/j.apcatb.2017.04.073>.
- (39) Laassiri, S.; Zeinalipour-Yazdi, C. D.; Bion, N.; Catlow, C. R. A.; Hargreaves, J. S. J. Combination of Theoretical and *in Situ* Experimental Investigations of the Role of Lithium Dopant in Manganese Nitride: A Two-Stage Reagent for Ammonia Synthesis. *Faraday Discuss.* **2021**, *229*, 281–296. <https://doi.org/10.1039/C9FD00131J>.
- (40) Mohammadi Aframehr, W.; Pfromm, P. H. Activating Dinitrogen for Chemical Looping Ammonia Synthesis: Nitridation of Manganese. *J Mater Sci* **2021**, *56* (22), 12584–12595. <https://doi.org/10.1007/s10853-021-06079-7>.
- (41) Shan, N.; Chikan, V.; Pfromm, P.; Liu, B. Fe and Ni Dopants Facilitating Ammonia Synthesis on Mn_4N and Mechanistic Insights from First-Principles Methods. *J. Phys. Chem. C* **2018**, *122* (11), 6109–6116. <https://doi.org/10.1021/acs.jpcc.7b12569>.
- (42) Gokcen, N. A. The Mn-N (Manganese-Nitrogen) System. *Bulletin of Alloy Phase Diagrams* **1990**, *11* (1), 33–42. <https://doi.org/10.1007/BF02841582>.
- (43) Alexander, A.-M.; Hargreaves, J. S. J.; Mitchell, C. The Reduction of Various Nitrides under Hydrogen: Ni_3N , Cu_3N , Zn_3N_2 and Ta_3N_5 . *Top Catal* **2012**, *55* (14–15), 1046–1053. <https://doi.org/10.1007/s11244-012-9890-3>.
- (44) Laassiri, S.; Zeinalipour-Yazdi, C. D.; Catlow, C. R. A.; Hargreaves, J. S. J. Nitrogen Transfer Properties in Tantalum Nitride Based Materials. *Catalysis Today* **2017**, *286*, 147–154. <https://doi.org/10.1016/j.cattod.2016.06.035>.
- (45) Zeinalipour-Yazdi, C. D.; Hargreaves, J. S. J.; Laassiri, S.; Catlow, C. R. A. DFT-D3 Study of H_2 and N_2 Chemisorption over Cobalt Promoted Ta_3N_5 -(100), (010) and (001) Surfaces. *Phys. Chem. Chem. Phys.* **2017**, *19* (19), 11968–11974. <https://doi.org/10.1039/C7CP00806F>.
- (46) Gao, Y.; Wu, Y.; Zhang, Q.; Chen, X.; Jiang, G.; Liu, D. N-Desorption or NH_3 Generation of TiO_2 -Loaded Al-Based Nitrogen Carrier during Chemical Looping Ammonia Generation Technology. *International Journal of Hydrogen Energy* **2018**, *43* (34), 16589–16597. <https://doi.org/10.1016/j.ijhydene.2018.07.042>.

- (47) Pearson, R. G. Recent Advances in the Concept of Hard and Soft Acids and Bases. *J. Chem. Educ.* **1987**, *64* (7), 561. <https://doi.org/10.1021/ed064p561>.
- (48) Kojima, R.; Aika, K. Cobalt Molybdenum Bimetallic Nitride Catalysts for Ammonia Synthesis Part 1. Preparation and Characterization. *Applied Catalysis A: General* **2001**, *215* (1–2), 149–160. (49) Kojima, R.; Aika, K. Cobalt Molybdenum Bimetallic Nitride Catalysts for Ammonia Synthesis Part 2. Kinetic Study. *Applied Catalysis A: General* **2001**, *218* (121–128), 8.
- (50) Kojima, R.; Aika, K. Cobalt Molybdenum Bimetallic Nitride Catalysts for Ammonia Synthesis Part 3. Reactant Gas Treatment. *Applied Catalysis A: General* **2001**, *219* (1–2), 157–170.
- (51) Grange, P.; Delmon, B. The Role of Cobalt and Molybdenum Sulphides in Hydrodesulphurisation Catalysts: A Review. *Journal of the Less Common Metals* **1974**, *36* (1), 353–360. [https://doi.org/10.1016/0022-5088\(74\)90119-2](https://doi.org/10.1016/0022-5088(74)90119-2).
- (52) Jacobsen, C. J. H.; Dahl, S.; Clausen, B. S.; Bahn, S.; Logadottir, A.; Nørskov, J. K. Catalyst Design by Interpolation in the Periodic Table: Bimetallic Ammonia Synthesis Catalysts. *J. Am. Chem. Soc.* **2001**, *123* (34), 8404–8405. <https://doi.org/10.1021/ja010963d>.
- (53) Hunter, S. M.; Gregory, D. H.; Hargreaves, J. S. J.; Richard, M.; Duprez, D.; Bion, N. A Study of ¹⁵N/¹⁴N Isotopic Exchange over Cobalt Molybdenum Nitrides. *ACS Catal.* **2013**, *3* (8), 1719–1725. <https://doi.org/10.1021/cs400336z>.
- (54) McKay, D.; Gregory, D. H.; Hargreaves, J. S. J.; Hunter, S. M.; Sun, X. Towards Nitrogen Transfer Catalysis: Reactive Lattice Nitrogen in Cobalt Molybdenum Nitride. *Chem. Commun.* **2007**, No. 29, 3051. <https://doi.org/10.1039/b707913c>.
- (55) Adamski, P.; Moszyński, D.; Komorowska, A.; Sarnecki, A.; Albrecht, A. AMMONOLYSIS OF COBALT MOLYBDENUM OXIDES – IN-SITU XRD STUDY. 19.
- (56) Smith, G. W.; Ibers, J. A. The Crystal Structure of Cobalt Molybdate CoMoO₄. *Acta Cryst* **1965**, *19* (2), 269–275. <https://doi.org/10.1107/S0365110X65003201>.
- (57) Eda, K.; Uno, Y.; Nagai, N.; Sotani, N.; Stanley Whittingham, M. Crystal Structure of Cobalt Molybdate Hydrate CoMoO₄·nH₂O. *Journal of Solid State Chemistry* **2005**, *178* (9), 2791–2797. <https://doi.org/10.1016/j.jssc.2005.06.014>.
- (58) Song, N.; Rhodes, C.; Johnson, D. W.; Hutchings, G. J. Comments on the Characterisation of Oxidation Catalysts Using TPR/TPO. *Catal Lett* **2005**, *102* (3–4), 271–279. <https://doi.org/10.1007/s10562-005-5868-0>.
- (59) Brown, S. W.; Jiang, C.; Wang, Q.; Caiola, A.; Hu, J. Evidence of Ammonia Synthesis by Bulk Diffusion in Cobalt Molybdenum Particles in a CLAS Process. *Catalysis Communications* **2022**, *167*, 106438. <https://doi.org/10.1016/j.catcom.2022.106438>.
- (60) Aslan, M. Y.; Hargreaves, J. S. J.; Uner, D. The Effect of H₂: N₂ Ratio on the NH₃ Synthesis Rate and on Process Economics over the Co₃Mo₃N Catalyst. *Faraday Discuss.* **2021**, *229*, 475–488. <https://doi.org/10.1039/C9FD00136K>.
- (61) Brown, S. W.; Robinson, B.; Wang, Y.; Wildfire, C.; Hu, J. Microwave Heated Chemical Looping Ammonia Synthesis over Fe and CoMo Particles. *J. Mater. Chem. A* **2022**, *10* (29), 15497–15507. <https://doi.org/10.1039/D2TA03241D>.
- (62) Al Sobhi, S.; Bion, N.; Hargreaves, J. S. J.; Hector, A. L.; Laassiri, S.; Levason, W.; Lodge, A. W.; McFarlane, A. R.; Ritter, C. The Reactivity of Lattice Nitrogen within the Ni₂Mo₃N and NiCoMo₃N Phases. *Materials Research Bulletin* **2019**, *118*, 110519. <https://doi.org/10.1016/j.materresbull.2019.110519>.

- (63) Bion, N.; Can, F.; Cook, J.; Hargreaves, J. S. J.; Hector, A. L.; Levason, W.; McFarlane, A. R.; Richard, M.; Sardar, K. The Role of Preparation Route upon the Ambient Pressure Ammonia Synthesis Activity of Ni₂Mo₃N. *Applied Catalysis A: General* **2015**, *504*, 44–50. <https://doi.org/10.1016/j.apcata.2014.10.030>.
- (64) Daisley, A.; Hargreaves, J. S. J.; Hermann, R.; Poya, Y.; Wang, Y. A Comparison of the Activities of Various Supported Catalysts for Ammonia Synthesis. *Catalysis Today* **2020**, *357*, 534–540. <https://doi.org/10.1016/j.cattod.2019.06.009>.
- (65) McAulay, K. Cobalt Rhenium Catalysts for Ammonia Synthesis. 186.
- (66) McAulay, K.; Hargreaves, J. S. J.; McFarlane, A. R.; Price, D. J.; Spencer, N. A.; Bion, N.; Can, F.; Richard, M.; Greer, H. F.; Zhou, W. Z. The Influence of Pre-Treatment Gas Mixture upon the Ammonia Synthesis Activity of Co–Re Catalysts. *Catalysis Communications* **2015**, *68*, 53–57. <https://doi.org/10.1016/j.catcom.2015.04.016>.
- (67) Itoh, M.; Machida, K.; Nakajima, H.; Hirose, K.; Adachi, G. Nitrogen Storage Properties Based on Nitrogenation and Hydrogenation of Rare Earth–Iron Intermetallic Compounds R₂Fe₁₇ (R=Y, Ce, Sm). *Journal of Alloys and Compounds* **1999**, *288* (1–2), 141–146. [https://doi.org/10.1016/S0925-8388\(99\)00105-X](https://doi.org/10.1016/S0925-8388(99)00105-X).
- (68) Uchida, H.-H.; Uchida, H.; Yanagisawa, T.; Kise, S.; Suzuki, T.; Matsumura, Y.; Koike, U.; Kamada, K.; Kurino, T.; Kaneko, H. Reaction Kinetics of N₂ Absorption by Sm₂Fe₁₇. *Journal of Alloys and Compounds* **1993**, *196* (1–2), 71–74. [https://doi.org/10.1016/0925-8388\(93\)90572-5](https://doi.org/10.1016/0925-8388(93)90572-5).
- (69) Koeninger, V.; Uchida, H. H.; Uchida, H. Nitrogen Absorption and Desorption of Sm₂Fe₁₇ in Ammonia and Hydrogen Atmospheres. *Journal of Alloys and Compounds* **1995**, *222* (1–2), 117–122. [https://doi.org/10.1016/0925-8388\(94\)04930-0](https://doi.org/10.1016/0925-8388(94)04930-0).
- (70) Machida, K.-I.; Ito, M.; Hirose, K.; Adachi, G. Formation and Hydrogenation of the Nitrogen Stored in Iron-Based Intermetallic Compounds. *Chemistry Letters* **1998**, 1117–1118.
- (71) Itoh, M.; Machida, K.; Hirose, K.; Sakata, T.; Mori, H.; Adachi, G. Nitrogenation and Hydrogenation Characteristics of Transition Metal–Iron Intermetallic Compounds. *J. Phys. Chem. B* **1999**, *103* (44), 9498–9504. <https://doi.org/10.1021/jp9916182>.
- (72) Itoh, M.; Masuda, M.; Machida, K. Hydrogen Generation by Ammonia Cracking with Iron Metal–Rare Earth Oxide Composite Catalyst. *Mater. Trans.* **2002**, *43* (11), 2763–2767. <https://doi.org/10.2320/matertrans.43.2763>.
- (73) Ogawa, T.; Kobayashi, Y.; Mizoguchi, H.; Kitano, M.; Abe, H.; Tada, T.; Toda, Y.; Niwa, Y.; Hosono, H. High Electron Density on Ru in Intermetallic YRu₂: The Application to Catalyst for Ammonia Synthesis. *J. Phys. Chem. C* **2018**, *122* (19), 10468–10475. <https://doi.org/10.1021/acs.jpcc.8b02128>.
- (74) Kitano, M.; Kujirai, J.; Ogasawara, K.; Matsuishi, S.; Tada, T.; Abe, H.; Niwa, Y.; Hosono, H. Low-Temperature Synthesis of Perovskite Oxynitride-Hydrides as Ammonia Synthesis Catalysts. *J. Am. Chem. Soc.* **2019**, *141* (51), 20344–20353. <https://doi.org/10.1021/jacs.9b10726>.
- (75) Goto, Y.; Daisley, A.; Hargreaves, J. S. J. Towards Anti-Perovskite Nitrides as Potential Nitrogen Storage Materials for Chemical Looping Ammonia Production: Reduction of Co₃ZnN, Ni₃ZnN, Co₃InN and Ni₃InN under Hydrogen. *Catalysis Today* **2020**, S092058612030136X. <https://doi.org/10.1016/j.cattod.2020.03.022>.
- (76) Gao, W.; Wang, P.; Guo, J.; Chang, F.; He, T.; Wang, Q.; Wu, G.; Chen, P. Barium Hydride-Mediated Nitrogen Transfer and Hydrogenation for Ammonia Synthesis: A Case Study of Cobalt. *ACS Catal.* **2017**, *7* (5), 3654–3661. <https://doi.org/10.1021/acscatal.7b00284>.

- (77) Ye, T.-N.; Park, S.-W.; Lu, Y.; Li, J.; Sasase, M.; Kitano, M.; Tada, T.; Hosono, H. Vacancy-Enabled N₂ Activation for Ammonia Synthesis on an Ni-Loaded Catalyst. *Nature* **2020**, *583* (7816), 391–395. <https://doi.org/10.1038/s41586-020-2464-9>.
- (78) *Pseudo catalytic ammonia synthesis by lithium-tin alloy | Elsevier Enhanced Reader*. <https://doi.org/10.1016/j.ijhydene.2019.12.190>.
- (79) Hara, M.; Kitano, M.; Hosono, H. Ru-Loaded C₁₂A₇:E⁻ Electride as a Catalyst for Ammonia Synthesis. *ACS Catal.* **2017**, *7* (4), 2313–2324. <https://doi.org/10.1021/acscatal.6b03357>.
- (80) Nakao, T.; Ogasawara, K.; Kitano, M.; Matsuishi, S.; Sushko, P. V.; Hosono, H. Ship-in-a-Bottle Synthesis of High Concentration of N₂ Molecules in a Cage-Structured Electride. *J. Phys. Chem. Lett.* **2021**, *12* (4), 1295–1299. <https://doi.org/10.1021/acs.jpcclett.0c03800>.
- (81) Wu, J.; Li, J.; Gong, Y.; Kitano, M.; Inoshita, T.; Hosono, H. Intermetallic Electride Catalyst as a Platform for Ammonia Synthesis. *Angew. Chem. Int. Ed.* **2019**, *58* (3), 825–829. <https://doi.org/10.1002/anie.201812131>.
- (82) Kishida, K.; Kitano, M.; Sasase, M.; Sushko, P. V.; Abe, H.; Niwa, Y.; Ogasawara, K.; Yokoyama, T.; Hosono, H. Air-Stable Calcium Cyanamide-Supported Ruthenium Catalyst for Ammonia Synthesis and Decomposition. *ACS Appl. Energy Mater.* **2020**, *3* (7), 6573–6582. <https://doi.org/10.1021/acsaem.0c00754>.

3. Microwave and Thermal Catalysis Reactions

3.1 Introduction

CLAS systems are a promising alternative process technology that can overcome traditional HB technological barriers such as high pressure and temperature. Modular CLAS reactors may be designed near sources of renewable energy or near the point of use to reduce the distance to ship ammonia. Microwave heating proceeds through different physical mechanisms than traditional thermal heating, thus microwave heating may provide a means to “switch” bed temperatures very rapidly. Among other possible benefits allowing modular CLAS to approach competitiveness with small scale, lower pressure HB systems.

Microwave heating of these metal nitrogen carriers was chosen as a way to increase both the rate of nitridation and the degree of nitrogen content in the material. Our hypothesis is that microwave treatment of materials lead to these effects due to both rapid volumetric heating, surface polarization and enhanced diffusion¹⁻³. Surface absorbed intermediates and N₂ will couple with microwave radiation and polarize, leading to higher rates of bond weakening and breakage⁴. The surface of metals under microwave radiation also experiences non-uniform electronic effects such as edge effects and high E fields between particles in packed beds⁵⁻⁷. These phenomena coupled with the thermal phenomena are expected to enhance the productivity of these materials.

Microwave heating offers a variety of benefits over conventional thermal heating owing to the difference in the physical processes by which this heating occurs. Uniform and non-uniform heating modes exist and depend upon the size, geometry, electric permittivity, and magnetic permeability of particles^{9,10}.

While bulk metals reflect microwaves due to the formation of eddy currents at the surface caused by magnetic fields ^{12,13}. This eddy current generation depends on skin depth and is a function of the magnetic field pushing the conduction electrons to the surface, commonly referred to as the “skin effect” ^{12,14}. Even though bulk metals often result in the high reflectance of microwaves, the heating of metallic powders is possible and is often exploited in alloying and sintering metals ^{14,15}. Particle size thus is a critical factor along with the dielectric and magnetic properties of the materials to be heated. Additionally composites of metals and microwave sorbents, like sintering cermets, may be exploited for the rapid heating of these structures.

Equation 12:
$$D_p = \sqrt{\frac{2}{(\omega^2 \mu \epsilon'')}}}$$

The penetration depth of microwave radiation may be calculated from data for a wide variety of materials (Equation 12) ¹². Penetration depths on the order of several micrometers are common, for Fe particles it is 3.2 μm , Mo is 2.4 μm , and for Co is 2.4 μm at 2.45 GHz ^{12,16}. Heating in metallic powders proceeds by both dielectric and magnetic properties ¹⁵. Here, dielectric properties were measured because these materials are composites with SiC, which primarily heats by the electric field. When the penetration depth, $D_p \approx d$, the particle diameter, almost all the particle becomes “skin,” in effect ^{14,17}.

Chemical reactions by their nature change the electronic properties of the systems they occur in; it is overserved that as nitridation occurs microwave power requirements for CLAS:SiC mixtures increase to maintain temperature. Oxides tend to heat differently than metallic materials, nitrides also shift electronic structures in a similar way, reducing the heating properties of the materials evaluated. While beneficial as lossy materials, these require more power input to maintain reaction temperatures.

SiC provided the best material for the composite due its physical, thermal, and chemical properties¹⁸. Under blank testing in both ammonia synthesis and CLAS conditions SiC was found to be unreactive. The rapid heat transfer and optimal microwave coupling capabilities of the material made it a useful inert to include in the system¹⁹. While other materials such as oxides, sulfides and carbon compounds couple well in the microwave heating systems, they are not chemically inert and do not allow as intrinsic evaluation of the metal-nitrogen systems being evaluated.

This work aims to evaluate single metals and bimetallic alloys in three ammonia synthesis cycles under realistic reactor conditions and to compare the effectiveness of microwave heating for enhanced ammonia productivity, the candidates were selected based on previous use in the literature, ready reducibility, availability, and low environmental impact.

3.2 Experimental Methods

3.2.1 Materials

Cobalt molybdenum oxide hydrate (CoMoO_4 , ~325 mesh, 99.9%, Alfa Aesar) and iron powder (Fe, <10 μm , >99.9%, Aldrich) samples were tested in both microwave and thermal heating experiments. Silicon carbide (SiC, 98%, 325 mesh, Aldrich) was used as an insulator, a microwave energy sorbent, and to separate particles. SiC and CLAS materials were physically mixed by hand until homogeneous before the reaction.

UHP gases (99.999%): H_2 , N_2 , Ar, and 10% H_2 balanced in He (Matheson and Airgas) were used for all gas-solid reactions. Outlet gases were measured by a CAI 600 Fourier Transform Infrared

Spectroscopy (FTIR) with a gas flow cell to determine outlet concentrations of ammonia product.

3.2.2 Chemical Looping Reactors

Two reactor setups were used to determine the differences between thermal and microwave heating. A continuous flow conventional thermal fixed bed (CTFB) and a continuous flow microwave fixed bed (MWFB). Chemical looping candidates were tested by mass using 500 mg samples physically mixed with 500 mg of inert SiC. Both reactors used quartz tubes (406.4 mm L, 10mm ID, 12 mm OD) to contain the catalyst between quartz wool supports in the center of the tube. All reactions were performed at atmospheric pressure. The procedure for each reaction is detailed below for both the CTFB and MWFB reactors.

3.2.2.1 Thermal Fixed Bed

The thermal fixed bed reactor consisted of a standard programmable tube furnace using a 24 °Cmin⁻¹ ramp rate. First, CoMoO₄ was pre-reduced for 3 h at 750 °C in 50 sccm of H₂ gas flow. Then sample nitridation was performed under N₂ gas flow at 50 sccm for 1 h at 750 °C for CoMo. Nitridation of the Fe samples was performed at 1 h at 450 °C for Fe.

Hydrogenation was performed under 50 sccm H₂ at 450 °C for 1 h. The reactor system was purged with 50 sccm Ar gas for 5 min at temperature between after each synthesis step of the chemical looping reaction cycle.

3.2.2.2 Microwave Fixed Bed Reactor

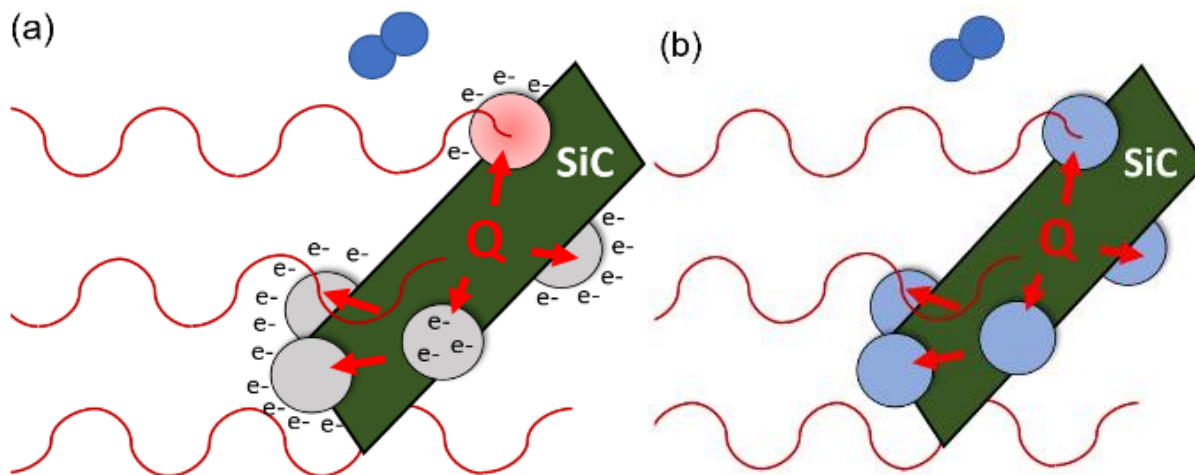


Figure 5. Metal particles heating under microwave. Particles heating from MW (a) and heat conduction from the SiC particles. Electrons are pushed to the surface where they can activate neutral molecules like N_2 . As the metal particles are nitrated (b) they become more oxidic and the heating process requires more energy to heat volumetrically and by conduction from SiC.

The nitridation reaction process proceeds according to Figure 5 (a), where microwave irradiation is absorbed by the metal particles, resulting in volumetric heating. In Figure 5 (b), more microwave power is required to maintain nitridation temperatures for both Fe and CoMo systems as they take on a different character due to oxidation by nitrogen.

Microwave testing was performed in a 2.45 GHz, 3 kW, magnetron generator with a mono-mode cavity microwave from Sairem (model GMP20K) (Figure 6). The temperature was measured using a laser aligned infrared pyrometer (IR) from Micro-Epsilon (model CTLM-3SF75H2) with a pre-calibrated temperature range between 200 and 1500 °C and a 6.5 mm radial spot size. The pyrometer measures the surface infrared emittance of both the reaction tube and its contents. A manual sliding short was positioned to minimize both leakage and reflected power. The power

applied was varied from 300-700 W to maintain target sample temperatures as the reaction proceeded.

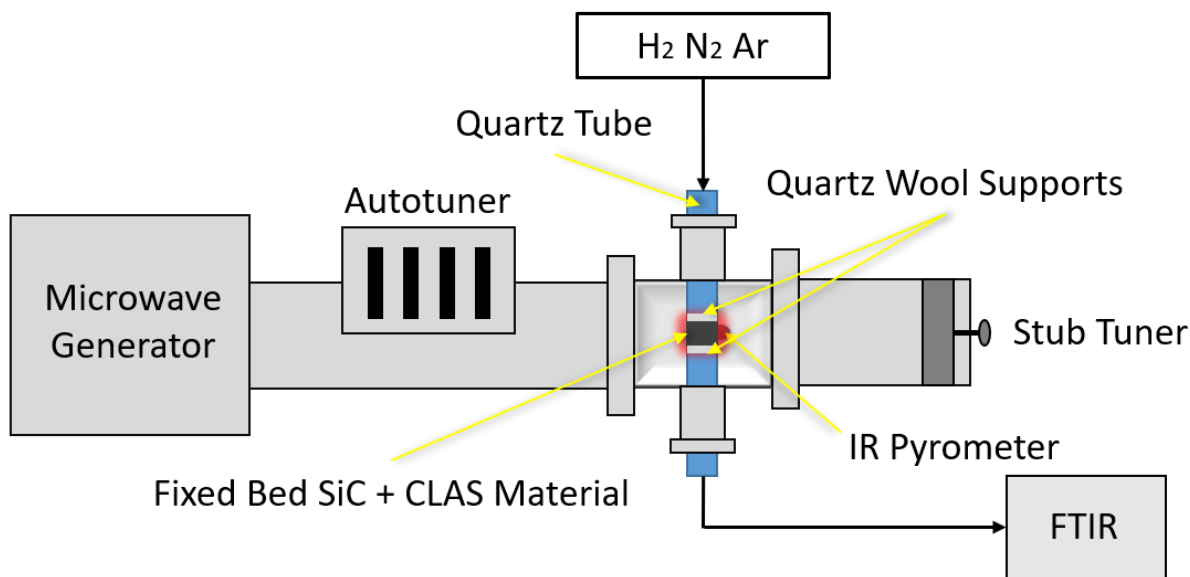


Figure 6. The microwave catalytic reactor. The complete microwave reactor assembly included the generator, waveguide, sliding short, 4-stub autotuner, IR pyrometer, mass flow controllers, and online gas phase FTIR analyzer for outlet gas.

MW heated nitridation was performed at temperatures of 750 °C for CoMo, and for 450 °C for Fe at 50 sccm N₂ flow for 1 h each. The hydrogenation step was performed under 50 sccm H₂ at 450 °C for 15 min to synthesize ammonia for both the CoMo and Fe samples. The reactor system was purged with 50 sccm of Ar for 5 min between each reaction step of the chemical looping reaction.

3.2.4 Particle Characterization

Powder x-ray diffraction (XRD) characterization was performed using PANalytical X'Pert Pro X-ray Diffractometer with CuK α radiation at 45 kV and 40 mA in the range from 10 ° and 20 ° to 100 ° (2θ) at a scan rate of 5 ° min⁻¹.

Thermogravimetric analysis (TGA) was performed (TA Instruments SDT-650 thermogravimetric analyzer) in 90 μ L alumina crucibles. The samples were purged for 1 h under 50 mLmin⁻¹ of 10% H₂/Ar balanced with 100 mLmin⁻¹ He for reduction, or 50 mLmin⁻¹ N₂ balanced in 100 mLmin⁻¹ He for nitridation. The temperature was ramped at a rate of 5 °Cmin⁻¹ to 750 °C and held for 4hrs.

Scanning electron microscopy (SEM) was performed (Hitachi S-4700 Scanning Electron Microscope) set at 5.0 kV and 10 μ A to determine particle size and morphology.

Inductively coupled plasma optical emission spectroscopy (ICP-OES) was performed to determine the composition of spent bimetallic samples. ICP was performed by dissolving spent CLAS materials in concentrated nitric acid, metallic films on glass reaction tubes were dissolved by rinsing with concentrated nitric acid.

Thermal analysis of the microwave catalyst bed was performed by an infrared thermal imaging camera (FLIR model number A6261). The camera was positioned 0.5 m away from the quartz waveguide port. FLIR (Research Max) software was used to analyze the temperature distribution recorded at each pixel of the bed.

Pulse chemisorption was performed (Micromeritics Autochem 2950) using UHP N₂. BET analysis was performed with He (Micromeritics ASAP 2020 adsorption analyzer).

Dielectric property measurement was performed between 100 MHz and 9 GHz (Keysight P5002A vector network analyzer) with a 7 mm by 3.12 cm air line (Maury Microwave model number 2653S3.12). Calibration was performed using a Keysight 85091C electronic calibration model on the autocalibration setting. The powdered materials of interest were included in a paraffin wax (Aldrich, mp 53-58 °C) matrix at 10% volume loading, homogenized, and cast into a plug following the method developed by Tempke et al.²⁰. The Landau-Lifshits-Loonyenga, (Equation 13), was used to separate the dielectric properties of the matrix and the powdered samples²¹. The variables in the equation are: ϵ_{mix} , the measured property, v_m , the volume of the matrix, ϵ_m , the dielectric property of the matrix, v_p , the volume of the particle, and ϵ_p , the dielectric property of the particle.

Equation 13:
$$(\epsilon_{mix})^{\frac{1}{3}} = (V_m \epsilon_m)^{\frac{1}{3}} + (V_p \epsilon_p)^{\frac{1}{3}}$$

3.3 Results and Discussion

Many possible materials for nitrogen fixation under thermal conditions were also considered in the microwave reactor (Table 1). The most outstanding materials for microwave heating included Fe, CoMo and Mg, while the conventional choice for CLAS reactions. The diamagnetic Mn did not couple well with the microwave, so it was excluded from further analysis.

Table 1. The time on stream experimental notes for nitrogen chemical looping catalysts.

Nitrogen Chemical Looping Candidate	Reaction Observation
Mo metal	Unfavorable stoichiometry, air sensitivity, and poor MW heating characteristics.

MoO ₂ /MoO ₃	The low vapor pressure of MoO ₃ causes some mass loss to reactor walls as a molybdenum film. The oxides do heat under microwave irradiation, but this effect decreases as the oxygen content is reduced.
Mn metal	Excellent candidate for nitrogen chemical looping as shown by the publication record, however, a distinct drawback is the massive loss of surface area when metal particles sinter together during nitridation.
MnO ₂	The temperature required to fully reduce MnO ₂ to Mn is above the range studied here, however, MnO still forms a limited nitride which can produce small amounts of ammonia. The Mn suboxide form can be easily observed by a pale green coloring and is easily re-oxidized. This material does not succumb to sintering like pure Mn metal does at ~700°C.
Co ₃ O ₄	Cobalt oxides reduce at a low temperature but retain very small amounts of nitrogen alone.
Mg metal	Heats well in the microwave.
2.5% Co 2.5 % Mo / γ -Al ₂ O ₃	Hydrodesulfurization catalyst shows some limited nitride formation despite low metal loading.
CoMoO ₄	Can be observed to heat in microwave reactor but this effect is limited to changing oxidation states and thus does not last and is not repeatable. Like MoO ₃ , temperature ramp rate can create metallic films which indicate loss of Mo species.
MgFe ₂ O ₄	No ammonia detected.
La _{0.6} Sr _{0.4} FeMnO (LSFM)	No ammonia detected.
CoMoO ₄ + SiC	Heats well in (1:1), less well in other ratios.
CoMoO ₄ + SiO ₂	Did not heat in microwave reactor.
MoO ₂ + SiC	Heats moderately well in (1:1) ration.
MoO ₂ + SiO ₂	Did not heat in microwave reactor.
Mn + SiC	Did not heat in microwave reactor.
Mn + SiO ₂	Did not heat in microwave reactor.
MnO ₂ + SiC	Did not heat in microwave reactor.
MnO ₂ + SiO ₂	Did not heat in microwave reactor.
Mo + SiC	Did not heat in microwave reactor.
Mo + SiO ₂	Did not heat in microwave reactor.
Ta ₂ O ₅	Did not heat in microwave reactor.
CoMoO ₄ :Al ₂ O ₃	Ground with mortar and pestle the 1:1 ratio and calcined at 550°C, this material did heat effectively in the microwave for at least one cycle. Rapidly deactivated and lost performance afterward.
4% Ru 4% Cs/ MgO	Model traditional catalyst used in this laboratory.

1% K 1% Ru/ γ - Al_2O_3	Model traditional catalyst used in this laboratory.
C12A7 (electride)	Did not heat in microwave reactor.
SiO_2	'Invisible' to microwave heating. Separates catalyst particles to allow heating and reduce electron conduction in the mass when homogeneously mixed.
SiC	Efficient absorber of microwave energy used to heat nearby particles when homogeneously mixed.
Al metal	The melting point of metallic Al is within the range of efficient nitride synthesis, $\sim 650^\circ\text{C}$, also making this a difficult material to work with alone.
Ti metal	No ammonia detected.
TiMn_2	No ammonia detected.
γ - Al_2O_3	Support for 2.5% Co 2.5 % Mo / γ - Al_2O_3 , no ammonia detected.
MgO	No ammonia detected.

3.3.1 CLAS Performance Comparison between Microwave and Thermal Heating

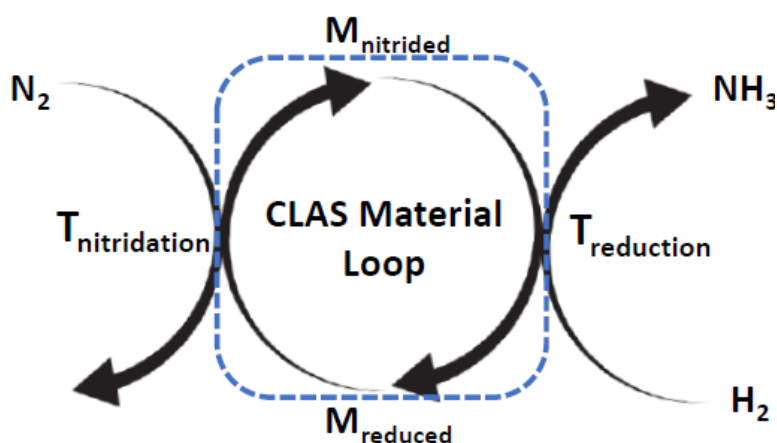


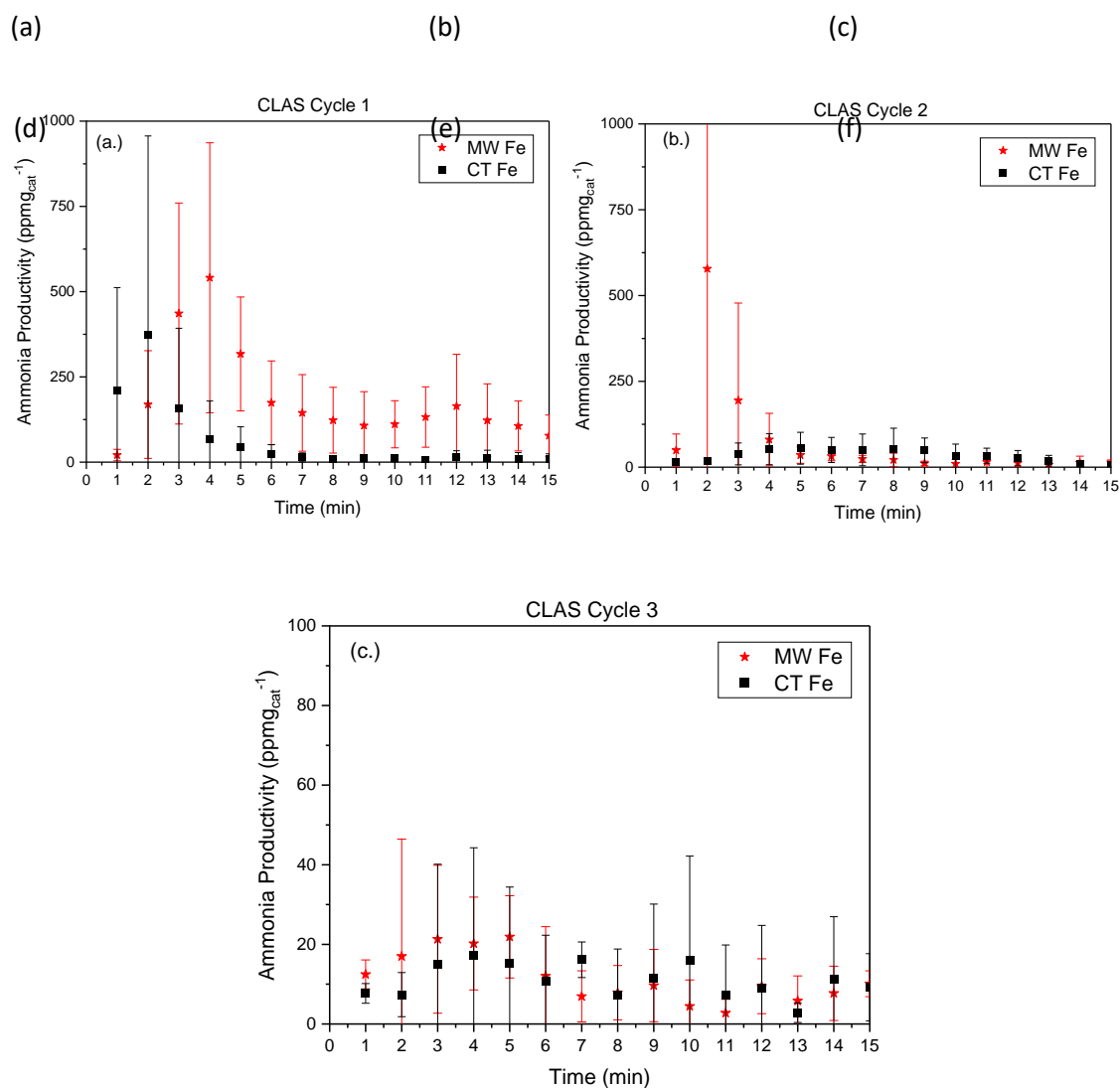
Figure 7. The CLAS loop visualized. A particle is first nitrided at the temperature of nitridation under N_2 , then is reduced at the temperature of hydrogenation to ammonia under H_2 .

A representative schematic diagram of the three-cycle chemical looping process is presented in Figure 7. Initiation steps include reduction of the oxide precursors followed by nitridation to the active phase, hydrogenation to form ammonia, and the eventual deactivation leading to the

formation of multiple stable phases that are no longer active stable inactive phases, which ultimately breaks the cycle. The ammonia synthesis reaction, or hydrogenation step, was performed three times for each chemical looping candidate.

Time on stream experiments was performed for both the CTFB and the MWFB with identical operating conditions. CoMo and Fe systems were examined at 450 °C for 15 min under H₂ flow.

The results of these experiments performed in three CLAS cycles are shown in Figure 8.



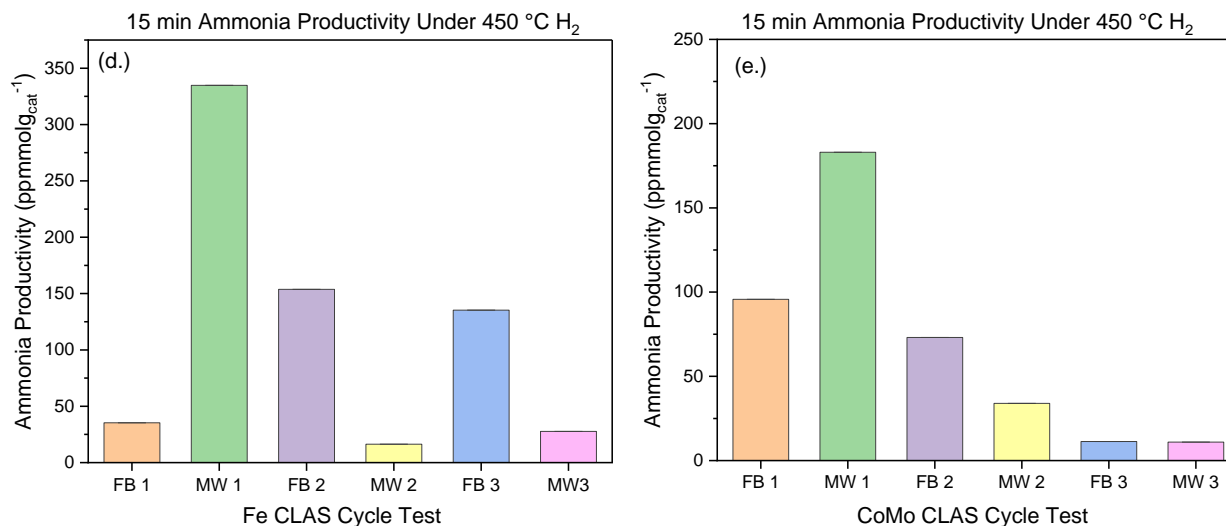


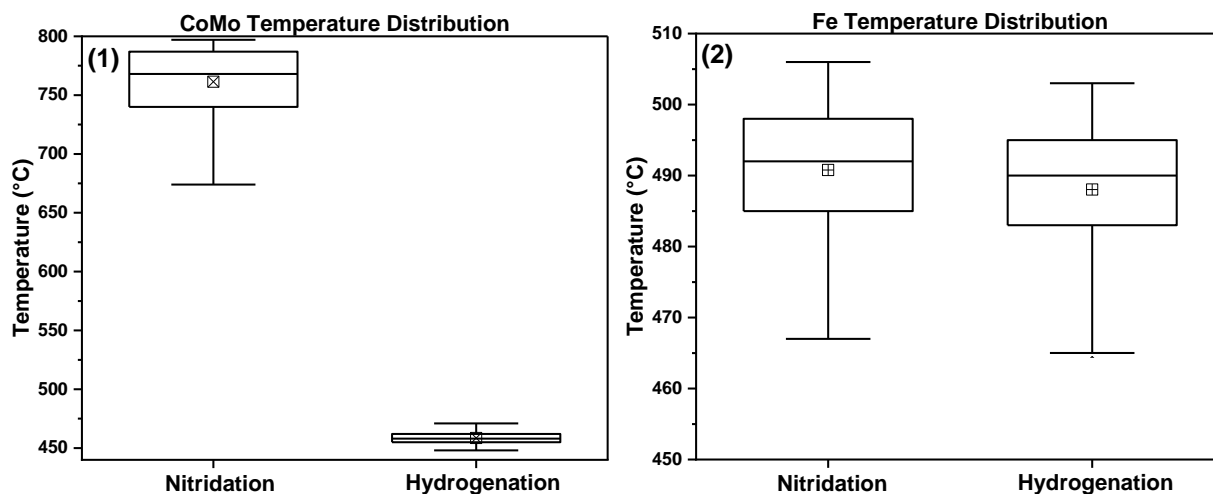
Figure 8. Microwave and thermal reactor results for a three cycle CLAS process. Samples of Fe:SiC are represented in red for cycle 1, (a), 2, (b), and 3 (c). Samples of CoMo:SiC are represented in blue for cycle 1 (d), 2 (e), 3 (f).

The MWFB system resulted in a significantly higher ammonia production rate in comparison to the CTFB for both the Fe and CoMo catalyst systems. In CLAS Cycle 1-3 for the CoMo system (Figure 8 (d-f)) shows significant deactivation for ammonia production for the MWFB in comparison to CTFB. However, the Fe system produces much higher amounts of ammonia over the entire process, especially (Figure 8 (a) and (b)). An induction period is overserved in the initial step of cycle 1 (Figure 8 (a)) for CoMo.

Several possible explanations for the differences in performance between the CTFB system and the MWFB system exist. Electronic activation enhanced ionic diffusion could lead to the advantage the microwave system presents²². Rapid heat transfer, however, likely results in the faster conversion to ammonia. Deactivation may proceed via formation of various inactive phases and the loss of surface features due to MW heating.

Due to both its particle size $<10\ \mu\text{m}$, and the ability of Fe to couple with both electric and magnetic fields it performs the best of all samples considered ²⁵. Fe metal is ferromagnetic and the heating process occurring is largely due to the internal eddy current variety which leads to volumetric heating ²⁶.

Mo is paramagnetic and do not couple well with MW radiation. Co metal is also ferromagnetic and does couple with the microwave, but the performance is offset by both the larger particle size of the CoMo sample, and the alloying with Mo. All samples were aided by the conductive heat transfer from SiC, which being insulating prevented the entire catalyst bed from becoming conductive and simply reflecting MW energy ⁷.



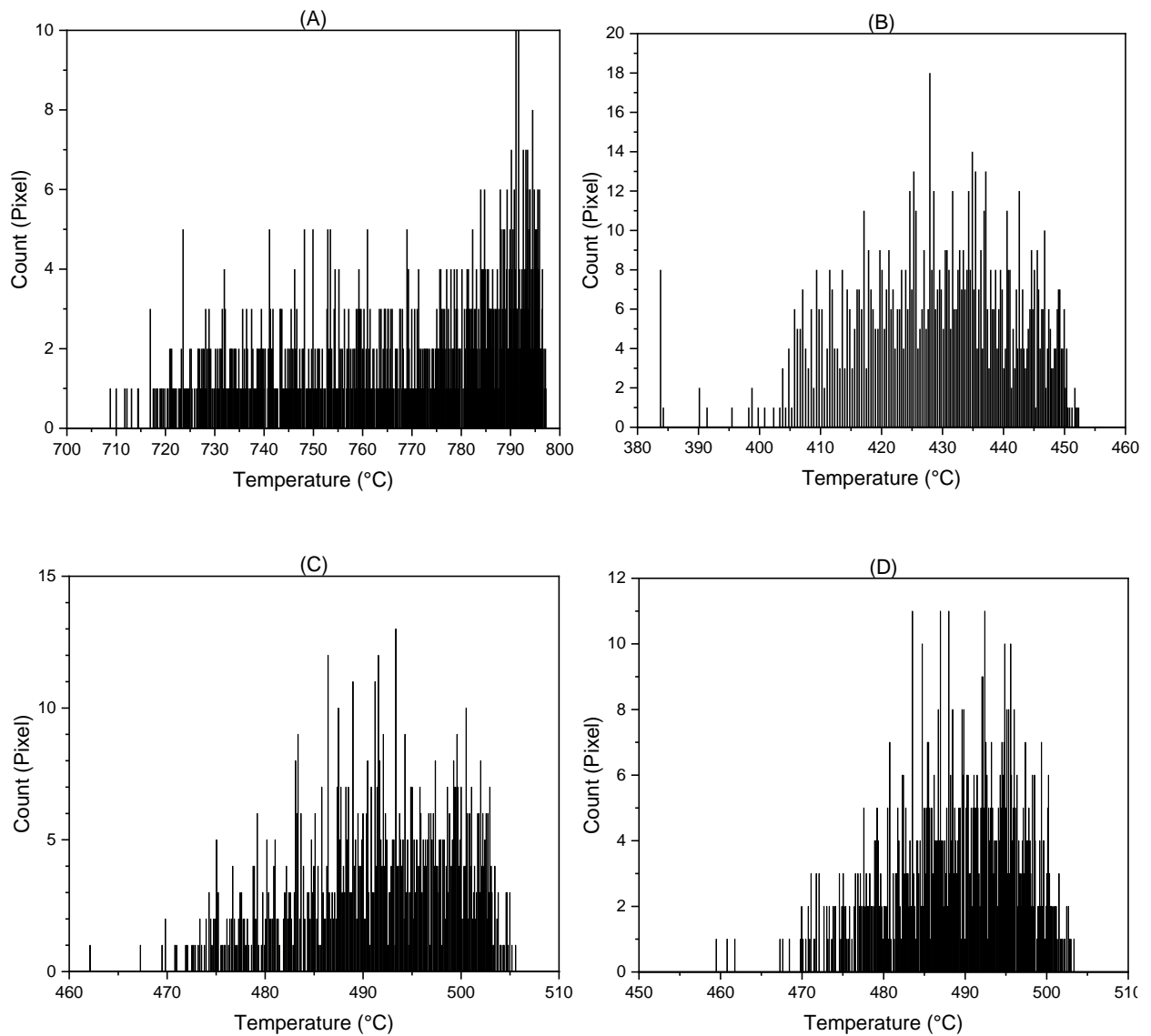


Figure 9. The temperature distribution for MWFB conditions under both N_2 and H_2 flow at 50 sccm was acquired with thermal imaging. (1) is the temperature distribution for the CoMo:SiC system where the set point is 750 °C and 450 °C respectively. (2) is the temperature distribution for the Fe:SiC system where the set point is 450 °C. Raw data is available for all temperature analyses in (A-D), CoMo nitridation, hydrogenation (A, B) and Fe nitridation, hydrogenation (C, D).

A discrepancy of 10 °C – 40 °C in the MW setpoint, controlled by an IR pyrometer. The temperature difference is attributed to how radiation is collected from the surface of the sample. The IR pyrometer can only observe a small fraction of the catalyst bed due to the small observation spot size, whereas the thermal imager observes the entire front-facing section of the catalyst bed. Therefore, a greater temperature distribution is observed when a per-pixel average is taken with the thermal imager due to heat losses at the top, bottom, and sides of the catalyst bed.

The Fe samples exhibited higher microwave absorption than the CoMo samples resulting in a more rapid heat generation from within the sample. Figure 9 (2) depicts the Fe samples heat distribution. The Fe sample nitridation step and the hydrogenation step both resulted in a similar temperature overshoot. The nitridation step and the hydrogenation step resulted in an on average temperature overshoots of about 40 °C from the 450 °C setpoint.

CoMo heating, in Figure 9 (2), appears to have more accurate temperature control during cycle 1, with an average of 761 °C during nitridation and an average temperature of 459 °C during hydrogenation. The error bars at the 750 °C setpoints are large which is to be expected at such elevated temperatures. While the 450 °C hydrogenation step is better controlled. We speculate this is due to lower energy requirements for the exothermic hydrogenation reaction.

The thermal imager is used outside the waveguide and focused on the quartz tube through a secondary quartz port. The temperature pixel data is collected and then processed using basic descriptive statistical analysis. There is a degree of error that is inherent in either temperature measurement system; the IR pyrometer averages colder with warmer regions within the spot size and the FLIR system does not compensate for emissivity changes and averages to a smaller spot

size. However as both are $< 50\text{ }^{\circ}\text{C}$ of each other this system is fairly accurate and consistent in temperature control between multiple runs. Because of the temperature of the bed, it is not possible to use a fiber to measure the temperature.

3.3.2 Material Characterization

To understand the physical changes occurring in CLAS fresh and spent particles were characterized. SEM, Vector Network Analysis, ICP, TGA and XRD were useful to examine particle morphology, chemical, and phase changes when undergoing the nitridation and hydrogenation reactions in both thermal and microwave heated settings.

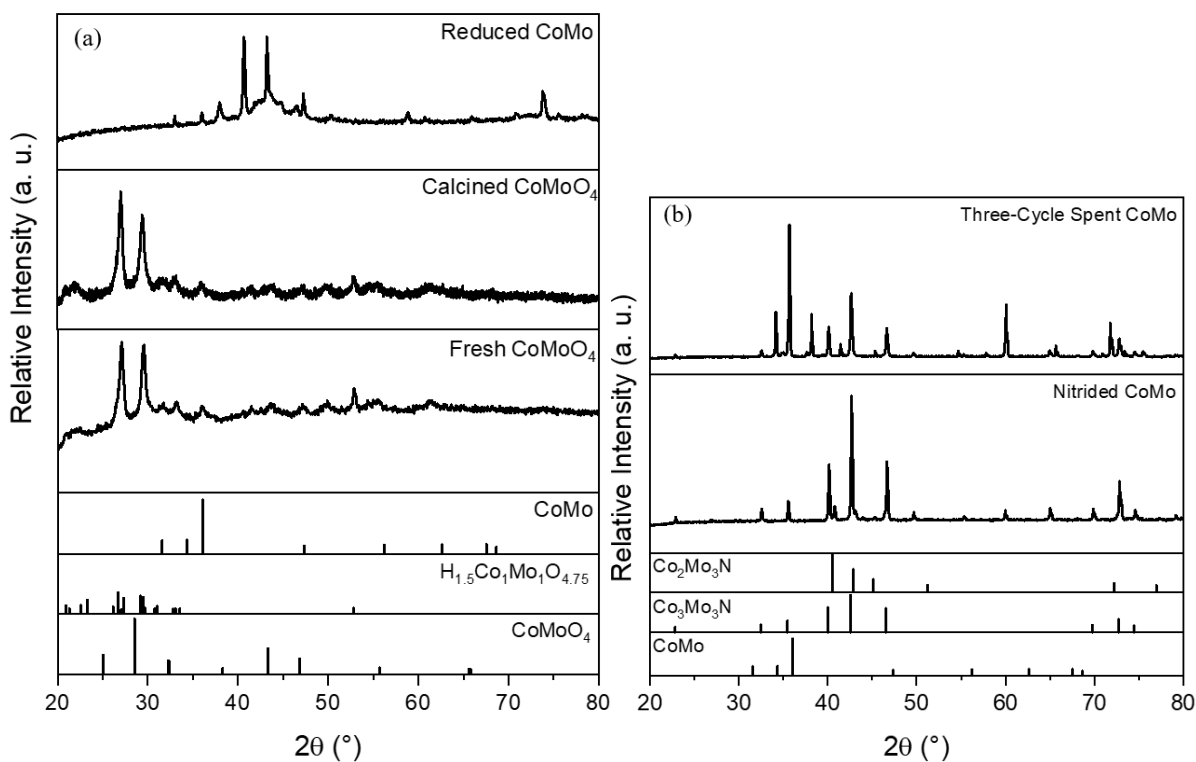


Figure 10. CoMoO₄ X-ray diffraction patterns as the sample are reacted under CLAS conditions.

The diffraction patterns in (a) the oxide species, and (b) the spent and nitride species.

The structure characterization of the CoMo sample was analyzed with XRD for each step of the reaction cycle; pre-reduction, nitridation, and spent samples. Figure 10 (a) indicates that reduction and calcination processes do not remove all complexed water, or rather, result in a mixed-phase product finally resulting in a partially reduced system.

The 3 h reduced CoMo system does not resemble CoMo metal alloy, nor the oxide precursor, so it must be some new intermediate collection of phases.

The active phases of many CLAS materials have been identified previously by researchers. The CoMo system has been well characterized by both Hargreaves and Moszyński²³⁻²⁵. Iron nitrides proved too unstable to prepare an ex-situ sample for crystallographic analysis due to the low overall conversion.

XRD results (Figure 10 (b)) indicate that the nitrated material is indeed $\text{Co}_3\text{Mo}_3\text{N}$, the desired active phase. After three cycles, however, this material is degraded, the coexistence of $\text{Co}_2\text{Mo}_3\text{N}$, $\text{Co}_3\text{Mo}_3\text{N}$, and a significant metallic and unreacted CoMo phase is inferred from the diffractogram. The existence of these metallic phases is likely the deactivation route that these particles undergo, diffusion along grain boundaries is traditionally thought to be the fastest process in nitridation but may lead to losses amongst metallic and partially nitrated phases due to slow intra-phase diffusion²⁶.

The XRD results indicate that a partially reduced system exists. This reflects the findings in Chapter 4 on nitridation-stabilized ammonia synthesis and CoMo structure rearrangement during OH^- loss processes, the nitride phases appear to be free from H_2O ²⁷.

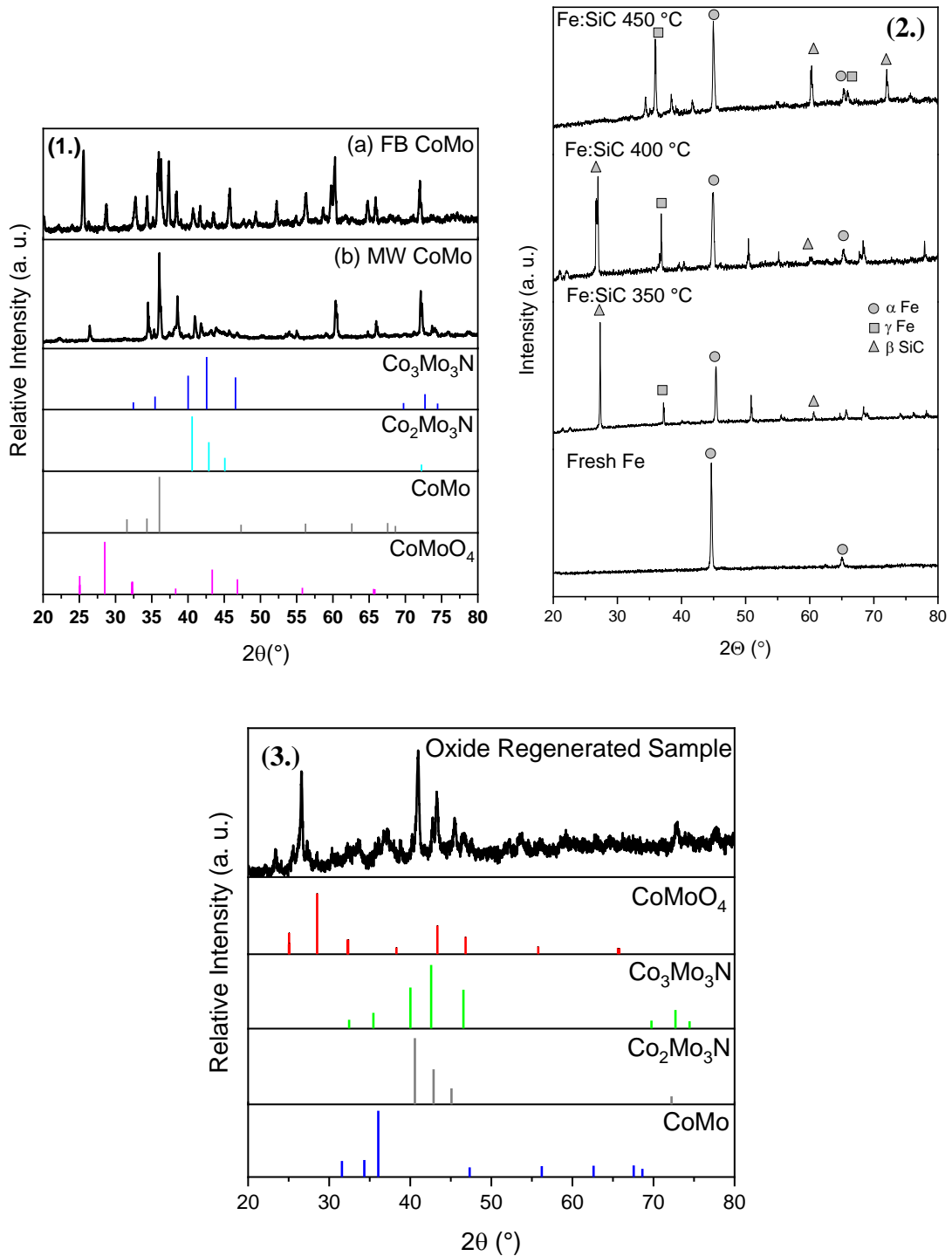
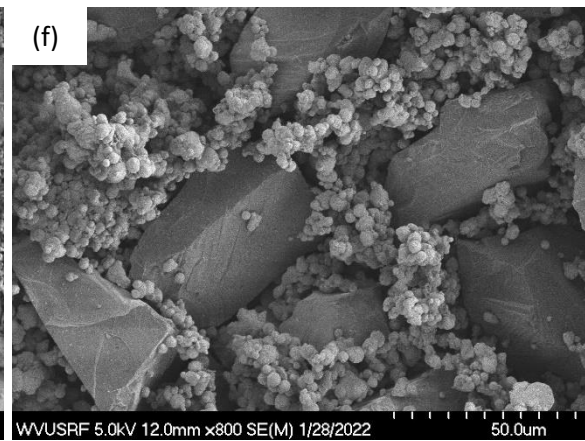
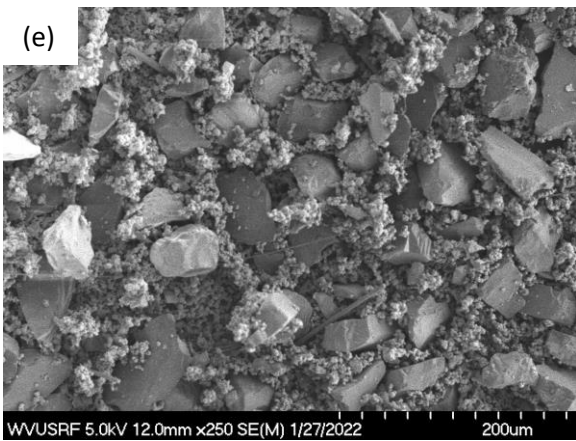
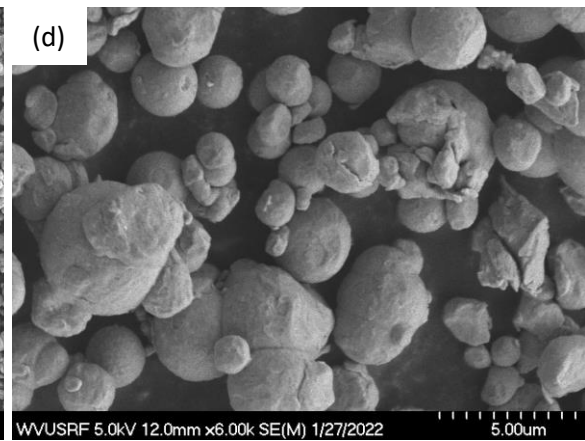
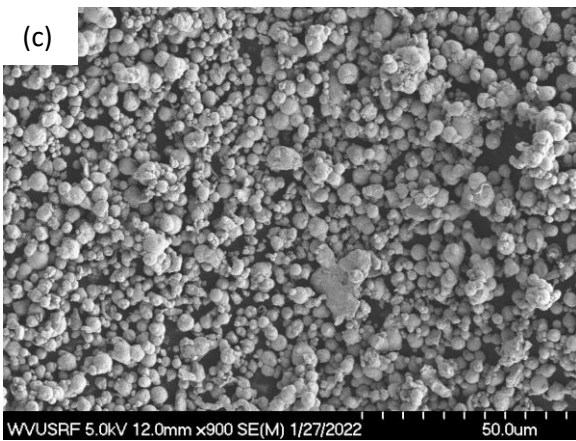
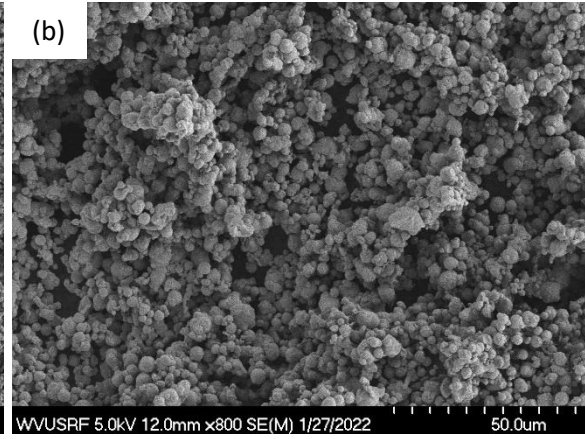
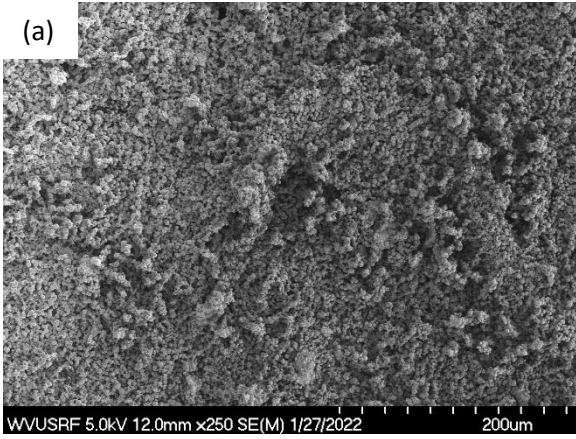


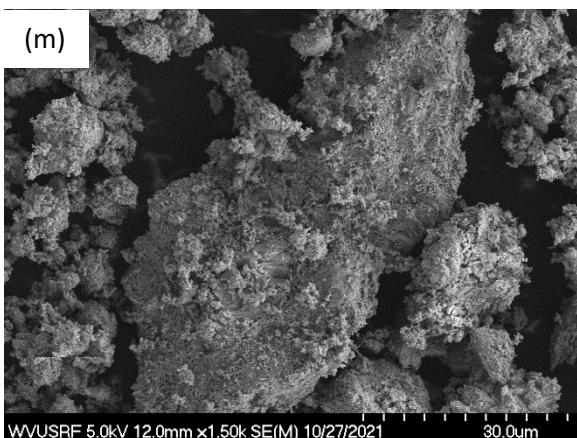
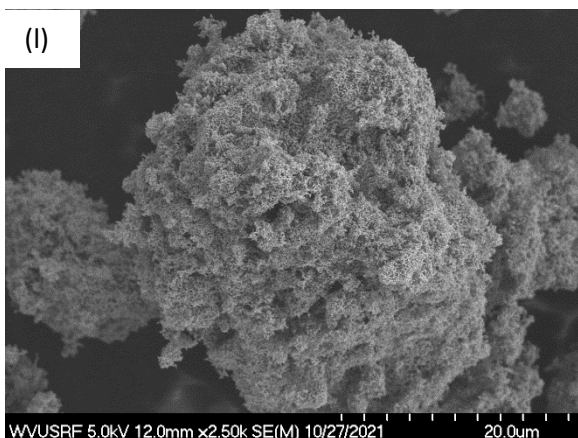
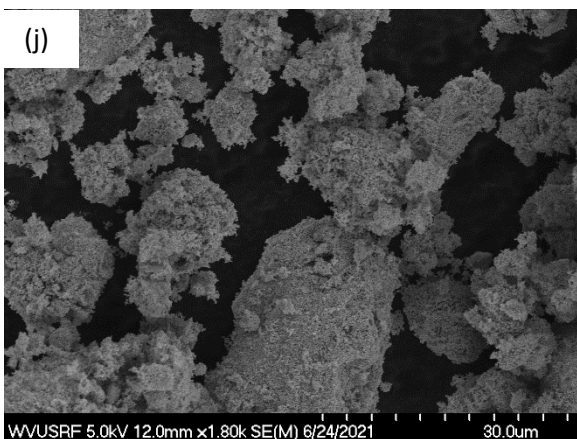
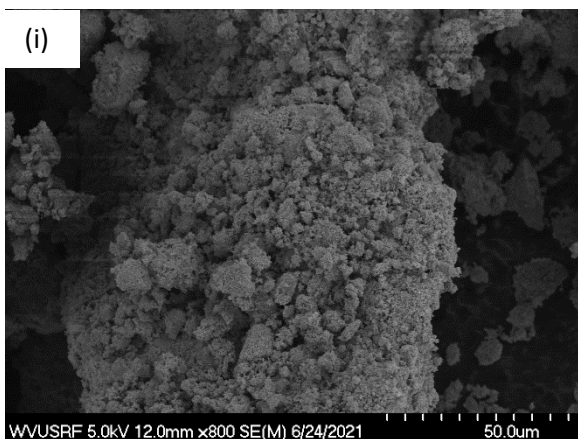
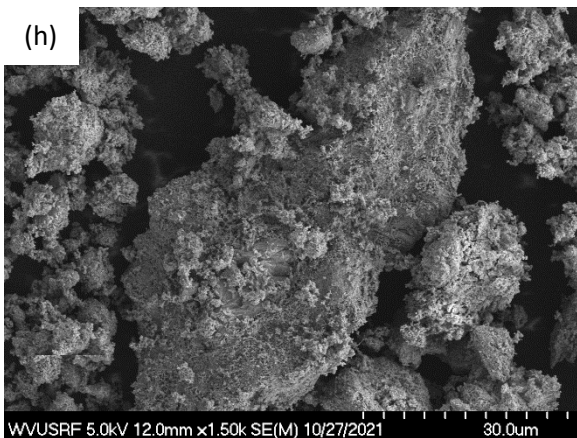
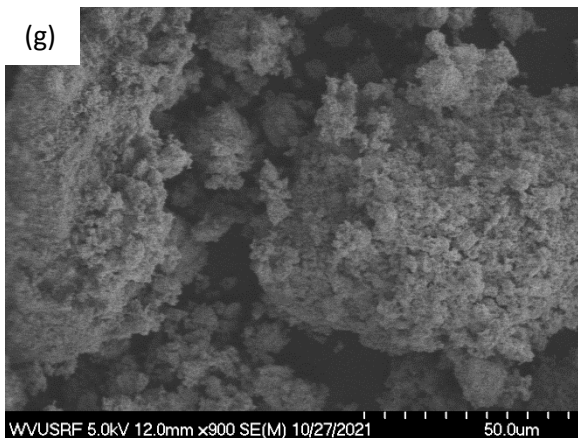
Figure 11. X-ray diffraction patterns of spent MW and regenerated samples. Spent MW and FB CoMo samples are compared (1.), spent Fe:SiC composites are compared in (2.) at different temperatures of reaction. (3.) the CoMo sample nitrated, oxidized and renitrated.

Deactivation of the CLAS candidates was evaluated with post reaction XRD. The spent MWFB and CTFB CoMo samples are compared in Figure 11 (1.). Many more oxidic phases formed in the deactivated FB sample, while the MW sample was shifted from nitride to its metallic alloy form. The effect of heat treatment on the Fe sample was evaluated at different temperatures of MW reaction, and it can be observed that the BCC Fe changes to FCC upon heating, likely owing to non-uniform heating in the microwave (Figure 11 (2.)). The formation of the FCC is less productive than the BCC phase.

To evaluate the impact of cyclical operation and redox capabilities the CoMo material was also tested cyclically from the CoMoO_4 state. The material was then reduced at 750 °C for 3 h under 50 sccm H_2 , nitrified under 750 °C 50 sccm N_2 , and reduced at 750 °C under 50 sccm H_2 . The final state representing a spent material. This spent material was then re-oxidized in air at 750 °C for 3 h. Once completely oxidized the material was reduced at 3 h 750 °C under 50 sccm H_2 and then nitrified at 750 °C under 50 sccm N_2 for 1 h. This final step representing a regenerated material. The resultant diffraction pattern in Figure 11 (3.), shows evidence of both regeneration of the $\text{Co}_3\text{Mo}_3\text{N}$ active phase and resultant oxide phases from incomplete conversion as well as reduced intensity and peak broadening likely due to loss of crystallinity.

Particle size and design could potentially be utilized to reduce and mitigate this effect, as well as high-temperature processing to anneal the crystal structure and grinding to further reduce the particle size after agglomeration.





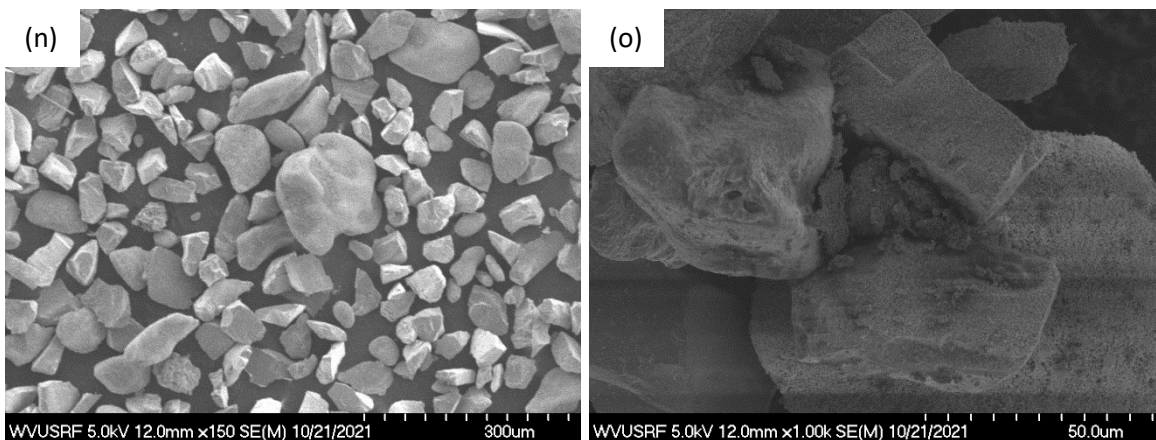


Figure 12. Electron micrography of CLAS Samples. Fresh Fe powder (a), (b), spent CTFB Fe powder (c), (d), spent MWFB Fe:SiC powder (e), (f), fresh CoMoO₄ (g), (h), reduced CoMo (i), (j), nitrided CTFB (k) and spent CTFB CoMo (l), and finally spent MWFB CoMo samples (m), (n).

Electron micrography of (Figure 12 (a), (b)) of fresh Fe powder, (Figure 12 (c), (d)) 1 h 450 °C, 50 mLmin⁻¹ CTFB nitrided Fe powder, and (Figure 12 (i), (f)) three-cycle spent MWFB 1:1 physically mixed with SiC. The SEM images in Figure 12 (a-d) indicate that the CTFB Fe powder had little morphological changes occurring between the fresh Fe powder and nitrided Fe powder samples. The spent Fe MWFB samples show slight evidence of agglomeration and exhibit evidence of sintering on removal from reaction tube.

The bimetallic CoMo starts as an oxide which is calcined from the nitrate form leaving a textured surface. Figure 12 (g, h) of the fresh oxide show very little change during the reduction step which results in a significant weight loss Figure 12 (i, j). CoMo volume typically decreases between the oxide precursor and the reduced samples, shown in Figure 12 (i, j). Nitrided thermal, (Figure 12 (i)), and spent (Figure 12 (f)), samples show no more volume or changed surfaces from the reduced samples which experienced thermal treatment.

Spent MWFB CoMo samples (Figure 12 (m, n)), show very little evidence of agglomeration or of significant morphological changes at all. It is believed that at the operating temperatures of the CTFB and the MWFB, there should be very limited sintering effects ²⁸. Nor do we expect to see particle surface area changes as reported by Pfromm under hydrolysis conditions, since we are cycling between the metal (0) oxidation state to the metal (+1.5, +3, +6) oxidation states under oxidation conditions with N₂, not the oxide ²⁹.

Metallic films were observed on the inner surface of the quartz tubes during some time on stream experiments with CoMo alloys. Because this represent a possible mass loss from the material, it was necessary to understand the nature of this phenomenon and how it can alter yields, performance, and reproducibility of ammonia synthesis. Thus, ICP was performed to identify the metallic film composition.

Table 2. ICP-OES results were collected from the metal films coated on quartz tubes used in CoMo experiments. Samples were washed with soap and water before being crushed and rinsed with fuming nitric acid.

Sample	Co [wt. %]	Mn [wt. %]	Mo [wt. %]
Spent Quartz Reaction Tube	0.01	0.09	99.90

The major constituent of the metallic films was found to be Mo, shown in Table 2. Loss of Mo occurred at reaction temperatures used in the literature, between 700 °C and 750 °C. This raised concerns about the stability of the material for possible scale-up. This phenomenon is likely owing to the low vapor pressure of the MoO₃ species ³⁰. In future work, pre-reduction of

CoMoO₄ should be carefully performed with a slow ramp rate to reduce the volatility of the MoO₃ species which can result in mass loss, undesirable vapor phase reactions and attrition of the particles.

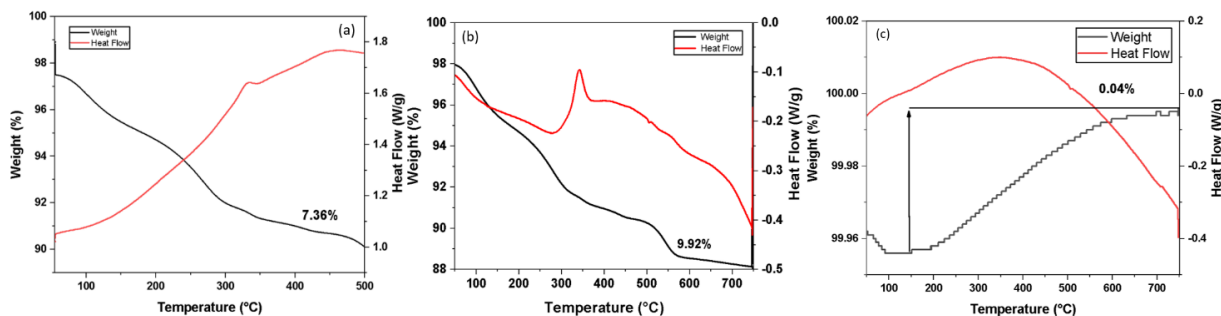


Figure 13. TGA-DSC results of CoMo samples. The calcination of CoMoO₄ hydrate in He (a), the reduction of CoMoO₄ under 10% H₂ balanced in He (b) and the nitridation process of CoMo under N₂ (c).

Thermogravimetric analysis was performed to correlate loss of water, nitrogen and other related processes under chemical looping conditions and collect relevant information on mass loss and phase change by employing TGA-DSC.

The calcination process results in a 7.36 % mass loss is attributable to complexed water upon heating in He (Figure 13 (a)). The reduction process of CoMoO₄ is shown in Figure 13 (b). The reduction process is found to be similar to the calcination process in the shape of the curve. Because the mass loss is 9.92% when it reaches temperature it can be inferred that the reduction process is slow compared with complex water loss process, though these processes occur simultaneously.

At 340 °C in Figure 13 (b), an endothermic change is observed, likely attributable to phase rearrangement. A slightly smaller peak is overserved in Figure 13 (a) during calcination There is another dehydration reaction found to occur at 610 °C where the β phase CoMoO_4 is formed ³¹.

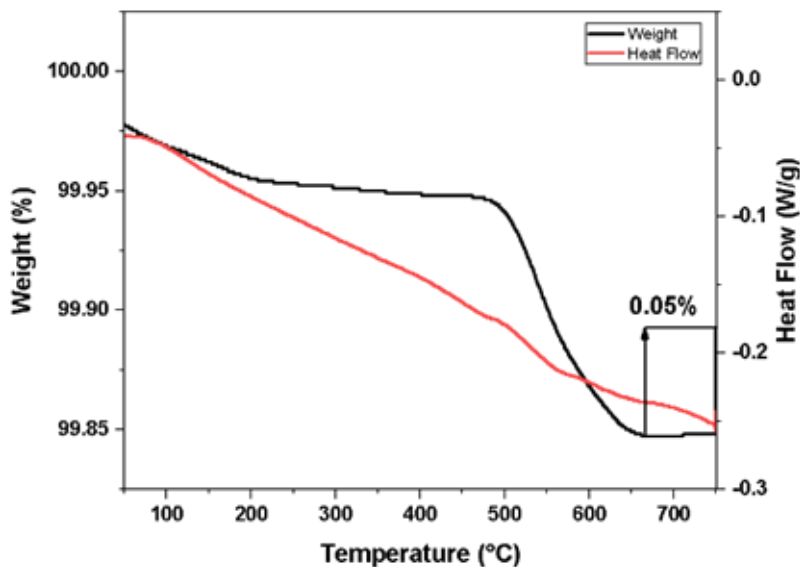


Figure 14. TGA nitridation of Fe under N_2 .

Nitridation of the three CLAS candidates was carried out in the TGA to determine nitrogen uptake. Mass transfer limitation inside the TGA pan is speculated to be the cause of many of these nitridation results not approaching stoichiometric yields even after many hours of treatment time. CoMo, (Figure 14 (c)) and Fe, (Figure 13) both indicated negligible nitrogen uptake in the TGA. This process then is inferred to be limited by gas phase diffusion to the particle surface and the formation of a small layer of nitride which blocks further N_2 diffusion to the particles beneath.

3.3.3 Deactivation

Multiple deactivation processes affect performance after the first CLAS cycle. In the CTFB, loss of surface area and phase segregation are the main concerns. Similarly, the MWFB suffers from the same issues, however, because of the increased material kinetics and some unique features of microwave heating, the deactivation process may happen faster and be dominated by a different set of physical processes.

BET surface areas measurements were conducted for the samples in their fresh, first nitridation cycle, second nitridation cycle, and three-cycle spent states for both CoMo and Fe in the thermal and microwave reactors. Results of these experiments (Table 3) indicate that the pre-reduced CoMoO₄ suffers from a drastic reduction in surface area through the reduction-nitridation-hydrogenation reaction cycles losing ~92% of its original area. The Fe samples can be seen to suffer from reduced surface areas, but the starting surface area is already extremely small, so the effect is limited.

Table 3. BET surface areas collected for Fe and CoMo for both thermal and MW heating.

CLAS Sample	Fresh [m ² /g]	CTFB Spent 1:1 SiC [m ² /g]	MWFB Spent 1:1 SiC [m ² /g]
Fe	0.62	0.35	0.47
CoMo	15.98	3.68	1.33

*1:1 CLAS Sample:SiC is physically mixed by mass

Pulse N₂ chemisorption was performed for both pre-reduced CoMo and Fe samples for two cycle each to determine the effects of deactivation. In pulse chemisorption the gas injection is precisely

controlled, and the process is repeated until the signal in the outlet stream remained stable, indicating that the sample is saturated with N₂.

The Fe samples was treated at 450 °C and the CoMo sample was treated at 750 °C, their given reaction temperatures. Next, the sample was reduced with H₂ at 450 °C for 30 min, and the N₂ injection process was repeated.

To attempt to regenerate the catalyst a 10% O₂ balanced in Ar gas was passed over the samples for 30 min at 450 °C between the chemisorption steps. the results presented in Table 4 indicated that the CoMo sample is negatively affected by the low-level oxygen treatment, while Fe experiences a slight increase in N₂ uptake. This is attributable to the increase in surface oxidation of Fe which increases surface area for adsorption. While the O₂ treatment of CoMo further removes the active phase Co₃Mo₃N and leads to inactive phase formation.

Table 4. Results from pulse N₂ chemisorption tests for both Fe and CoMo samples. Two cycles were used to determine N₂ uptake. The samples were nitrided, reduced and re-nitrided. The second set of N₂ uptake experiments featured a nitride, reduction, oxidation, and nitridation step.

CLAS Sample	N ₂ Uptake Cycle 1 [Peak Area]	N ₂ Uptake Cycle 2 [Peak Area]	N ₂ Volume Uptake Cycle 1 [mL]	N ₂ Volume Uptake Cycle 2, post oxidation [mL]
Fe	0.1478	0.1040	0.1448	0.1508
CoMo	0.1443	0.1506	0.1355	0.1062

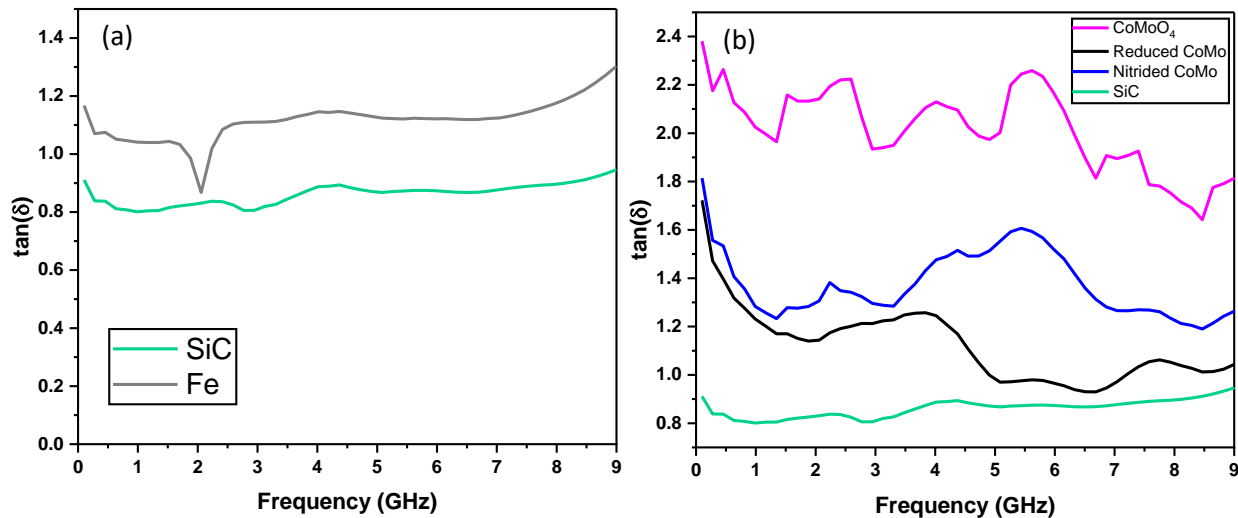


Figure 15. The dielectric properties for both CoMo and Fe samples. SiC (a), Fe (a), CoMoO₄ (b), reduced CoMo (b), nitrided CoMo (b), SiC (b).

Dielectric properties of the 1:1 CLAS materials and SiC were measured using vector network analysis. The dielectric property can be presented in the loss tangent, which is a ratio of how lossy a material is to how conductive it is. The results are presented in Figure 15, indicate that the results of the various stable chemical states that made up the CLAS reactions, nitrided Fe was not examined in the network analyzer because of the inherent instability of the compound as prepared.

The trends which can be inferred from the results in Figure 15 are that materials tend to heat best when they are in an optimal zone, somewhat greater than 1 loss tangent. However, as the chemical nature of the system changes, such as with nitrided CoMo, the system becomes more difficult to heat and requires more microwave input energy. The observed chemical change of the bimetallic is more like that of the precursor oxide and thus the material is too lossy and does not heat well (Figure 15).

Microwave sintering is a well-studied process using small metallic powders ⁷. This phenomenon, along with differential heating in radial volumes based on the penetration depth may lead to restructuring of the surface to leading to a smoother and less porous surface. The BET results indicate that surface area slowly increases due to repeated oxidation by nitrogen followed by reduction with hydrogen. The microwave may enhance the formation of unreactive phases near the surface, where the wave is at its strongest. This in turn leads to less site and higher activation barriers for N⁻³ ion diffusion into the crystal structure. Ultimately this process breaks the chemical looping cycle.

The Fe samples deactivation seems to be more linked to the sintering and agglomeration of small particles because the chemical state of the nitrated Fe particles is short lived. This observation indicates that the heating process is more linked to the penetration depth as the particle sizes grow. The particles become larger due to sintering and thus heat less efficiency as they take on more reflective character under irradiation. The effect of penetration depth means that when the size of the particle is on the order of the penetration depth, then the entire particle becomes “skin” and heating is volumetric ¹³. If the particle is too small, the particle may become invisible to the irradiation, a problem possibly encountered with certain nanoparticle catalysts under microwave conditions, if the particle is too large the surface skin effect will reflect the radiation and heating will be non-uniform ¹³. This may also occur if conductive particles share electrons forming a “super-particle” which may reflect incident radiation.

On the other hand, the CoMo bimetallic shows much less evidence of sintering, but as the material is completely changed from its metallic state to the ‘lossier’ nitrated state the dielectric properties take on more of the original oxide character. This leads to a less efficient heating process, the tendency for the reaction not to run to completion or to deplete the CoMo samples

supports this interpretation. Additionally, the larger CoMo particles likely heat more from the E-field rather than the combination of both magnetic and electric field for the Fe particles.

3.4 Conclusions

Chemical looping ammonia synthesis materials, Fe and CoMo, were subjected to three chemical looping cycles to evaluate respective productivity under both microwave and traditional thermal heating. An in-depth investigation into the prevalent microwave heating mechanisms, reaction engineering parameters, and particle characterization was performed. The three cycles were selected to begin to analyze longer and more representative chemical looping processes which may last for many cycles and many hours ³².

Dielectric properties of microwave catalyst samples were found to have a significant impact on how materials interact with electromagnetic radiation, but the penetration depth is a critical factor for considering microwave-matter interaction in microwave-enhanced catalysis. Taken together the dielectric and magnetic properties must be tuned to fall into an optimal lossy region, with a penetration depth which avoids surface only heating, or reflection and avoids on too-small scales, transparency to microwave radiation. These features may be tuned depending on the purpose of the catalyst.

Finally, the regeneration and attrition of these materials was considered with gaseous oxygen to increase surface area and introduce defects back into the lattice. The findings of this study indicate that, re-oxidation may be a useful strategy depending on the starting material composition and morphology. Spherical Fe particles responded more favorably than the more air sensitive CoMo system and future work may consider other geometries and combinations of microwave sorbents and metals ³³.

Microwave chemical treatment of metals offers possible advantages over conventional thermal fixed bed reactors that include both higher productivity and more operational flexibility. These features matched with microwave sensitive catalyst design may prove to be useful in future decentralized ammonia production applications.

3.5 References

- (1) Huang, J.-W.; Li, J.; Peng, H. Microwave Synthesis of Manganese Nitride. *Powder Metallurgy* 2007, 50 (2), 137–141. <https://doi.org/10.1179/174329007X153323>.
- (2) Houmes, J. D.; zur Loye, H.-C. Microwave Synthesis of Ternary Nitride Materials. *Journal of Solid State Chemistry* 1997, 130 (2), 266–271. <https://doi.org/10.1006/jssc.1997.7303>.
- (3) Rao, K. J.; Vaidhyanathan, B.; Ganguli, M.; Ramakrishnan, P. A. Synthesis of Inorganic Solids Using Microwaves. *Chem. Mater.* 1999, 11 (4), 882–895. <https://doi.org/10.1021/cm9803859>.
- (4) Muley, P. D.; Wang, Y.; Hu, J.; Shekhawat, D. Microwave-Assisted Heterogeneous Catalysis. In *Catalysis*; Spivey, J., Han, Y.-F., Shekhawat, D., Eds.; Royal Society of Chemistry: Cambridge, 2021; Vol. 33, pp 1–37. <https://doi.org/10.1039/9781839163128-00001>.
- (5) Bai, X.; Muley, P. D.; Musho, T.; Abdelsayed, V.; Robinson, B.; Caiola, A.; Shekhawat, D.; Jiang, C.; Hu, J. A Combined Experimental and Modeling Study of Microwave-Assisted Methane Dehydroaromatization Process. *Chemical Engineering Journal* 2022, 433, 134445. <https://doi.org/10.1016/j.cej.2021.134445>.
- (6) Egorov, S. V.; Ereemeev, A. G.; Plotnikov, I. V.; Semenov, V. E.; Sorokin, A. A.; Zharova, N. A.; Bykov, Y. V. Edge Effect in Microwave Heating of Conductive Plates. *J. Phys. D: Appl. Phys.* 2006, 39 (14), 3036–3041. <https://doi.org/10.1088/0022-3727/39/14/024>.
- (7) Jie, X.; Chen, R.; Biddle, T.; Slocombe, D. R.; Dilworth, J. R.; Xiao, T.; Edwards, P. P. Size-Dependent Microwave Heating and Catalytic Activity of Fine Iron Particles in the Deep Dehydrogenation of Hexadecane. *Chem. Mater.* 2022, 34 (10), 4682–4693. <https://doi.org/10.1021/acs.chemmater.2c00630>.
- (10) Will, H.; Scholz, P.; Ondruschka, B. Heterogeneous Gas-Phase Catalysis Under Microwave Irradiation—a New Multi-Mode Microwave Applicator. *Topics in Catalysis* 2004, 29 (3/4), 175–182. <https://doi.org/10.1023/B:TOCA.0000029800.57024.7d>.
- (11) Mishra, R. R.; Sharma, A. K. Microwave–Material Interaction Phenomena: Heating Mechanisms, Challenges and Opportunities in Material Processing. *Composites Part A: Applied Science and Manufacturing* 2016, 81, 78–97. <https://doi.org/10.1016/j.compositesa.2015.10.035>.
- (12) Microwaves - Theory. In *Microwaves and Metals*; John Wiley & Sons (Asia) Pte Ltd: Singapore, 2011; pp 25–41. <https://doi.org/10.1002/9780470822746.ch2>.
- (13) Buchelnikov, V. D.; Louzguine-Luzgin, D. V.; Xie, G.; Li, S.; Yoshikawa, N.; Sato, M.; Anzulevich, A. P.; Bychkov, I. V.; Inoue, A. Heating of Metallic Powders by Microwaves: Experiment and Theory. *Journal of Applied Physics* 2008, 104 (11), 113505. <https://doi.org/10.1063/1.3009677>.
- (14) Jie, X.; Wang, J.; Gonzalez-Cortes, S.; Yao, B.; Li, W.; Gao, Y.; Dilworth, J. R.; Xiao, T.; Edwards, P. P. Catalytic Activity of Various Carbons during the Microwave-Initiated Deep Dehydrogenation of Hexadecane. *JACS Au* 2021, 1 (11), 2021–2032. <https://doi.org/10.1021/jacsau.1c00326>.
- (15) Sun, J.; Wang, W.; Yue, Q.; Ma, C.; Zhang, J.; Zhao, X.; Song, Z. Review on Microwave–Metal Discharges and Their Applications in Energy and Industrial Processes. *Applied Energy* 2016, 175, 141–157. <https://doi.org/10.1016/j.apenergy.2016.04.091>.
- (16) Microwave Heating of Metal-Based Materials. In *Microwaves and Metals*; John Wiley & Sons (Asia) Pte Ltd: Singapore, 2011; pp 65–157. <https://doi.org/10.1002/9780470822746.ch4>.

- (17) Brown, S. W.; Robinson, B.; Wang, Y.; Wildfire, C.; Hu, J. Microwave Heated Chemical Looping Ammonia Synthesis over Fe and CoMo Particles. *J. Mater. Chem. A* **2022**, 10.1039/D2TA03241D. <https://doi.org/10.1039/D2TA03241D>.
- (18) Kulkarni, S. R.; Velisoju, V. K.; Tavares, F.; Dikhtiarenko, A.; Gascon, J.; Castaño, P. Silicon Carbide in Catalysis: From Inert Bed Filler to Catalytic Support and Multifunctional Material. *Catalysis Reviews* **2022**, 1–64. <https://doi.org/10.1080/01614940.2022.2025670>.
- (19) Sugawara, H.; Kashimura, K.; Hayashi, M.; Ishihara, S.; Mitani, T.; Shinohara, N. Behavior of Microwave-Heated Silicon Carbide Particles at Frequencies of 2.0–13.5 GHz. *Appl. Phys. Lett.* **2014**, 105 (3), 034103. <https://doi.org/10.1063/1.4890849>.
- (20) Tempke, R.; Wildfire, C.; Shekhawat, D.; Musho, T. Dielectric Measurement of Powdery Materials Using a Coaxial Transmission Line. *IET Science, Measurement & Technology* **2020**, 14 (10), 972–978. <https://doi.org/10.1049/iet-smt.2020.0055>.
- (21) Dube, D. C. Study of Landau-Lifshitz-Looyenga's Formula for Dielectric Correlation between Powder and Bulk. *J. Phys. D: Appl. Phys.* **1970**, 3 (11), 1648–1652. <https://doi.org/10.1088/0022-3727/3/11/313>.
- (22) Booske, J. H.; Cooper, R. F.; Freeman, S. A.; Rybakov, K. I.; Semenov, V. E. Microwave Ponderomotive Forces in Solid-State Ionic Plasmas. *Physics of Plasmas* **1998**, 5 (5), 1664–1670. <https://doi.org/10.1063/1.872835>.
- (23) AlShibane, I.; Daisley, A.; Hargreaves, J. S. J.; Hector, A. L.; Laassiri, S.; Rico, J. L.; Smith, R. I. The Role of Composition for Cobalt Molybdenum Carbide in Ammonia Synthesis. *ACS Sustainable Chem. Eng.* **2017**, 5 (10), 9214–9222. <https://doi.org/10.1021/acssuschemeng.7b02168>.
- (24) Hargreaves, J. S. J.; McKay, D. A Comparison of the Reactivity of Lattice Nitrogen in $\text{Co}_3\text{Mo}_3\text{N}$ and $\text{Ni}_2\text{Mo}_3\text{N}$ Catalysts. *Journal of Molecular Catalysis A: Chemical* **2009**, 305 (1–2), 125–129. <https://doi.org/10.1016/j.molcata.2008.08.006>.
- (25) Adamski, P.; Moszyński, D.; Komorowska, A.; Nadziejko, M.; Sarnecki, A.; Albrecht, A. Ammonolysis of Cobalt Molybdenum Oxides - In Situ XRD Study. *Inorg. Chem.* **2018**, 57 (16), 9844–9850. <https://doi.org/10.1021/acs.inorgchem.8b00685>.
- (26) Balluffi, R. W. Grain Boundary Diffusion Mechanisms in Metals. *METALLURGICAL TRANSACTIONS B* **27**.
- (27) Brown, S. W.; Jiang, C.; Wang, Q.; Caiola, A.; Hu, J. Evidence of Ammonia Synthesis by Bulk Diffusion in Cobalt Molybdenum Particles in a CLAS Process. *Catalysis Communications* **2022**, 167, 106438. <https://doi.org/10.1016/j.catcom.2022.106438>.
- (28) Exner, H. E. SINTERING PROCESSES. *Sintering processes* **36**.
- (29) Michalsky, R.; Pfromm, P. H. An Ionicity Rationale to Design Solid Phase Metal Nitride Reactants for Solar Ammonia Production. *J. Phys. Chem. C* **2012**, 116 (44), 23243–23251. <https://doi.org/10.1021/jp307382r>.
- (30) Maissel, L. I.; Glang, R. *The Handbook of Thin Film Technology*; McGraw-Hill: New York, 1970.
- (31) Eda, K.; Uno, Y.; Nagai, N.; Sotani, N.; Stanley Whittingham, M. Crystal Structure of Cobalt Molybdate Hydrate $\text{CoMoO}_4 \cdot n\text{H}_2\text{O}$. *Journal of Solid State Chemistry* **2005**, 178 (9), 2791–2797. <https://doi.org/10.1016/j.jssc.2005.06.014>.
- (32) Fan, L.-S. *Chemical Looping Systems for Fossil Energy Conversions*; John Wiley & Sons, Incorporated & AIChE: Hoboken, NJ, USA, 2010.

- (33) Musho, T. D.; Wildfire, C.; Houlihan, N. M.; Sabolsky, E. M.; Shekhawat, D. Study of Cu₂O Particle Morphology on Microwave Field Enhancement. *Materials Chemistry and Physics* **2018**, *216*, 278–284. <https://doi.org/10.1016/j.matchemphys.2018.05.059>.

4. Thermal Kinetics and Thermal Phenomena

4.1 Introduction

To further elucidate the differences between microwave and conventional thermal heated modes, time-on-stream reaction data was further analyzed. The complex gas-surface reactions have been modelled before by Pfromm et al. by using the shrinking core model (SCM) ¹. Additionally, unique features of the nitridation process of the CoMo nitride alloy were discovered and characterized ².

Researchers have shown that under $H_2:N_2$ conditions there is a significant exchange between the lattice nitrogen and gaseous nitrogen ³. While controversial, they propose that ammonia synthesis reaction proceeds by a Mars-van Krevlen type mechanism involving both surface and bulk contributions ^{4,5}. It was observed that ammonia-synthesis-on-nitridation occurred under an atmosphere of pure N_2 gas ². This was observed when a reduced CoMo bimetallic alloy was heated to 750 °C ². To the author's knowledge this phenomenon has not been previously described in the literature, however another group approached it with sequential TPR/TPO studies ⁶.

Chemical looping kinetics represent complex systems of reactions which occur between gas and particles. Whether this is the oxidation or reduction of an oxide or nitride, the basic form of the reaction is the same. In the past, this reaction was modelled with a SCM model, but this has been found to be an inaccurate approach which does not yield correct results. Other workers, such as Ostace et al. have developed other models which can sometimes more accurately predicted the performance of these materials ^{7,8}. Combustion, however, is a mature field – nitrogen storage is not, thus here the SCM was applied, and the limitations of it are identified for future work.

The kinetic insights gained from proper modeling and analysis of chemical reaction rates for CLAS type reactions would also aid in determining the effectiveness of the various promotion schemes identified in Section 2. Various oxides were physically mixed with Mn powder in a 10:1 mass ratio to establish their relative effectiveness. Both reducible and irreducible, at the temperatures of operation, were analyzed. In the now typical process, samples were nitrided under 50 sccm N₂ at 700 °C for 3 h following a purge with 50 sccm to the hydrogenation temperature, 400 °C before the addition of 50 sccm H₂. In Figure 16 both alumina and magnesia are seen to obviously enhance productivity while partially reduced oxides limit the productivity of the sample. These preliminary results show the necessity of model development and kinetic parameter determination.

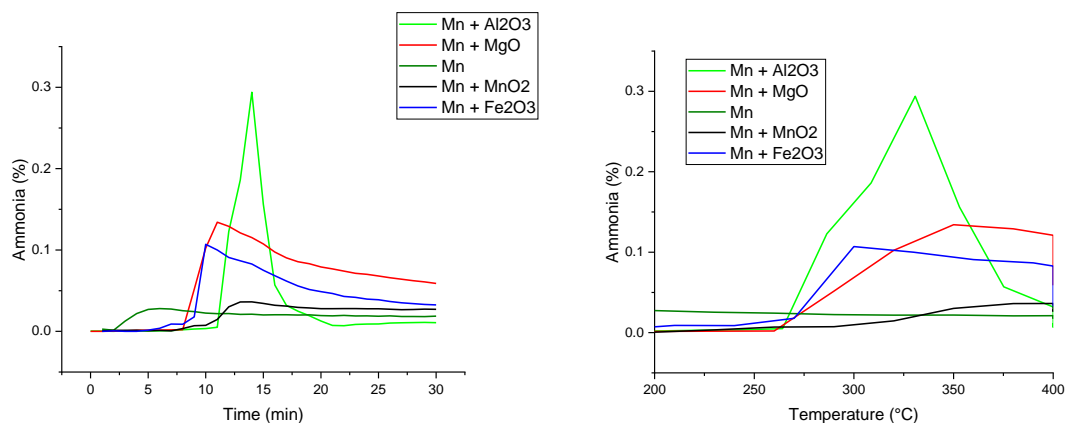


Figure 16. The effect of 10:1 addition of Fe₂O₃, MnO₂, MgO, and Al₂O₃ to Mn in a 10:1 Mn to oxide weight ratio.

4.2 Experimental Methods

4.2.1 Thermal Phenomena and Characterization

Materials were used as received from the manufacturer, Fe (99.9%, <10 μm particle size, Aldrich), Fe nanoparticles (10-30 nm particle size, Thermoscientific), Mn (99.6%, <10 μm particle size, Alfa Aesar), and Mn nanoparticles (30-50 nm particle size, Alfa Aesar). CoMoO_4 (99.9%, ~44 μm particle size, Alfa Aesar) was reduced under 50 sccm H_2 for 180 min at 750 $^\circ\text{C}$ before use in the CLAS process.

Thermal kinetics were performed in a tubular furnace (Lindberg), mass flow controllers, and quartz tube to contain the catalyst. The inlet to the reactor was 0.15875 cm to minimize turbulence and the outlet line was insulated and heated to the UV-Vis inlet. 300 mg of the sample was loaded into quartz reaction tubes (12 mm OD, 8 mm ID, 40.64 cm L) and supported by quartz wool prior to reaction.

Nitridation was performed under 50 sccm N_2 (UHP, Airgas) for 1 h at the respective temperatures from the literature; 450 $^\circ\text{C}$ Fe, and 750 $^\circ\text{C}$ CoMo, and Mn. Reactor temperature was changed under 50 sccm Ar (UHP, Airgas).

Ammonia synthesis reactions were performed under 50 sccm H_2 (UHP, Matheson) for 30 min at the reaction temperature. Ammonia synthesis performance was analyzed with a UV-Vis ammonia analyzer (Applied Analytical, OMA-406R) taking one point every 18 s. The typical time of reaction was limited to the initial reaction kinetics, a time step for hydrogenation was chosen at 15 minutes.

4.2.2 Thermal Phenomena and Characterization

The bimetallic and its constituent oxides were obtained, cobalt (II) molybdenum oxide (CoMoO_4 , 99%, American Elements), molybdenum (IV) oxide (99%, MoO_2 , Alfa Aesar),

molybdenum (VI) oxide (99%, MoO₃, Aldrich), cobalt (II, III) oxide (99.7%, Co₃O₄, Alfa Aesar), molybdenum (0) powder (99%, Mo, Alfa Aesar).

Reactions were performed using a traditional tubular furnace, with powdered catalyst samples loaded into (406.4 mm L, 10 mm ID, 12 mm OD) quartz tubes. Oxide samples were pre-reduced for 3 hours under 50 mLmin⁻¹ H₂, then the system was purged with 50 mLmin⁻¹ Ar for 5 min, and the sample was nitrated under 50 mLmin⁻¹ N₂ for 1 h. This process was operated at 750 °C to obtain the Co₃Mo₃N product. This material was synthesized by the ammonolysis route with 50 mLmin⁻¹ 15% NH₃ balanced in Ar at 750 °C according to Hargreaves et al.

Reactant gases were of ultra-high purity grade (UHP, 99.999%): H₂, N₂, Ar, and 15% NH₃ balanced in Ar were obtained from Airgas, Inc. Outlet gas concentrations were measured by CAI 600 Fourier transform infrared spectrometer (FTIR) with a gas flow cell.

Characterization of the spent materials was performed with Micromeritics Autochem 2950, Physical Electronics PHI 5000 VersaProbe X-ray photoelectron spectrometer (XPS), Hitachi S-4700 scanning electron microscope (SEM), and Renishaw InVia Raman Microscope.

The Raman spectroscopy was performed at 532 nm excitation wavelength, at 5 mW laser power (5% of the Max. 100 mW was adopted) for all samples. Extended wavelength: 100~3200 cm⁻¹; Exposure time =10 s; Accumulation = 2 times.

XPS was performed with monochromatic Al K-alpha X-ray source at 1486.6 eV with 100 um beam size. All XPS measurement were carried out at room temperature at a pressure below 10⁻⁸ Torr. Compositional survey scans were obtained using a pass energy of 117.4 eV and energy step

of 0.5 eV. High-resolution detailed scans of each element were acquired using a pass energy of 23.5 eV and energy step of 0.1 eV.

4.3 Thermal Kinetic Results and Discussion

To determine kinetic parameters of the chemical looping ammonia synthesis reaction, time on stream experiments were performed for Fe, Mn, and CoMo particles. Ammonia synthesis was performed at various hydrogenation temperatures to determine reaction rates and apparent activation energies assuming a first order reaction. Additional time on stream experiments were performed with varying particle sizes and with varying flow rates to determine mass transfer effects on the ammonia synthesis reaction rate.

Typically, chemical looping reactions are considered in a SCM for particles of unchanging size^{1,9}. Applying the SCM framework allows the determination of limiting regimes, gas diffusion, surface reaction, and bulk diffusion, in lieu of more detailed elementary step analysis. However, the literature on the hydrogenation of nitrides also suffers from a lack of repeated time on stream studies, instead relying on pH metering during extended reaction times^{1,9,10}. The SCM kinetics were used to determine the apparent activation energies, ($E_{a,app}$), of the Fe process, 13 kJmol⁻¹ in Figure 17. The simple Arrhenius formulation of the activation energy is used for the SCM kinetics to determine the approximate activation energies of these reactions. The specialized activation energy models for diffusion limited processes were not considered because the kinetic model was not optimized globally, rather it was fit to the local reaction conditions, thus the apparent activation energy is used.

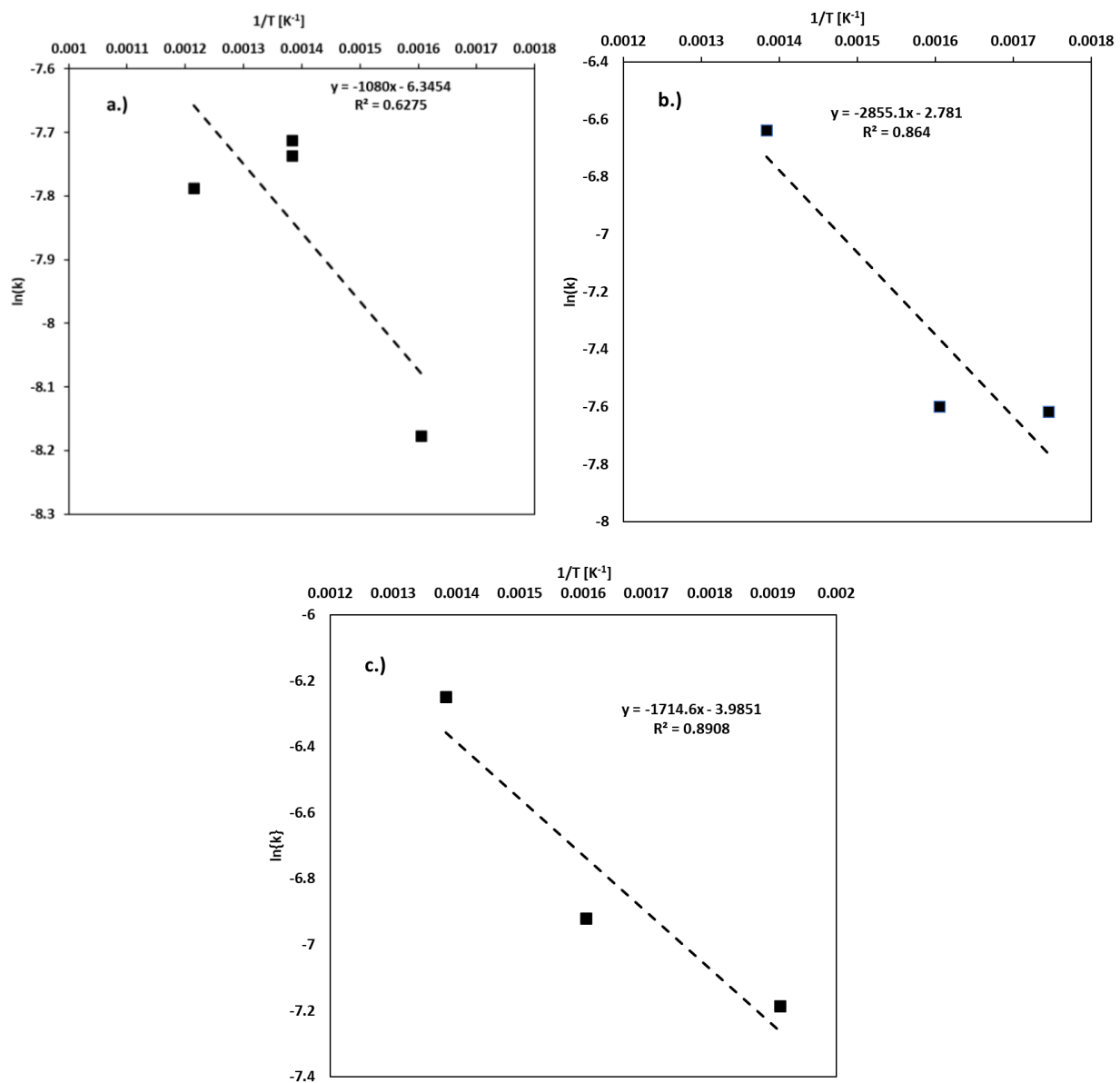
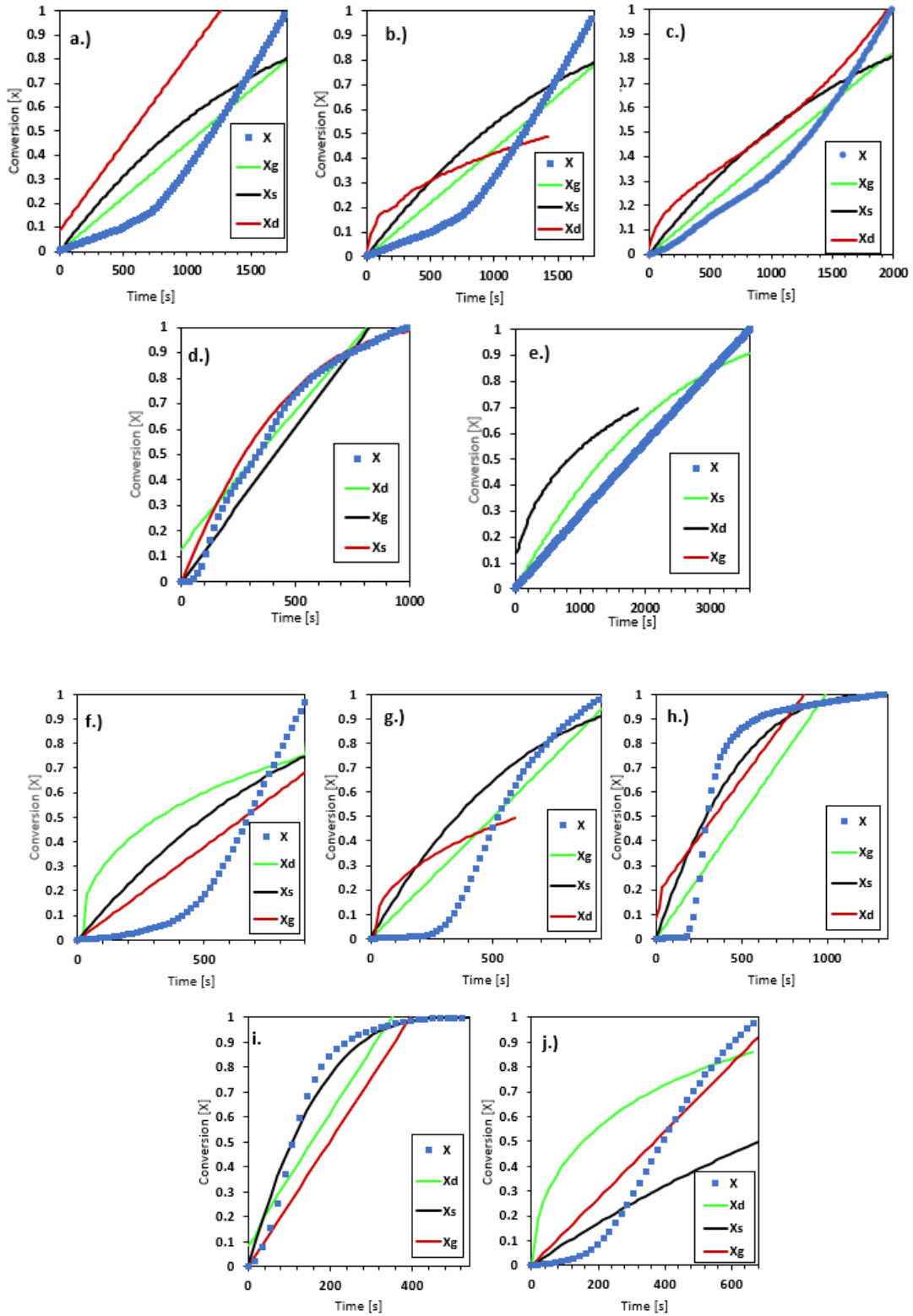


Figure 17. Shrinking core model activation energy. Apparent activation energies were calculated by using the Arrhenius plot method for each catalyst treated thermally, a.) CoMo, b.) Mn, c.) Fe.



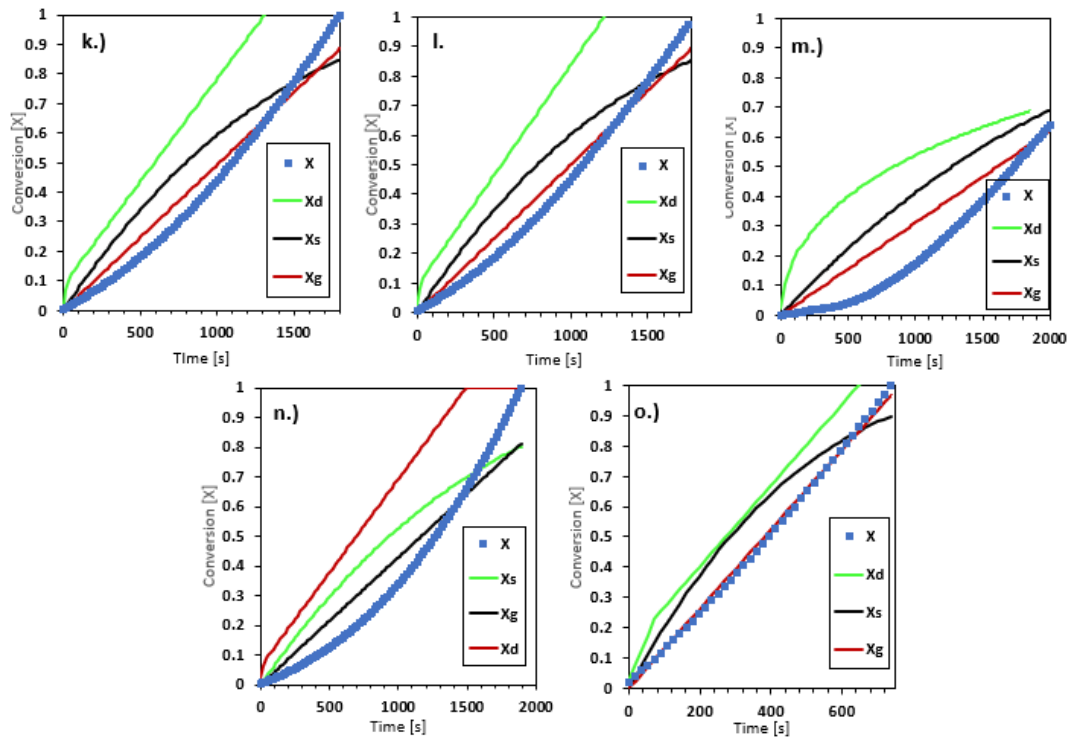


Figure 18. Shrinking core best fit models. Representative kinetics of the ammonia synthesis process over thermally nitrated particles. CoMo a.) 450 °C 25 sccm, b.) 450 °C 100 sccm, c.) 550 °C, d.) 450 °C, e.) 350 °C. Fe, f.) 250 °C, g.) 350 °C, h.) 400 °C, i.) 450 °C, j.) 500 °C. Mn k.) 300 °C, l.) 350 °C, m.) 450 °C, n.) 500 °C, o.) 450 °C 100 sccm (all flows are 50 sccm unless noted).

Ammonia synthesis kinetics for thermal only hydrogenation reactions of CoMo, Mn, and Fe samples are presented in Table 2, and the SCM best fit curves for time on stream results are in Figure 18 (a, b, c, d, e, for CoMo, f, g, h, I, j, for Fe, and k, l, m, n, o, for Mn).

Shrinking core equations were used to analyze the thermal fixed bed kinetics of Mn, Fe, and CoMo as chemical looping ammonia synthesis materials ^{1,9}. These equations fit three different rate determining steps in a gas-solid reaction of unchanging volume, Equation 14, the gas diffusion limit, Equation 15, the bulk diffusion limit, and Equation 16, the surface reaction limit. Where t is the time in s, k is the rate constant in s^{-1} , and X is the conversion. The SCM was

solved individually for each reaction condition while changing temperature and flow. There are two approaches to the solution of the SCM for reactions of this type, individual solutions, which result in weaker data, but potentially better local fits and globally optimized solutions which result in more coherent kinetic results but are more difficult to fit and require more data trimming to achieve.

Equation 14: $tk_{gas} = X_{NH_3}$

Equation 15: $tk_{bulk} = 1 - 3(1 - X_{NH_3})^{\frac{2}{3}} + 2(1 - X_{NH_3})$

Equation 16: $tk_{surface} = 1 - (1 - X_{NH_3})^{\frac{1}{3}}$

The produced results may be compared with similar studies published elsewhere, CoMo, Fe and Mn for instance were found to have initial rates between: $\sim 98 \mu\text{molh}^{-1}\text{g}^{-1}$ (400 °C, 1/3 Ar/H₂, 60 mLmin⁻¹, 0.4 g), $\sim 50 \mu\text{molh}^{-1}\text{g}^{-1}$ (400 °C, 1/3 Ar/H₂, 60 mLmin⁻¹, 0.3 g), $\sim 635 \mu\text{molh}^{-1}\text{g}^{-1}$ (500 °C, H₂O, 0.1 mLmin⁻¹, 0.5 g), respectively ^{1,10,11}.

Many of the lines of best fit suggest that multiple reaction schemes may be controlling, but lacking fundamental information on the reaction, we instead rely on the SCM. The model selected is the one which best fits the reaction. Future work is intended to address the issues in the SCM fit by using alternate model developed for chemical looping combustion. The results of the SCM fitting are and other kinetic parameters are included in Table 5.

Table 5. Thermal-only fixed bed kinetics determined by the shrinking core reaction model for spheres of constant volume*.

Material	Rate [$\mu\text{mol g}^{-1}\text{min}^{-1}$]	Temperature [°C]	k [s ⁻¹]	Rate Limiting Step	Flow rate [sccm]	Time on stream [min]	R ²
CoMo	45.6	350	2.8×10^{-4}	Gas	50	60	0.9998
	62.4	450	4.47×10^{-4}	Gas	25	15	0.9387
	31.2	450	1.21×10^{-3}	Surface	50	16.5	0.9950
	180.0	450	4.37×10^{-4}	Gas	100	30	0.9321
	66.7	550	4.15×10^{-4}	Gas	50	33	0.9821
Mn	64.4	300	4.92×10^{-4}	Gas \ddagger	50	30	0.9839
	41.1	350	5.01×10^{-4}	Gas \ddagger	50	30	0.9871
	191.3	450	3.10×10^{-4}	Gas \ddagger	50	44.1	0.9559
	261.9	450	2.56×10^{-4}	Gas \ddagger	25	60	0.9935
	211.3	450	1.31×10^{-3}	Gas \ddagger	100	12.3	0.9977
	306.1	500	4.29×10^{-4}	Gas	50	31.4	0.9603
	29.1	350	1.99×10^{-3}	Gas	50	9	0.9865
Mn np	689.1	450	1.93×10^{-4}	Gas \ddagger	50	60.3	0.8952
	312.9	250	7.57×10^{-4}	Gas	50	15.3	0.8614
Fe	606	350	9.88×10^{-4}	Gas	50	16.2	0.9512
	362.2	400	7.09×10^{-4}	Surface	50	22.2	0.9222
	61.9	450	4.81×10^{-4}	Gas	25	28.2	0.9494
	588.7	450	1.93×10^{-3}	Surface	50	9	0.9804
	388	550	3.02×10^{-4}	Gas	50	11.4	0.9678
Fe np	100	250	3.24×10^{-4}	Gas	50	47.4	0.9812

110.7	350	7.13×10^{-4}	Gas	50	18.6	0.9376
92.7	450	4.79×10^{-4}	Gas	50	35.1	0.9923
187.3	550	4.79×10^{-4}	Gas	50	69	0.9479

*Shrinking core conversions (X) determined by maximum conversion after integration of the concentration across time on stream data.

‡The model selected had the highest R^2 value but, the other rate determining steps, bulk diffusion and surface reaction were also found to be highly significant.

4.4 Nitridation of CoMo Alloys

The typical synthesis of $\text{Co}_3\text{Mo}_3\text{N}$ begins with the stoichiometric combination of $\text{Co}(\text{NO}_3)_2$ and $(\text{NH}_4)_6\text{Mo}_7\text{O}_{24}$. The metal salts are dissolved in solution with deionized water and heated, the resulting precipitate is dried overnight following by calcination to form a deep purple powder at 700 °C for several hours¹². The result is the oxide precursor, CoMoO_4 , is reduced by H_2 and then nitrided by N_2 , a mixture of H_2 and N_2 , or directly ammonolyzed by pure NH_3 at 700 °C depending on the preferred synthesis method^{12,13}. The resulting $\text{Co}_3\text{Mo}_3\text{N}$ powder is then sometimes passivated with dilute oxygen to protect it from oxidation when exposed to the atmosphere⁶.

A recent study has remarked on surface activation with varying compositions of H_2 and N_2 gas. Previous studies have mentioned that pre-activation with H_2/N_2 is necessary for increased productivity, there has not been any significant research into the related phenomena leading to surface enhancement effects observed¹⁴. During our previous research on CLAS materials it was found that when synthesizing $\text{Co}_3\text{Mo}_3\text{N}$ by pre-reduction with H_2 followed by nitridation by N_2 , on the initial nitridation step, ammonia synthesis was observed in the absence of gaseous H_2 .

This ammonia-synthesis-on-nitridation step effect was unexpected, the system was usually cooled to 25 °C and purged with inert gas between reaction steps, removing reactive gases.

4.4.1 Time on Stream Nitridation Experiments

To determine whether the ammonia-synthesis-on-nitridation effect was limited to the CoMoO₄ alloy or if it was present in either Co or Mo systems each was tested independently. Samples of powdered Mo, MoO₂, MoO₃, Co₃O₄ and CoMoO₄ were all subjected to identical conditions.

The results presented in Figure 19 indicate that ammonia formation is likely related to MoO₃ within the CoMoO₄ bimetallic under nitriding conditions. Mo metal appears to have a weak propensity towards ammonia-synthesis-on-nitridation, but it is suspected this is due to oxidation of the Mo metal surface in air. MoO₂ and Co₃O₄ were not found to have any ammonia synthesis activity under H₂ at 700 °C followed by N₂ at 700 °C. This led to the conclusion that MoO₃ hydroxides must be involved in the observed phenomena.

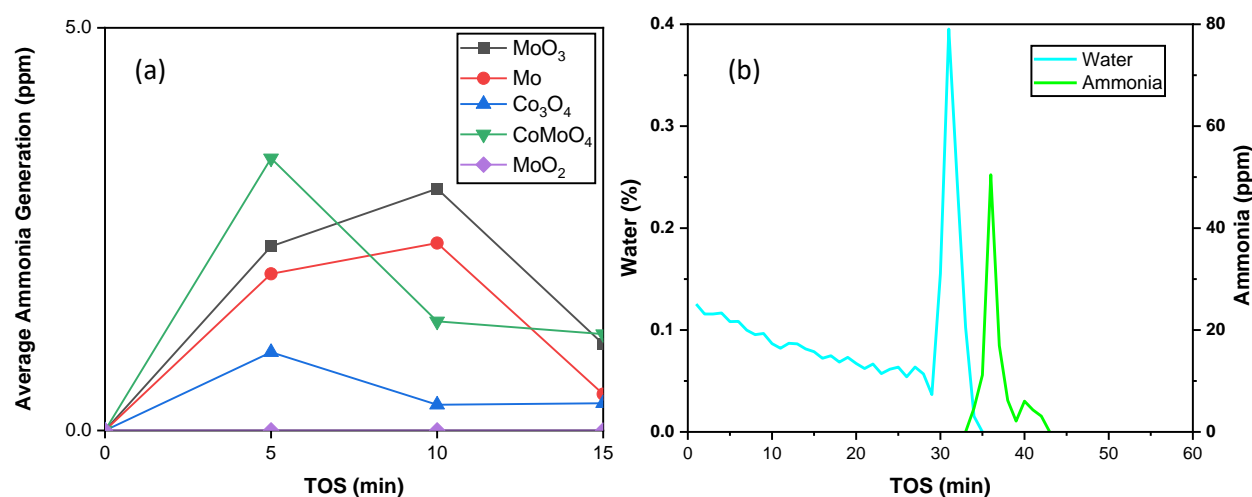


Figure 19. CoMo nitridation time on stream. The time on stream results of the pre-reduced 500 mg samples of CoMoO₄, MoO₃, and Mo and their relative ammonia productivity on nitridation by N₂ (a) and the typical result of CoMo nitridation H₂O and NH₃ (b).

Hada et. al. report TPR profiles for H₂, H₂O and N₂ treatment of CoMo¹⁵. Under an NH₃ atmosphere, water was observed leaving the system broadly at 477°C and 627°C¹². In the chemical looping reaction, reduction by H₂ is followed by nitridation by N₂, therefore the chemical changes in the particles are potentially easier to observe¹⁶. It is suspected that there exists a shrinking unreacted core as the TPR profiles indicate that the operating temperature is above the reduction temperature.

4.4.2 Characterization of CoMo Particles

To understand both the surface and bulk chemical phenomena observed, XPS, H₂-TPD, SEM, and Raman spectroscopy were performed on fresh oxide, reduced, nitrided and spent particles.

Scanning electron microscopy indicated very limited morphological changes in the particles between, fresh oxide, nitride and spent states (Figure 20 (a) and (b)). Likewise, H₂-TPD of the reduced surface showed negligible H₂ adsorption on the reduced surface.

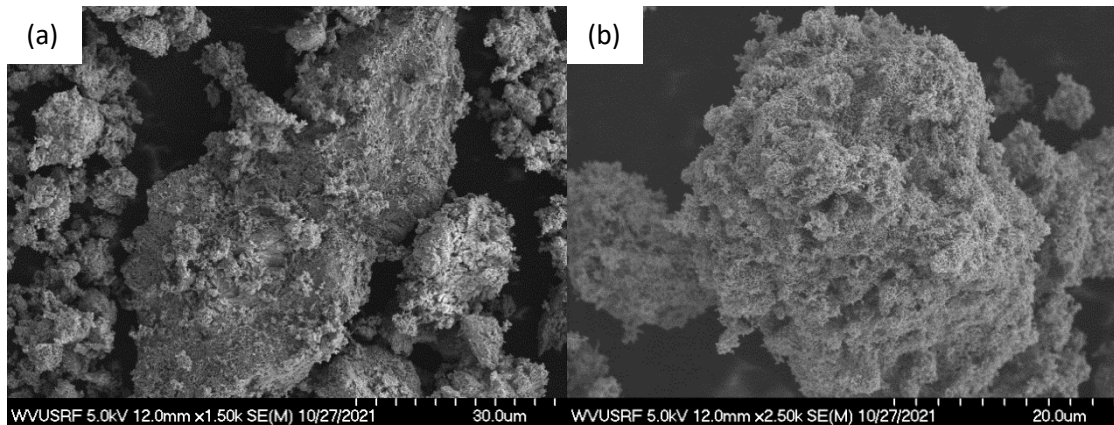


Figure 20. Micrography of CoMo particles. Scanning electron micrographs of (a) fresh CoMoO_4 , and (b) $\text{Co}_3\text{Mo}_3\text{N}$ as synthesized.

XPS and Raman were used to gather information on the surface chemistry of the CoMo particles (Figures 21 and 22).

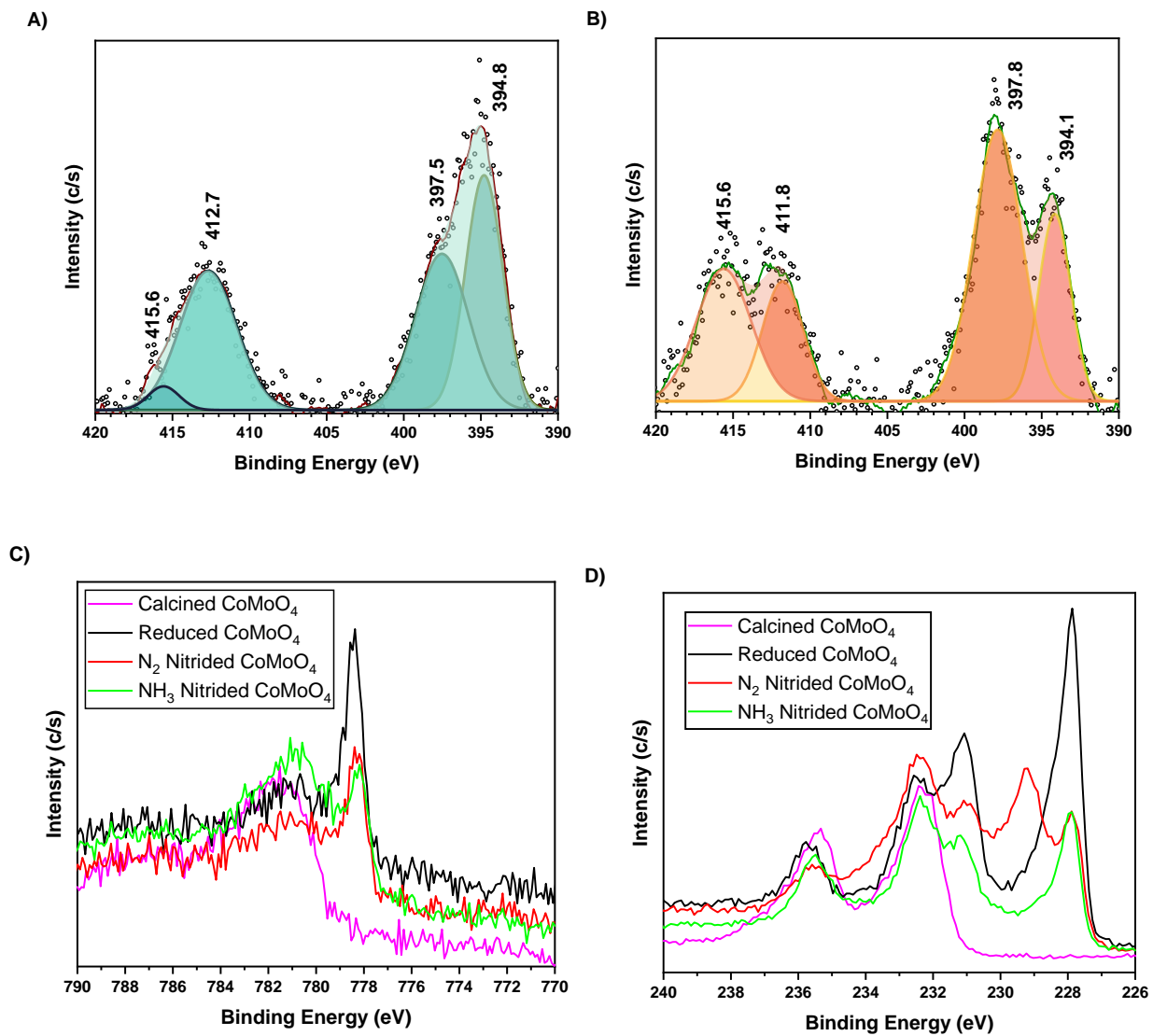


Figure 21. XPS results for CoMo samples. The spectra collected for (A) N_2 nitrided and (B) 15% NH_3 balanced in Ar, nitrided Mo 3p peaks (C) Co 2p peaks, (D) Mo 3d peaks.

The spectroscopy collected for calcined, reduced and nitrated (H_2/N_2 and NH_3 routes) are presented in Figure 20. Inspection of the Mo peaks is useful for understanding the degree of nitridation of the surface of the particles. Mo 3p (394 eV) peaks overlap with the N 1s (397 eV) peaks and required deconvolution. Nitridation with N_2 (Figure 21 (A)) results in relatively more nitrogen in surface as compared with nitridation with 15% ammonia (Figure 21 (B)).

Time on stream results and theory suggests that the rate determining step of particle nitridation is the partial pressure of nitrogen. Nitride formation then is enhanced with higher partial pressure nitrogen, in pure N_2 this leads to higher bulk nitrogen content despite a less “active” nitrogen source ¹⁷.

Following Mo, Co results present a similar phenomenon. The Co 2p peaks are compared amongst the calcined, H_2 reduced, and both nitrated samples. Co^0 (777 eV) peaks can be observed most strongly in the H_2 reduced sample, while the intensity of the NH_3 and N_2 nitrated samples are somewhat reduced due to oxidation by N_2 . Oxidized Co 2p can be observed as Co^{3+} (781 eV) and Co^{2+} (779 eV), a trend then exists with the nitrated samples having less Co^0 and increased Co^{3+} in the case of the NH_3 treated sample.

The collected Mo 3d peaks present the triplet associated with the chemical states of Mo^0 , Mo^{4+} , and Mo^{6+} (Figure 21 (D)). The calcined sample is the exception, only the Mo^{6+} peak is present associated with the higher oxidation state, MoO_3 present in the bimetallic. The same oxidation state trend may be observed for the Co 2p.

Metallic Mo^0 (228 eV) is increased after H_2 reduction, the N_2 nitrated system shows the existence of the Mo^{5+} (229 eV) and Mo^{6+} (233 eV) oxidation states ¹⁶. Mo^{5+} likely represents an oxynitride, while Mo^{6+} is representative of the presence of the fully oxidized MoO_3 ¹⁸. The

relative red-shifting observed in the nitrated samples is representative of the uptake and oxidation by nitrogen.

Raman spectroscopy was used to determine the bulk oxidation states of the particles (Figure 20).

Coupled with XPS, Raman is used to resolve both the surface and bulk chemistry occurring during the nitridation of reduced CoMo particles.

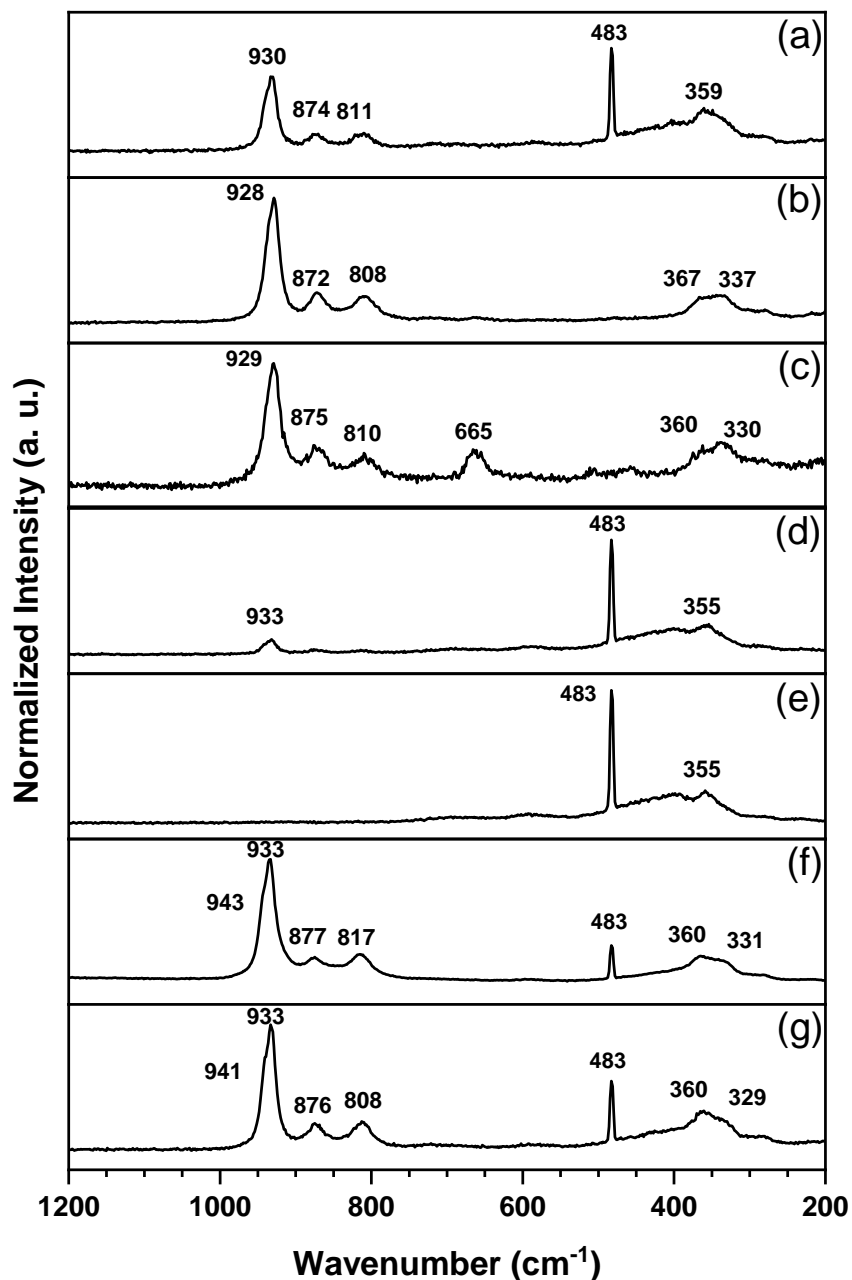


Figure 22. Raman spectroscopy of CoMo. Results for CoMo samples treated at each step of the cycle: (a) 15 h 15% NH₃ balanced in Ar ammonolyzed sample, (b) 5 h 15% NH₃ balanced in Ar ammonolyzed sample, (c) 3 h 15% NH₃ balanced in Ar ammonolyzed sample, (d) 3 h N₂ nitrated sample, (e) 3 h H₂ reduced sample, (f) 5 h 250 °C calcined sample, (g) fresh hydrate sample.

Bulk oxidation state changes can be observed in the Raman results between fresh CoMo, calcined CoMo, reduced CoMo, and the various nitrated samples. Between the fresh (Figure 22 (g)) and the samples calcined at 250 °C for 5 h (Figure 22 (f)), the peak attributable to Co and its hydroxide at 483 cm⁻¹ is observed to reduce in intensity and the spectrum is clearer¹⁹.

The 3 h H₂ reduction yields a spectrum where the oxide peaks related to MoO₃ and Co oxides at 943, 933, 877, 817 cm⁻¹ are no longer present (Figure 21 (i))^{20,21}. However, on 3 h N₂ nitridation (Figure 22 (d)) the 933 cm⁻¹ is observed to return, indicating an increased oxidation state and the possible presence of MoO₃ in the bulk structure.

The range between 330-370 cm⁻¹ is associated with Mo oxide and Mo hydroxide^{20,22,23}. The peak observed in (Figure 22 (i)) at 665 cm⁻¹ is likely attributable to the Co-Mo-O symmetric stretch reported at 698 cm⁻¹, indicating partial oxidation, likely shifted by the partial formation of oxynitride species and crystal structure changes²⁴.

The samples treated in 15% NH₃ atmosphere (Figure 22 (a, b, c)) show the presence of various oxidation states at long treatment times despite a more aggressive nitriding agent. This is attributable to the slowly reacting core, where when interpolating from the XPS the shell is more fully nitrated by NH₃ but at less depth. This reinforces the confirmation of partial pressure of N as the driving force of nitridation in the bulk, but not the surface scale.

The proposed mechanism in Figure 20 describes the reaction explaining the observation of both ammonia and water synthesis occurring in a reduced CoMo bimetallic with no gaseous H_2 present. It is suspected that the particle follows the shrinking core model of non-catalytic reacting gas-solid reacting particles originally published by Wen ²⁵. This approximation does not entirely hold, as the Co_3Mo_3N surface is known to be an active catalyst for ammonia synthesis, however at this level of consideration the model is appropriate and suggests the existence of an unreduced, or partially reduced core.

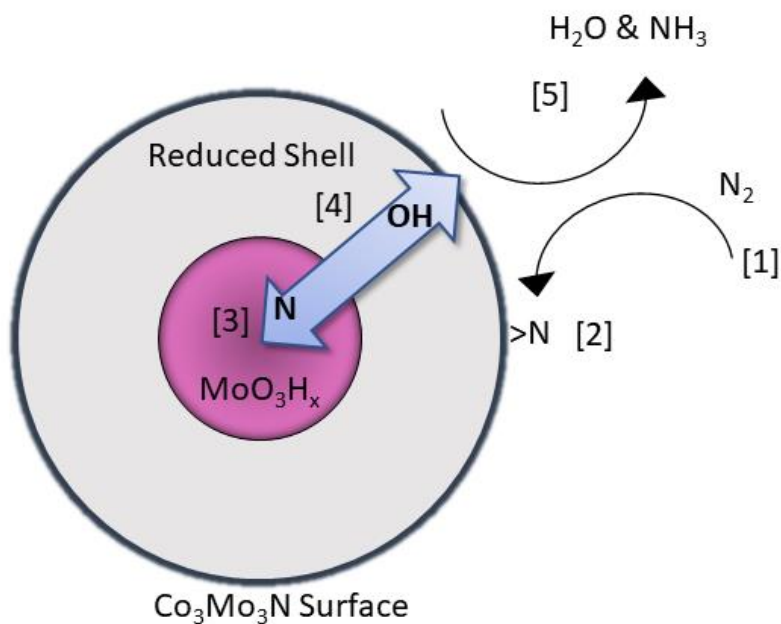


Figure 23. Proposed Co_3Mo_3N mechanism. Schematic representing the dynamic surface and unreduced core.

The mechanism of reaction in the nitridation model are: (1) dinitrogen dissociates at the surface and diffuses inward (Figure 23 (1)). In step two, the nitrogen begins to diffuse into the particle and a nitrided shell forms (Figure 23 (2)). Then in step three atomic nitrogen continues to diffuse inward, the crystal structure stabilizes, lose oxygen, and forms a nitride compound (Figure 23 (3)).

Based on the literature and the indirect observations, it is speculated that molybdenum bronzes, H_xMoO_3 , play a role in this rearrangement process ²⁶. In step four the hydrogen and oxygen begin to diffuse out as the Mo is oxidized by nitrogen (Figure 23 (4)). Finally, in step five the hydroxyl group reach the surface where they encounter nitrogen species, recombine, and diffuse away as both ammonia and water (Figure 23 (5)). It is likely that this phase transformation requires nitrogen in the bulk to facilitate the final loss of oxygen from the lattice. This atomic diffusion likely requires the catalytic surface at the gas interface to complete the reduction to water and ammonia before diffusing away.

In-situ XRD of $CoMoO_4$ ammonolysis and calcination has been performed in the past however the literature lacks consecutive, H_2 reduction, N_2 nitridation treatment studies as would be commonly encountered in CLAS processes.

4.5 Conclusions

This work has analyzed thermal SCM kinetics of ammonia synthesis by hydrogenation of nitrides, and the synthesis of ammonia on the nitridation of a partially reduced metal nitrogen carrier.

The SCM is a common model encountered in undergraduate chemical engineering and can be fit to fluid-solid reactions. The models developed indicate that the resistances, specifically the gas and surfaces resistances at first, followed by the bulk resistance are the limiting steps. It is difficult to establish which step is rate limiting, but upon repeated experiments trends become apparent for the typical particle reaction. The limitations of this model have been established by other researchers and are present in the results above.

It is believed that this is the first time that this ammonia-synthesis-on-nitridation effect has been reported for CoMo bimetallics. To summarize, ammonia synthesis was observed on the nitridation step under atmosphere of pure N₂ gas, to determine the nature of this effect we performed XPS to explore surface chemistry, time on stream testing and Raman spectroscopy to determine the bulk chemistry. It is believed that an understanding of the phase changes, reaction dynamics, and surface chemistry within CLAS processes will lead to more insight in future particle development and process scale-up.

This ammonia-synthesis-on-nitridation reaction proved to be an unexpected finding, and one not remarked upon before in the literature. This led to the question of where the hydrogen in the system was coming from, whether a hydride or an OH group. There are parallels in the research on metal hydride and imide CLAS materials, as well as the use of metal oxides to increase nitridation rates in Al and Mg systems²⁷. It is also known that the inclusion of H₂ or water may enhance Mo nitridation process²⁸. Some of the transient ammonia concentrations were found to be larger than those found under pure H₂, lending some motivation to this study.

Future research directions of interest include the development of more advanced models to represent the reduction of nitride particles and the use of and inclusion of stable oxides, and Brønsted acid sites to enhance ammonia productivity and lower attrition rates.

4.6 References

- (1) Michalsky, R.; Pfromm, P. H. An Ionicity Rationale to Design Solid Phase Metal Nitride Reactants for Solar Ammonia Production. *J. Phys. Chem. C* **2012**, *116* (44), 23243–23251. <https://doi.org/10.1021/jp307382r>.
- (2) Brown, S. W.; Jiang, C.; Wang, Q.; Caiola, A.; Hu, J. Evidence of Ammonia Synthesis by Bulk Diffusion in Cobalt Molybdenum Particles in a CLAS Process. *Catalysis Communications* **2022**, *167*, 106438. <https://doi.org/10.1016/j.catcom.2022.106438>.
- (3) Hunter, S. M.; Gregory, D. H.; Hargreaves, J. S. J.; Richard, M.; Duprez, D.; Bion, N. A Study of ¹⁵N/¹⁴N Isotopic Exchange over Cobalt Molybdenum Nitrides. *ACS Catal.* **2013**, *3* (8), 1719–1725. <https://doi.org/10.1021/cs400336z>.
- (4) Zeinalipour-Yazdi, C. D.; Hargreaves, J. S. J.; Catlow, C. R. A. Low-T Mechanisms of Ammonia Synthesis on Co₃Mo₃N. *J. Phys. Chem. C* **2018**, *122* (11), 6078–6082. <https://doi.org/10.1021/acs.jpcc.7b12364>.
- (5) Zeinalipour-Yazdi, C. D.; Hargreaves, J. S. J.; Catlow, C. R. A. Nitrogen Activation in a Mars–van Krevelen Mechanism for Ammonia Synthesis on Co₃Mo₃N. *J. Phys. Chem. C* **2015**, *119* (51), 28368–28376. <https://doi.org/10.1021/acs.jpcc.5b06811>.
- (6) Song, N.; Rhodes, C.; Johnson, D. W.; Hutchings, G. J. Comments on the Characterisation of Oxidation Catalysts Using TPR/TPO. *Catal Lett* **2005**, *102* (3–4), 271–279. <https://doi.org/10.1007/s10562-005-5868-0>.
- (7) Okoli, C. O.; Parker, R.; Chen, Y.; Ostace, A.; Lee, A.; Bhattacharyya, D.; Tong, A.; Biegler, L. T.; Burgard, A. P.; Miller, D. C. Application of an Equation-oriented Framework to Formulate and Estimate Parameters of Chemical Looping Reaction Models. *AIChE Journal* **2022**, *68* (10). <https://doi.org/10.1002/aic.17796>.
- (8) Ostace, A.; Chen, Y.-Y.; Parker, R.; Mebane, D. S.; Okoli, C. O.; Lee, A.; Tong, A.; Fan, L.-S.; Biegler, L. T.; Burgard, A. P.; Miller, D. C.; Bhattacharyya, D. Kinetic Model Development and Bayesian Uncertainty Quantification for the Complete Reduction of Fe-Based Oxygen Carriers with CH₄, CO, and H₂ for Chemical Looping Combustion. *Chemical Engineering Science* **2022**, *252*, 117512. <https://doi.org/10.1016/j.ces.2022.117512>.
- (9) Levenspiel, O. *Chemical Reaction Engineering*, 3rd ed.; Wiley: New York, 1999.
- (10) Alexander, A.-M.; Hargreaves, J. S. J.; Mitchell, C. The Denitridation of Nitrides of Iron, Cobalt and Rhenium Under Hydrogen. *Top Catal* **2013**, *56* (18–20), 1963–1969. <https://doi.org/10.1007/s11244-013-0133-z>.
- (11) Hargreaves, J. S. J.; McKay, D. A Comparison of the Reactivity of Lattice Nitrogen in Co₃Mo₃N and Ni₂Mo₃N Catalysts. *Journal of Molecular Catalysis A: Chemical* **2009**, *305* (1–2), 125–129. <https://doi.org/10.1016/j.molcata.2008.08.006>.
- (12) Kojima, R.; Aika, K. Cobalt Molybdenum Bimetallic Nitride Catalysts for Ammonia Synthesis Part 1. Preparation and Characterization. *Applied Catalysis A: General* **2001**, *215* (1–2), 149–160.
- (13) Kojima, R.; Aika, K. Cobalt Molybdenum Bimetallic Nitride Catalysts for Ammonia Synthesis Part 2. Kinetic Study. **2001**, *8*.
- (14) Aslan, M. Y.; Hargreaves, J.; Uner, D. The Role of H₂:N₂ Ratio on the NH₃ Synthesis Rate and on Process Economics over the Co₃Mo₃N Catalyst. *Faraday Discuss.* **2020**, 10.1039/C9FD00136K. <https://doi.org/10.1039/C9FD00136K>.

- (15) Hada, K.; Nagai, M.; Omi, S. XPS and TPR Studies of Nitrided Molybdena–Alumina. *J. Phys. Chem. B* **2000**, *104* (9), 2090–2098. <https://doi.org/10.1021/jp993631s>.
- (16) Hada, K.; Tanabe, J.; Omi, S.; Nagai, M. Characterization of Cobalt Molybdenum Nitrides for Thiophene HDS by XRD, TEM, and XPS. *Journal of Catalysis* **2002**, *207* (1), 10–22. <https://doi.org/10.1006/jcat.2001.3495>.
- (17) Addemir, O.; Tekin, A.; Gupta, C. K. Nitridation in the Processing and Preparation of Metals and Ceramics. *High Temperature Materials and Processes* **1996**, *15* (4), 273–280. <https://doi.org/10.1515/HTMP.1996.15.4.273>.
- (18) Podila, S.; Zaman, S. F.; Driss, H.; Al-Zahrani, A. A.; Daous, M. A.; Petrov, L. A. High Performance of Bulk Mo_2N and $\text{Co}_3\text{Mo}_3\text{N}$ Catalysts for Hydrogen Production from Ammonia: Role of Citric Acid to Mo Molar Ratio in Preparation of High Surface Area Nitride Catalysts. *International Journal of Hydrogen Energy* **2017**, *42* (12), 8006–8020. <https://doi.org/10.1016/j.ijhydene.2017.01.044>.
- (19) Li, Y.; Qiu, W.; Qin, F.; Fang, H.; Hadjiev, V. G.; Litvinov, D.; Bao, J. Identification of Cobalt Oxides with Raman Scattering and Fourier Transform Infrared Spectroscopy. *J. Phys. Chem. C* **2016**, *120* (8), 4511–4516. <https://doi.org/10.1021/acs.jpcc.5b11185>.
- (20) Yuan, H.; Qiherima; Xu, G.-T.; Li, H.-F.; Lu, L.-J. Study of Oxidic and Sulfided Selective Hydrodesulfurization Catalysts for Gasoline Using Raman Spectroscopy. *Chinese Chemical Letters* **2013**, *24* (12), 1041–1044. <https://doi.org/10.1016/j.cclet.2013.07.009>.
- (21) Villa, P. L.; Trifirb, F.; Pasquon, I. Study of the Interaction between CoMoO_4 and $\gamma\text{-Al}_2\text{O}_3$ by Raman Spectroscopy. *Reaction Kinetics and Catalysis Letters* **1974**, *1* (3), 341–344.
- (22) Seguin, L.; Figlarz, M.; Cavagnat, R.; Lassègues, J.-C. Infrared and Raman Spectra of MoO_3 Molybdenum Trioxides and $\text{MoO}_3 \cdot x\text{H}_2\text{O}$ Molybdenum Trioxide Hydrates. *Spectrochimica Acta Part A: Molecular and Biomolecular Spectroscopy* **1995**, *51* (8), 1323–1344. [https://doi.org/10.1016/0584-8539\(94\)00247-9](https://doi.org/10.1016/0584-8539(94)00247-9).
- (23) Tang, C.-W.; Wang, C.-B.; Chien, S.-H. Characterization of Cobalt Oxides Studied by FT-IR, Raman, TPR and TG-MS. *Thermochimica Acta* **2008**, *473* (1–2), 68–73. <https://doi.org/10.1016/j.tca.2008.04.015>.
- (24) Moura, A. P. de; Oliveira, L. H. de; Pereira, P. F. S.; Rosa, I. L. V.; Li, M. S.; Longo, E.; Varela, J. A. Photoluminescent Properties of CoMoO_4 Nanorods Quickly Synthesized and Annealed in a Domestic Microwave Oven. *ACES* **2012**, *02* (04), 465–473. <https://doi.org/10.4236/aces.2012.24057>.
- (25) Wen, C. Y. NONCATALYTIC HETEROGENEOUS SOLID-FLUID REACTION MODELS. *Ind. Eng. Chem.* **1968**, *60* (9), 34–54. <https://doi.org/10.1021/ie50705a007>.
- (26) Birtill, J. J.; Dickens, P. G. Thermochemistry of Hydrogen Molybdenum Bronze Phases H_xMoO_3 . *Journal of Solid State Chemistry* **1979**, *29* (3), 367–372. [https://doi.org/10.1016/0022-4596\(79\)90193-2](https://doi.org/10.1016/0022-4596(79)90193-2).
- (27) Szabó, Z. G.; Perczel, S.; Gábor, M.; Zsolt, G.; Galwey, A. K. The Role of Magnesia and Alumina in Promoting the Nitridation of Magnesium and Aluminium. *Thermochimica Acta* **1983**, *64* (1–2), 167–178. [https://doi.org/10.1016/0040-6031\(83\)80140-3](https://doi.org/10.1016/0040-6031(83)80140-3).
- (28) Wise, R. S.; Markel, E. J. Synthesis of High Surface Area Molybdenum Nitride in Mixtures of Nitrogen and Hydrogen. *Journal of Catalysis* **1994**, *145* (2), 344–355. <https://doi.org/10.1006/jcat.1994.1043>.

5. Plasma-Catalysis and Pretreatment

5.1 Introduction

Microwave plasma was used to pretreat on Fe particles before ammonia synthesis under non-plasma H₂ gas conditions. Time on stream analysis, plasma characterization, and a kinetic analysis is performed comparing the post-plasma species with a traditional thermal system to develop more fundamental basic insights on nitride-gas phase reactions. Samples of iron were selected because the experiments using Mn and CoMo metals exhibited much slower rates of reaction and required much higher temperatures of operation.

5.2 Methods

5.2.1 Catalyst Materials

Chemical looping ammonia synthesis metals were used as received from the manufacturer, Fe (99.9%, <10 μm particle size, Aldrich).

5.2.2 Thermal Fixed Bed Reactor Experiments

Thermal fixed bed kinetics were performed using a tubular furnace (Lindberg), mass flow controllers, and quartz tube to contain the catalyst. A 0.15875 cm inlet line to the thermal fixed bed reactor was used to minimize turbulence, the outlet line was insulated and heated to the UV-Vis inlet. 300 mg of sample was loaded into quartz reaction tubes (12 mm OD, 8 mm ID, 40.64 cm L) and supported by quartz frit prior to reaction. The typical reaction was performed in the same reactor as the plasma reaction, only without the plasma present (Figure 24 (a)).

Nitridation reactions were performed under 50 sccm N₂ (UHP, Airgas) for 1 h at 450 °C Fe. The system was allowed to change temperature and purge N₂ gas under 50 sccm Ar (UHP, Airgas).

Ammonia synthesis reactions were performed under 50 sccm H₂ (UHP, Matheson) for 30 min at the temperature of consideration. Gas phase detection of ammonia was performed with a UV-Vis ammonia analyzer (Applied Analytical, OMA-406R) collecting concentration data every 18 s.

5.2.3 Plasma Fixed Bed Reactor Experiment

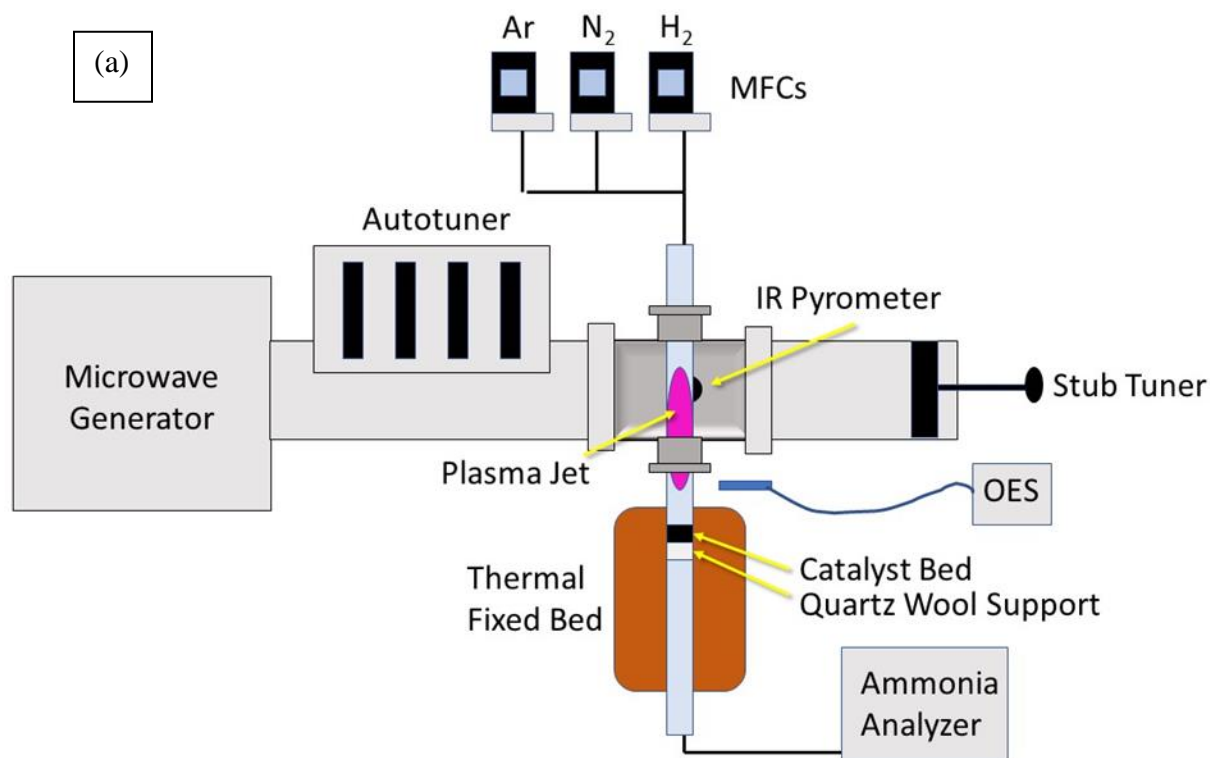
Plasma experiments were performed in the reactor (Figure 24 (a)) with mass flow controllers, and a quartz tube to contain the catalyst materials. 0.15875 cm diameter inlet line to the thermal fixed bed reactor was used to minimize turbulence, the outlet line was insulated and heated to the UV-Vis inlet. 300 mg of sample was loaded into quartz plasma reaction tubes (12 mm OD, 8 mm ID, 61.1 cm L) with a 100-160 μm quartz frit situated 205 mm from the end of the tube, allowing plasma generation above the catalyst which is outside the enclosure of the waveguide choke (Figure 23 (b)).

Plasma-enhanced nitridation was performed under 50 sccm N₂ (UHP, Airgas, Matheson), a tubular furnace (Mellen) controlled the temperature of the catalyst bed which is located outside the waveguide and beyond the plasma plume in the dark zone (Figure 24 (b)). The plasma was removed, and Ar (UHP, Matheson) gas is used to sweep reactive products between steps after the completion of nitridation.

Plasma generation is performed via a 2.54 GHz, 3 kW, fixed frequency microwave (Sairem, GMP20K) with a spark plasma inducer. A quartz tube placed in the waveguide at 300 W power in continuous wave mode, and plasma was ignited with 50 sccm Ar (UHP, Matheson) flow.

Then, 10 sccm N₂ (UHP, Airgas) feed was then introduced into the system with 40 sccm Ar balance. Once the flow normalized, a color change was observed from bright blue to a deeper purple indicating the activation of N₂ gas.

Ammonia synthesis reactions were performed under 50 sccm H₂ (UHP, Hydrogen) gas flow for 15 min at the temperature of consideration. Gas phase detection of ammonia was performed using an online UV-Vis ammonia analyzer (Applied Analytical, OMA-406R) collecting concentration data every 18 s.



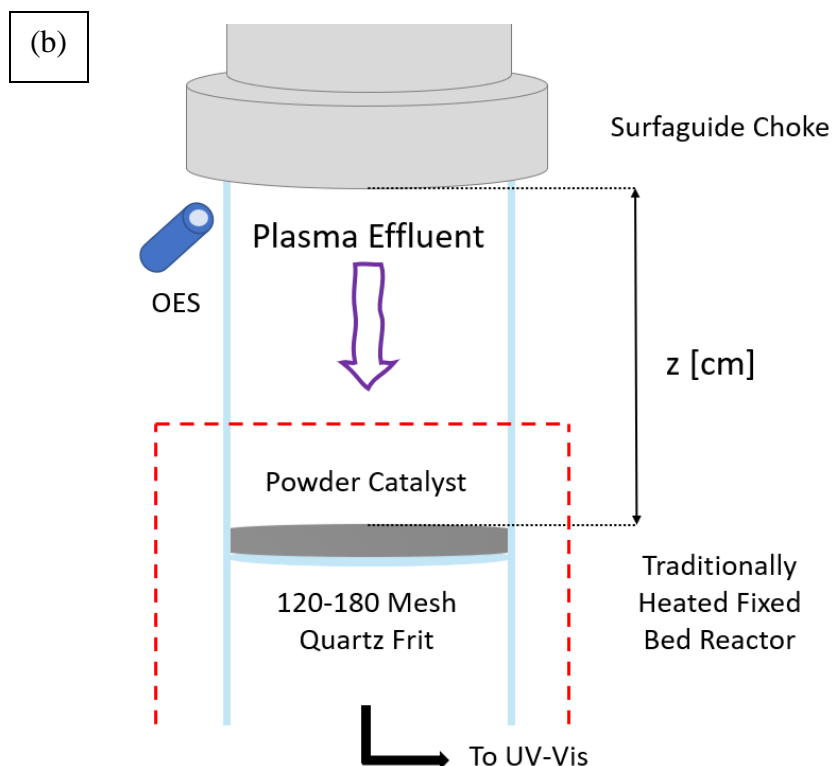


Figure 24. Plasma reactor schematic and reactor outlet. The microwave plasma reactor (a) with OES, catalyst bed, tubular furnace, and ammonia analyzer, the outlet of the reactor (b) with the distance z between the outlet of the waveguide and the catalyst bed.

Optical emission spectroscopy (OES) was used to determine the active species present in the plasma and the electron temperature. Optical emissions of photons occur when molecules and atoms undergo an energy transition change, these photons may be collected, and their respective frequency paired with what is known about the chemistry of the plasma can allow more insight into the reactions occurring. Spectrometry of both Ar and Ar:N₂ plasma was collected at the choke of the waveguide without catalyst present. The spectral range of the OES is 200-1100 nm, with 1 nm FWHM resolution, an optical fiber and USB spectrometer (Ocean Optics, HR2000_ES). OES emission counts were collected every 18 s.

5.3 Results and Discussion

Results from the time-on-stream experiments are presented in several ways, by total integration over 15 min of time on stream by time of plasma treatment, time of plasma treatment, and as raw time on stream data.

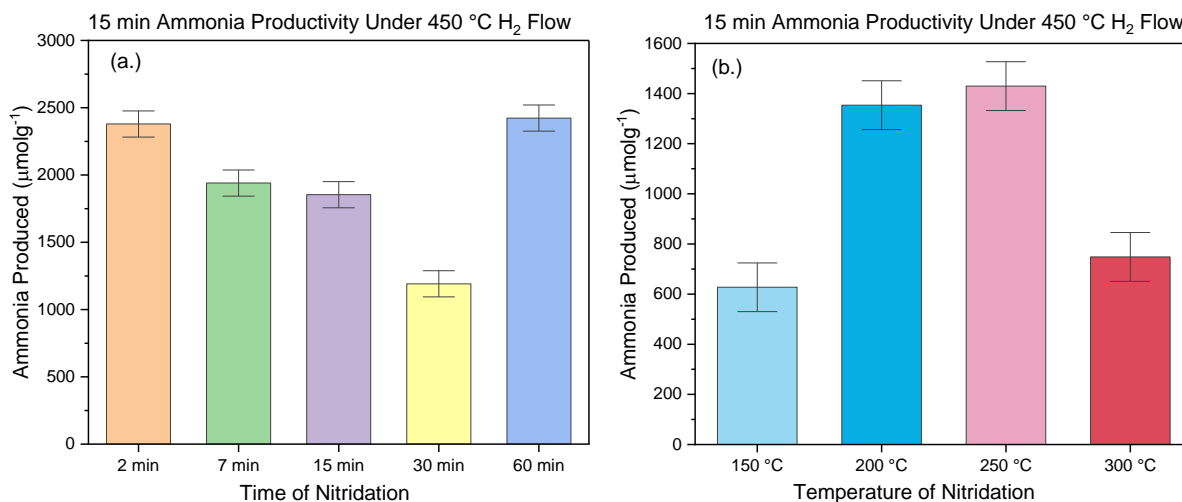


Figure 25. Plasma time on stream results for time of treatment and temperature. (a) Plasma nitridation treatment times impact on productivity were investigated by holding all other variables constant. (b) Optimal temperature of fixed bed nitridation for Fe particles were investigated by holding constant all variables except for bed temperature.

Time on stream experiments were performed for Fe particles using nitridation temperatures to determine the productivity increase associated with MWP pre-treatment during the nitridation step (Figure 25 (a)). Changing the time of the fixed bed under plasma-nitridation conditions was also investigated (Figure 25 (b)). The ammonia productivity was analyzed by integrating time on stream concentration results for the ammonia produced from the various nitrided Fe samples.

The integration was performed over 15 min under flowing 50 sccm H₂ at the temperature of hydrogenation, 250 °C. Higher ammonia productivities, 2379 μmolg⁻¹, are achieved for short plasma treatment times at moderate temperatures, 250 °C, with 60 min treatment times only marginally increased at 2423 μmolg⁻¹.

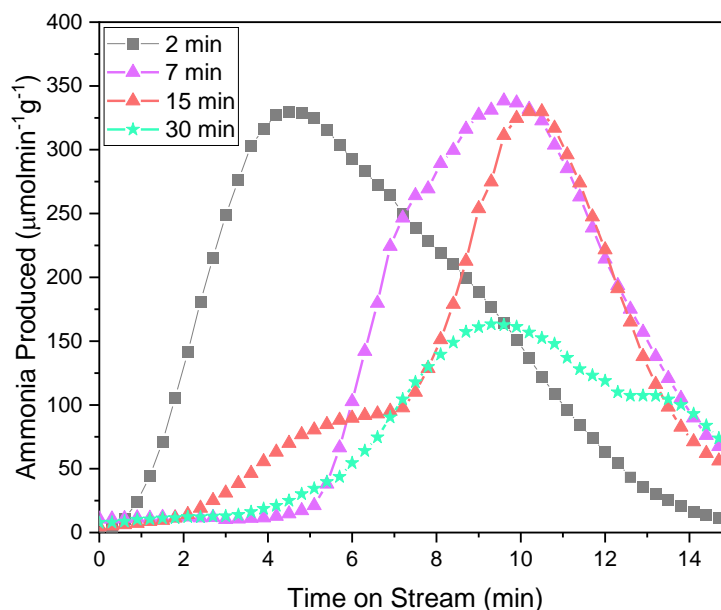


Figure 26. Time on stream MWP ammonia synthesis. Five run averaged time on stream reaction results of the hydrogenation of Fe nitrogen carriers under H₂.

Iron is known to form various nitride phases (Fe_xN, _{x=2-4}) under plasma nitridation conditions¹. Iron nitrides have inherently low stability in air thus we were unable to confirm the phases present with x-ray diffractometry at low conversions under plasma.

Empty tube results yielded no ammonia conversion, so we can surmise that the Fe catalyst is the active site for ammonia synthesis in this reaction. An interesting phenomenon is observed when analyzing Figure 25 (a) and the time on stream results in Figure 26. Inspection of the time on stream plot in Figure 26 shows a changing shape of the ammonia concentration curve. The

shortest plasma-treatment time, 2 min of sustained N₂ plasma, indicates a rapid evolution of ammonia upon reaction with H₂.

As plasma-nitridation times increase, the productivity was reduced, and the shapes of the curves were observed to change towards a more sigmoid modality. We propose that this increase in ammonia productivity is due to competing resistances in bulk-controlled diffusion rates on long nitridation times, versus higher densities of active surface nitrogen on lower nitridation times. Comparing the initial rates of each nitridation time supports this interpretation. A more thorough development is considered in the mechanistic section and discussion of the limitations of the kinetic model.

The plasma reaction order was determined via power law kinetics at 0.72. Rates, and kinetic parameters were determined via the shrinking core model (SCM) for each run in Table 6. The rates obtained indicate a comparable production of ammonia from the lower temperature MWP pre-treatment process as to a traditional thermochemical route. The SCM kinetics were used to determine the apparent activation energies, ($E_{a,app}$), of the Fe process, 13 kJmol⁻¹, 20.6 kJmol⁻¹, for plasma and thermal treatments respectively. Several of the experimental fits of the SCM suggested multiple reaction limiting steps as ammonia synthesis proceeded. The SCM fit for these reactions is presented in Figure 27.

Table 6. SCM to obtain initial rates of ammonia synthesis on plasma treated Fe particles.

Temperature of Nitridation [°C]	Rate [$\mu\text{molg}^{-1}\text{min}^{-1}$]	Apparent rate constant [s^{-1}]	Temperature of Hydrogenation [°C]	Rate Determining Step	Flow rate [sccm]	Time on stream [min]	R ²
---------------------------------	---	--	-----------------------------------	-----------------------	------------------	----------------------	----------------

150	130.5	1.05×10^{-3}	450	Gas	50	16.8	0.993 9
200	304.3	1.43×10^{-3}	450	Surface	50	10.5	0.943 6
250	420.9	5.07×10^{-4}	450	Gas†	50	29.7	0.926 7
300	150.9	9.07×10^{-4}	450	Gas	50	17.4	0.942 7
450	505	$7.70 \times 10^{-2*}$	450	n.a.	50	49	0.918 7

†The model selected had highest R^2 value but, for the other rate determining steps, surface reaction was also found to be very significant.

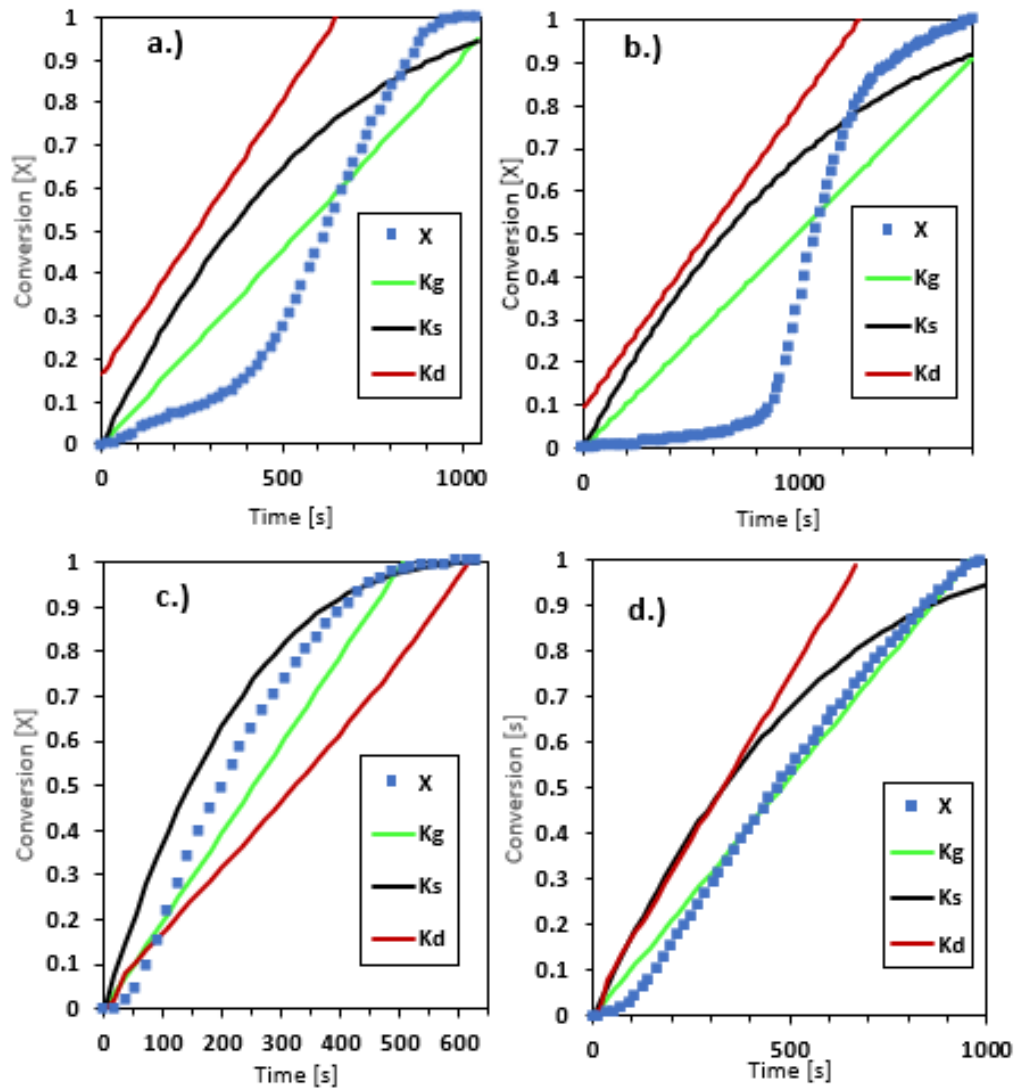


Figure 27. Representative kinetics of the ammonia synthesis process over plasma nitrided Fe particles, a.) 300 °C, b.) 250 °C, c.) 200 °C, and d.) 150 °C.

5.3.1 Plasma Characterization

To understand the plasma system, input variables such as power, frequency, flowrate, and composition were modified to find ideal settings. Additionally, emission spectra were collected via OES optical fiber from the plasma plume. The optimal plasma composition and flow was found to be at 300 kW input power, 40 sccm Ar and 10 sccm N₂, additional compositions

considered include 50:50 and 90:10 Ar:N₂. A review of the literature suggests that an optimum exists for MWP with a 20% N₂ and 80% Ar composition for the formation of activated nitrogen in the plasma ^{2,3}.

Spectra was obtained from the choke at the outlet to the tubular furnace. While not true “in-situ” spectroscopy, the placement of the OES allows observation of the plasma <3 cm before effluent gases reach the catalyst surface. Fortunately, lifetimes of activated species may be calculated by using electron temperature and the number of ions, electrons, and activated species. With this information from analysis of the spectra collected in (Figure 28 (b)) using the Boltzmann plot method, flowrates, and basic geometry of the system the species reaching the Fe catalyst surface may be inferred.

Microwave plasmas typically have an electron density (n_e) of $10^{20} - 10^{24} \text{ m}^{-3}$, and a gas temperature (T_g) that is $\sim 2000\text{-}3000 \text{ K}$ in the plasma zone ^{4,5}. This results in a non-equilibrium plasma system, which maintains neutrality and has considerably hotter electrons than ions, atoms, and molecules. Testing in the MWP reactor with a thermal couple in the catalyst bed only resulted in slightly elevated gas temperatures from ambient, meaning most of the thermal energy is conserved in the plasma discharge region. By consulting molecular and atomic spectra for the Ar/N₂ system we can assign some of the peaks in (Figure 28 (a)) to species expected in a MWP discharge. These include the first negative state of N₂⁺ (388 and 391 nm) and the activated vibrational states of N₂ (358 and 776 nm), and Ar I (417 nm), along with lesser peaks in the range of neutral Ar I and N₂^v ⁶⁻⁸.

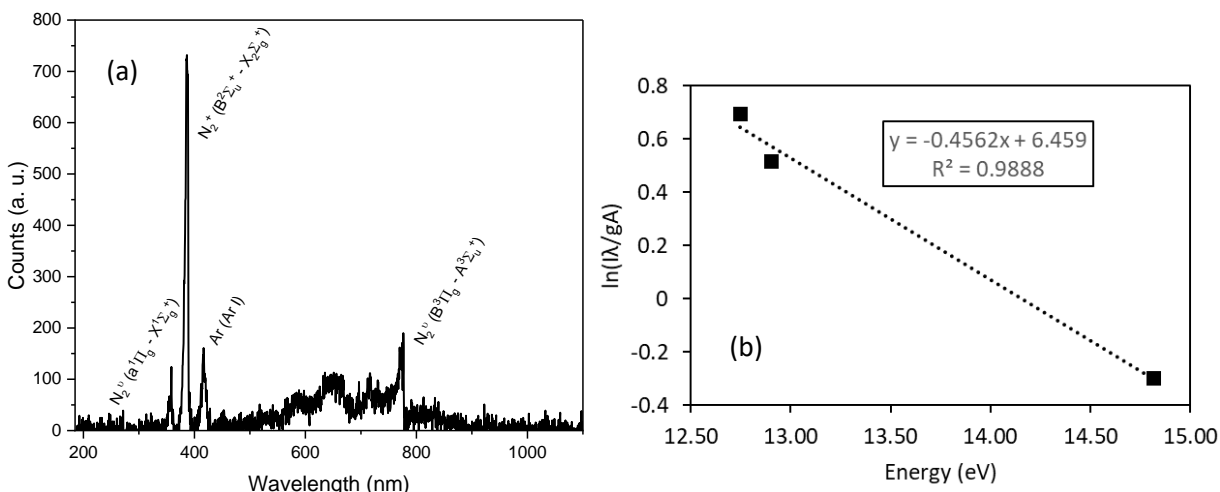


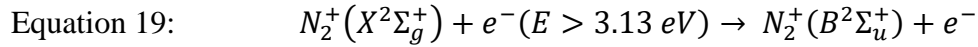
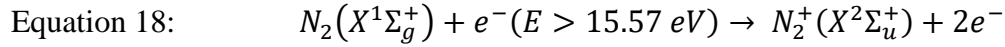
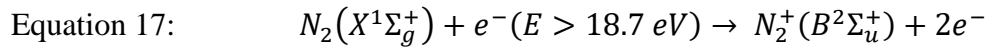
Figure 28. Optical emission spectra and Boltzmann plot. (a) The optical emission spectra collected from the outlet choke of the surfaguide waveguide (10 sccm N_2 balanced in 40 sccm Ar, 300 W), and (b) the Boltzmann plot of electron temperature.

The possible reactions between Ar and N_2 in the plasma are many, but N_2^+ and the two N_2 vibrational states are the major products. Lesser intensity Ar I emissions are grouped between 696 nm and ~800 nm 27,29. The typical lifespan of N_2^+ is only 67 ns, and the time for the average flow rate to travel the 3 cm from the end of the waveguide to the catalyst bed is ~1.9 s . Thus, we must infer that all the species reaching the surface are in a vibrationally active state and not ions. This topic has become increasingly relevant which publications suggesting that under plasma conditions vibrationally active species interact differently with surfaces, altering bond energies ^{9,10}.

To rule out a simple thermal increase in the system due to MWP, a thermocouple was inserted where the catalyst typically sits during normal operation. Several runs under the Ar: N_2 plasma condition revealed only a small ~5 °C temperature change. This is supported by experimental

evidence which found that elevated MWP Ar:N₂ temperatures (3000 K) return to normal (400 K) only 3 cm outside the plasma zone ³.

Proposed reactions to form the observed transition at ~391 nm (Equation 17). In Equation 17 the direct conversion from neutral N₂ to the activated N₂⁺ species is observed ¹¹. The more likely route in a low temperature plasma is the combined reaction followed by Equation 18 ¹¹. The energy of the final transition step, Equation 19, is only 3.13 eV.

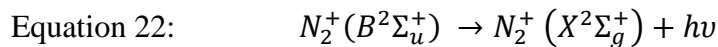


Atomic nitrogen emissions, N* ~425 nm, is difficult to distinguish from the Ar I excited state ~419.8 nm in the collected spectra. The energy of each transition is very similar; however, the lifetime of these species is very short, 39 ns for Ar ¹¹.

Electron temperature of plasma can be determined by the Boltzmann plot method, Equation 20 ⁶. The approximate number of N₂⁺ in low temperature, Equation 21, plasma can be directly related to the intensity observed of the transition at ~391 nm, Equation 22 ¹¹.

$$\text{Equation 20: } \ln \left(\frac{I_{ki}\lambda_{ki}}{g_k A_{ki}} \right) = -\frac{E_k}{k_B T_e} + C$$

$$\text{Equation 21: } I(N_2^+, \lambda = 391.4 \text{ nm}) \approx N_u^+$$



Average velocity in the reaction tube was determined by the flow rate, Q, 50 sccm, and the cross-sectional area, A, of the tube using Equation 23. The average lifetime of the N₂⁺ species, 67 ns,

was compared with the length between the plasma and the catalyst, $z = 3$ cm, and the average fluid velocity, v , 1.5 s^{-1} .

Equation 23: $Q = vA$

This is an approximate method, and not necessarily representative of the true electron energy distribution function. In addition, some higher energy ions may travel faster than the average fluid velocity in the tube, this is open problem in low temperature and pressure plasmas.

One of the major limitations of the above analysis, which lends weight to the plasma enhancement of the reaction is the lack of accurate analysis of the entire electron distribution function, only a simple analysis has been performed. More in-depth understanding of the system is possible but effective modeling of this atomic-molecular plasma at atmospheric pressure does not exist, so the simpler analysis above is proposed for now.

5.3.2 Proposed Mechanism

SCM models applied to chemical looping combustion lack the complexity to accurately model these reactions. Even with a “simple” system such as the oxidation of Fe particles, modeling can become both difficult and require modification of the original model¹². Kinetic parameters determined from SCM can result in loss of data and incorrect assumptions of rate limiting steps as critical kinetic steps are overlooked¹².

In our system, this is complicated by the inclusion of the Ar/N₂ MWP reactions which result in many possible reactions that depend upon plasma conditions. Modeling of the catalyst system under the plasma condition is further complicated by charge accumulation^{13,14}. Increased ammonia production was observed in our plasma reactor when using a higher surface area quartz

wool support for the catalyst bed than a fritted tube. Electrostatic interactions rely on particle chemistry, geometry, and plasma properties and while a full analysis is impossible the review by Nyets and our recent work by Tiwari et al currently under review supports this observation ¹⁵. The charging effect can both increase and decrease reaction rates of interest ¹⁴.

A reaction mechanism is proposed in Figure 29, panel (1), the catalyst bed is brought to the temperature of nitridation ($T_{\text{nitridation}}$), and the plasma is initiated. In Figure 29 panel (2), after the plasma is stable, N_2 is introduced into the system and the nitridation reaction begins. In Figure 29 panel (3) activated nitrogen species accumulates on and interacts with the surface. In Figure 29 panel (4) a nitride diffusion layer is present, in a real system likely this would be impacted by grain boundaries and morphology, here it is idealized as spherical. Once the processing time is complete, the plasma is stopped, and nitrogen is purged from the system with Ar flow as seen in Figure 29 panel (5) surface absorbed species may remain. Next in Figure 29 panel (6) the temperature is adjusted to the hydrogenation temperature and H_2 is added. In Figure 29 panel (7) ammonia is liberated from both the surface due to the ease of H_2 dissociation and diffusion in Fe in the bulk. Finally in Figure 29 panel (8), the reaction decreases as most of the lattice nitrogen is removed and the experiment is ended.

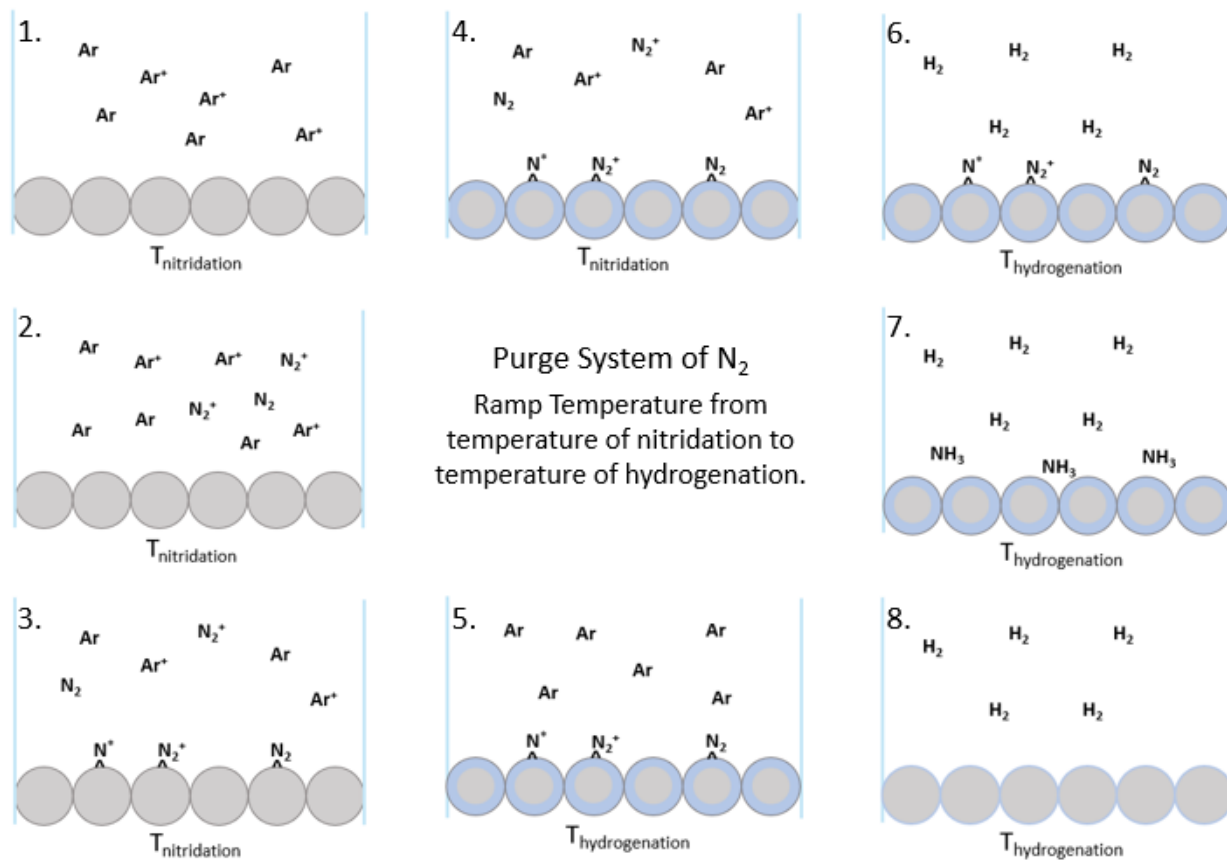


Figure 29. Stepwise plasma-enhanced chemical looping ammonia synthesis reaction with idealized catalyst bed and gaseous species. (1.) Ar plasma is initiated in the waveguide, (2.) N_2 is introduced into to the plasma stream, (3.) activated nitrogen interacts with the catalyst surface, (4.) after the time of nitridation, a layer of metal nitride forms on the catalyst, (5.) Ar is purged through the system to remove gaseous N_2 and temperature is changed to the temperature of ammonia synthesis, (6.) H_2 is introduced into the system, (7.) H_2 reacts readily with the nitride catalyst at the temperature of hydrogenation, (8.) once the catalyst is spent very little nitrogen remains in the lattice.

While this reaction mechanism is generated in the context of a CLAS Fe material, it can also be generalized for other simple metal-based nitrogen carriers without specific catalytic islands or

promoters. The affinity towards surface nitrogen may differ, as well as the temperature require to form nitride bonds for different materials of interest. This particularly impacts nitrides of Mn and CoMo which tend to be more thermodynamically favorable than Fe at forming stable nitrogen-metal bonds¹⁶. More stable bonds may result in longer nitridation times as more “catalytic nitrides” may have better kinetic properties 1. As CLAS process cycle times shorten more to match those of chemical looping combustion and process conditions become milder – this approach may become preferable. Nitrogen reactions which fall into a “surface mediated” rather than “bulk mediated” regime may overcome some of the energy requirements for lattice diffusion. Eventually as process time is shortened, it approaches the time scale of transport limitations much sooner than those of ambient pressure HB reactions. Thus, there likely exists some sort of optimum conditions between limiting cases, CLAS reaction and ambient pressure HB catalytic reactions.

5.3.3 Kinetic Parameter Determination

In lieu of estimating the nitrogen content of each treated sample with TGA or XRD and risking exposure to air, the concentration of ammonia synthesized over a given reaction time was integrated as (C_{total}), Equation 24. Conversion (X), Equation 25, could be determined and plotted as a function of time by the simple ratio of the $C(t)$ in ppm over the integrated concertation. The power law equations are given in Equations 26 and 27 for the linearization of the plot.

Equation 24:
$$X = \frac{C(t)}{C_{total}}$$

Equation 25:
$$C_{total} = \int_{t_0}^{t_f} C(t) dt$$

Equation 26:
$$r = kP_{H_2}^n$$

Equation 27: $\ln(r) = \ln(k) + n \ln(P_{H_2})$

Similarly, reaction rates were calculated by converting the concentration in ppm to μmoles and dividing by time of reaction and normalizing by mass of catalyst.

Apparent activation energies, Figure 30, were calculated by using the Arrhenius plot method.

Kinetic parameters were calculated using the power law kinetic model with Equation 23 and

Equation 24. A plot of a best fit line using the power law model for the plasma enhanced

catalytic system are presented in Figure 31.

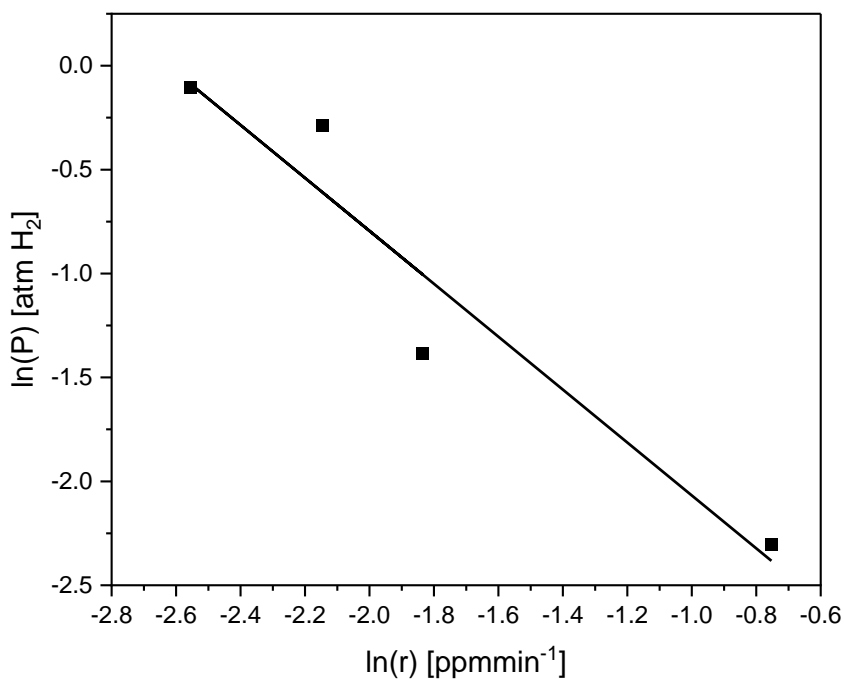


Figure 30. Representative kinetics of the ammonia synthesis process over plasma nitrated Fe particles.

The power law model determined that order is $n = 0.72$ (approaching first order), and $k = 12.92$ s^{-1} with an R^2 of 0.9187.

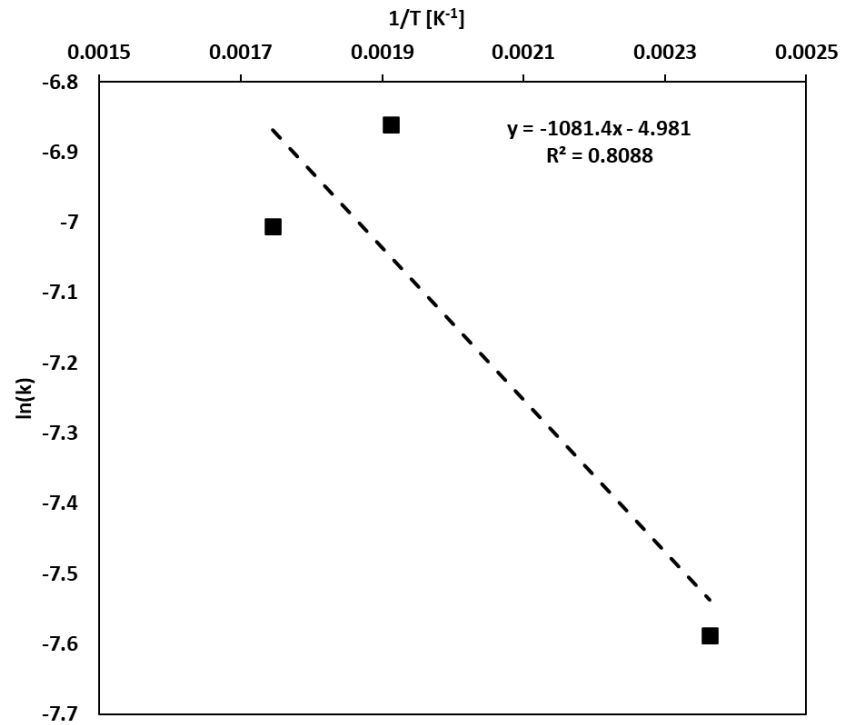


Figure 31. Apparent activation energy of ammonia synthesis over plasma nitrated Fe by the Arrhenius plot method.

5.4 Conclusions

Time on stream chemical looping experiments were carried out to evaluate the efficacy of pre-activation of nitrogen by microwave-plasma and to study the inherent kinetics of nitrogen storage materials by solely thermochemical means. Nitrogen plasma is found to enhance overall reaction productivity and to reduce temperatures of the nitridation reaction by first pre-activating nitrogen before depositing it on the surface of the catalyst. Rates of up to $420.9 \mu\text{molmin}^{-1}\text{g}^{-1}$ at $250 \text{ }^\circ\text{C}$ nitridation temperatures were found to be optimal. Analysis of the plasma, flow and kinetics was performed, and limitations of this process were identified. Additionally, a surface-mediated and bulk-mediated reaction domain was found to exist depending on the length of the plasma treatment times.

5.5 References

- (1) Chen, C.-Z.; Shi, X.-H.; Zhang, P.-C.; Bai, B.; Leng, Y.-X.; Huang, N. The Microstructure and Properties of Commercial Pure Iron Modified by Plasma Nitriding. *Solid State Ionics* **2008**, *179* (21–26), 971–974. <https://doi.org/10.1016/j.ssi.2008.03.019>.
- (2) Henriques, J.; Tatarova, E.; Ferreira, C. M. Microwave N₂–Ar Plasma Torch. I. Modeling. *Journal of Applied Physics* **2011**, *109* (2), 023301. <https://doi.org/10.1063/1.3532055>.
- (3) Henriques, J.; Tatarova, E.; Dias, F. M.; Ferreira, C. M. Microwave N₂–Ar Plasma Torch. II. Experiment and Comparison with Theory. *Journal of Applied Physics* **2011**, *109* (2), 023302. <https://doi.org/10.1063/1.3532056>.
- (4) Bruggeman, P. J.; Iza, F.; Brandenburg, R. Foundations of Atmospheric Pressure Non-Equilibrium Plasmas. *Plasma Sources Sci. Technol.* **2017**, *26* (12), 123002. <https://doi.org/10.1088/1361-6595/aa97af>.
- (5) Baeva, M.; Bösel, A.; Ehlbeck, J.; Loffhagen, D. Modeling of Microwave-Induced Plasma in Argon at Atmospheric Pressure. *Phys. Rev. E* **2012**, *85* (5), 056404. <https://doi.org/10.1103/PhysRevE.85.056404>.
- (6) Qayyum, A.; Zeb, S.; Naveed, M. A.; Rehman, N. U.; Ghauri, S. A.; Zakauallah, M. Optical Emission Spectroscopy of Ar–N₂ Mixture Plasma. *Journal of Quantitative Spectroscopy and Radiative Transfer* **2007**, *107* (3), 361–371. <https://doi.org/10.1016/j.jqsrt.2007.02.008>.
- (7) Kramida, A.; Ralchenko, Y. NIST Atomic Spectra Database, NIST Standard Reference Database 78, 1999. <https://doi.org/10.18434/T4W30F>.
- (8) Lofthus, A.; Krupenie, P. H. The Spectrum of Molecular Nitrogen. *Journal of Physical and Chemical Reference Data* **1977**, *6* (1), 113–307. <https://doi.org/10.1063/1.555546>.
- (9) Rouwenhorst, K. H. R.; Kim, H.-H.; Lefferts, L. Vibrationally Excited Activation of N₂ in Plasma-Enhanced Catalytic Ammonia Synthesis: A Kinetic Analysis. *ACS Sustainable Chem. Eng.* **2019**, *7* (20), 17515–17522. <https://doi.org/10.1021/acssuschemeng.9b04997>.
- (10) Mehta, P.; Barboun, P. M.; Engelmann, Y.; Go, D. B.; Bogaerts, A.; Schneider, W. F.; Hicks, J. C. Plasma-Catalytic Ammonia Synthesis beyond the Equilibrium Limit. *ACS Catal.* **2020**, *10* (12), 6726–6734. <https://doi.org/10.1021/acscatal.0c00684>.
- (11) Qayyum, A.; Zeb, S.; Naveed, M. A.; Ghauri, S. A.; Zakauallah, M.; Waheed, A. Diagnostics of Nitrogen Plasma by Trace Rare-Gas–Optical Emission Spectroscopy. *Journal of Applied Physics* **2005**, *98* (10), 103303. <https://doi.org/10.1063/1.2132514>.
- (12) Okoli, C. O.; Parker, R.; Chen, Y.; Ostace, A.; Lee, A.; Bhattacharyya, D.; Tong, A.; Biegler, L. T.; Burgard, A. P.; Miller, D. C. Application of an Equation-oriented Framework to Formulate and Estimate Parameters of Chemical Looping Reaction Models. *AIChE Journal* **2022**, *68* (10). <https://doi.org/10.1002/aic.17796>.
- (13) Wan, M.; Yue, H.; Notarangelo, J.; Liu, H.; Che, F. Deep Learning-Assisted Investigation of Electric Field–Dipole Effects on Catalytic Ammonia Synthesis. *JACS Au* **2022**, *2* (6), 1338–1349. <https://doi.org/10.1021/jacsau.2c00003>.
- (14) Che, F.; Gray, J. T.; Ha, S.; Kruse, N.; Scott, S. L.; McEwen, J.-S. Elucidating the Roles of Electric Fields in Catalysis: A Perspective. *ACS Catal.* **2018**, *8* (6), 5153–5174. <https://doi.org/10.1021/acscatal.7b02899>.
- (15) Neyts, E. C. Plasma–Surface Interactions in Plasma Catalysis. *Plasma Chem Plasma Process* **2016**, *36* (1), 185–212. <https://doi.org/10.1007/s11090-015-9662-5>.
- (16) Ettmayer, P.; Lengauer, W. Nitrides. In *Ullmann's Encyclopedia of Industrial Chemistry*; Wiley-VCH Verlag GmbH & Co. KGaA, Ed.; Wiley-VCH Verlag GmbH & Co. KGaA: Weinheim, Germany, 2000; p a17_341. https://doi.org/10.1002/14356007.a17_341.

6. General Conclusions

6.1 Conclusions

Some general principles emerged from this work on the cyclical storage and removal of nitrogen in the form of ammonia from transition metals. These included material properties for nitridation, microwave-materials interaction strategies, and plasma chemical looping ammonia synthesis phenomena.

When approaching this work we applied increasing levels of process intensification, from the initial thermal only nitridation of these materials which is the current state of the art, to the application of microwave heating, finally to pre-treatment of the gas with microwave plasma. Thus, each step of the increasingly intense process brought with it new challenges, complexity, and findings.

Throughout the entire project the focus of the work from thermal fixed bed, to microwave fixed bed, to microwave plasma fixed bed reactors was on high resolution reaction data. This data provides a basis for evaluation of kinetic properties and limitations of these material systems which are necessary for further development and potential future scale-up.

Microwave heating appears to increase the rate and productivity of metal-like nitrides for chemical looping ammonia applications, though the physical mechanisms by which that proceeds are unclear. Microwave plasma pre-activation of the N_2 molecule when coupled with low temperature heating leads to unexpected rate increases through a unique surface dominated reaction mechanism leading to higher productivities at lower temperatures

6.2 Future Work

The future work which naturally follows from these processes relate to the materials for nitrogen storage and to the microwave heating process. The microwave-plasma enhanced process which proceeds from an altogether different physical process is best described separately.

First, as described in the review, materials for nitrogen fixation have been long known. These basic material trends are not new, thus what is needed is materials engineering and synthesis of older findings and concepts. The critical question is whether this kind of process is desired and justified, that sort of work falls to thermodynamic and techno-economic modeling which has at least begun and shows promising results¹⁻⁴. All these modeling efforts would be greatly benefited by rationalization of kinetics and data reporting for these materials for bench scale testing. The generation of more complicated and accurate kinetic models such as those which exist in chemical looping combustion is quite easily achievable by translating computational methods from the more mature field, despite still not knowing the definitive chemistry of these systems.

The use of bi-metallics, oxides, and promoters has long been a feature of the literature, but with more rationalize design as considered by Sun and others⁵. While proceeding with highly reactive species is an attractive starting place, low cost but highly reactive and cyclable materials are likely to make more economic sense when considering other forms of energy storage technologies such as batteries and other catalysts⁶⁻⁷. The development of “oxide nitrides” or ionic nitrides where the mobile ion is not the typical cation ex. Mg^{+2} , but N^{-3} , is also still a possibility but the chemistry of these materials is complex and difficult and requires more future research⁸.

Microwave and microwave plasma reactions hold an enormous amount of possibility for the electrification of the chemicals and materials industries which is a goal of greenhouse gas emission reduction strategies⁹. Future materials of interest for microwave-catalytic nitridation include low cost and common materials such as Cu, Fe, and Mg which can be coupled with common oxides and advanced carbon materials from other low carbon processes that are known to enhance reaction rates under MW.

6.3 Contributions to the Field

My contributions to the field include the peer reviewed publications that I have published from the work in this thesis and the presentations I have made of this work at national conferences. These activities are listed in the following sections.

6.3.1 Publications

1. Tiwari, S., Ibrahim, S., A., Robinson, B., Brown, S., Wang, Q., Che, F., Hu, J., “Post-plasma catalysis: Charge effect on product selectivity in conversion of methane and nitrogen plasma to ethylene and ammonia” *Catalysis Science & Technology*, March 21st 2023.
<https://doi.org/10.1039/D2CY02077G>
2. Brown, S., “Vector Network Analysis of Powdered Materials Guide” Zenodo April 27th, 2023. <https://doi.org/10.5281/zenodo.7595964>.
3. Araia, A., Wang, Y., Jiang, C., Brown, S., Caiola, A., Robinson, B., Hu, J., “Intuitive study on the effect of support morphology over Cs-Ru/CeO₂ catalyst for microwave-initiated ammonia synthesis” *Catalysis Communications*, October 27th, 2022.
<https://doi.org/10.1016/j.catcom.2022.106551>.
4. Aira, A. Wang, Y., Robinson, B., Jiang, C., Wildfire, C., Brown, S., Hu, J. “Microwave-assisted ammonia synthesis over Cs-Ru/CeO₂ catalyst at ambient pressure: Effect of metal loading and support particle size” *Catalysis Communications* 2022,
<https://doi.org/10.1016/j.catcom.2022.106491>.
5. Hu, J., Brown, S., Tiwari, S., Wang, Y., Robinson, B., “Methods and compositions for chemical looping ammonia synthesis at low pressure”, Provisional Patent, US Application No. 63/358,516, July 5th, 2022.
6. Brown, S., Robinson, B., Wang, Y., Wildfire, C., Hu, J. “Microwave heated chemical looping ammonia synthesis over Fe and CoMo particles”, *RSC Journal of Materials Chemistry A*, 2022, <https://doi.org/10.1039/D2TA03241D>.

7. Brown, S., Ellison, C., Shekhawat, D., Hu, J. “Chemical Looping Ammonia Synthesis: Microwave and Thermal Fixed Bed Systems”, Conference Proceedings of the International Microwave Power Institute, Annual Microwave Power Symposium 56, Savannah, GA, 2022
8. Brown, S., Jiang, C., Wang, Q., Caiola, A., Hu, J. “Evidence of Ammonia Synthesis by Bulk Diffusion in Cobalt Molybdenum Particles in a CLAS Process”, Catalysis Communications 2022, 106438. <https://doi.org/10.1016/j.catcom.2022.106438>.
9. Hu, J., Brown, S., Tiwari, S., Wang, Y., Robinson, B., “Methods and compositions for chemical looping ammonia synthesis at low pressure”, Provisional Patent, US Application No. 63/313,672, February 24th, 2022.

6.3.2 Oral Presentations

1. Brown, S., Hu, J., "Plasma-enhanced chemical looping ammonia synthesis", Oral presentation at the AIChE Annual Conference, Phoenix, AZ, November 14th, 2022.
2. Brown, S., Hu, J. "Chemical looping ammonia synthesis: microwave and thermal fixed bed systems", Poster presentation at International Microwave Power Institute, Savannah, GA, June 14th-16th, 2022.
3. Brown, S., Hu, J. "Next generation catalysis by microwave, plasma, and materials design", Oral presentation at CHMJC, Virtual, June 8th, 2022.
4. Brown, S., Hu, J. "Kinetic study of chemical looping ammonia synthesis candidates: Manganese nitride as a model material", Oral presentation at American Chemical Society Spring Conference, San Diego, CA, March 20th, 2022.
5. Brown, S., Wang, Y., Hu, J. "Chemical Looping Synthesis of Ammonia over Cobalt Molybdenum Nitride: Effects of Surface Hydrogen on Productivity", Oral presentation at the AIChE Annual Conference, Boston, MA, November 10th, 2021.

6.3.3 Poster Presentations

1. Brown, S., Hu, J. "Chemical looping ammonia synthesis by thermal, microwave, and plasma", Poster presentation at WIC session, AIChE Annual Conference, Phoenix, AZ, November 15th, 2022.
2. Brown, S., Hu, J. "Microwave and plasma enhanced catalysis for chemical looping ammonia synthesis", Poster presentation at the AIChE Annual Conference, Phoenix, AZ, November 14th, 2022.
3. Brown, S., Hu, J. "Next Generation Catalysis by Microwave, Plasma, and Materials Design", Faculty/postdoc poster presentation at the AIChE Annual Conference, Phoenix, AZ, November 13th, 2022.
4. Brown, S., Hu, J. "Chemical looping ammonia synthesis: thermal, microwave, and plasma approaches", Poster presentation at the American Chemical Society Fall Conference, Chicago, IL, August 24th, 2022.
5. Brown, S., Ellison, C., Shekhawat, D., Hu, J. "Chemical looping ammonia synthesis: microwave and thermal fixed bed systems", Poster presentation at International Microwave Power Institute, Savannah, GA, June 14th-16th, 2022.
6. Brown, S., Hu, J. "Chemical Looping Ammonia Synthesis: Thermal, Microwave, and Plasma Approaches", Poster presentation at WVU WVU Graduate Student Research Symposium, Morgantown, WV, April 12th, 2022

7. Caiola, A.; Robinson, B.; Brown, S., Hu, J. “Ethane Dehydroaromatization Using Molybdenum Promoted Microwave Synthesized Zeolites”, Poster presentation at the WVU Graduate Student Research Symposium, Morgantown, WV, April 12th, 2022
8. Brown, S., Robinson, B., Wang, Y., Wang, Q., Hu, J. “Thermal & Microwave Assisted Synthesis of Ammonia with a Chemical Looping Approach”, Poster presentation at the AIChE Annual Conference, virtual, November 16th-20th, 2020.
9. Brown, S., Robinson, B., Wang, Y., Wang, Q., Hu, J. “Thermal & Microwave Assisted Synthesis of Ammonia with a Chemical Looping Approach”, Poster presentation at the AIChE Annual Conference, virtual, November 16th-20th, 2020.
10. Bai, et. al. “Catalytic Dehydroaromatization of Ethane in Microwave Reactor”, Poster presentation at STARS: Students, Teachers, And Researchers Conference, Morgantown WV, November 16th, 2019.

6.4 References

- (1) Wang, X.; Su, M.; Zhao, H. Process Design and Exergy Cost Analysis of a Chemical Looping Ammonia Generation System Using AlN/Al₂O₃ as a Nitrogen Carrier. *Energy* **2021**, *230*, 120767. <https://doi.org/10.1016/j.energy.2021.120767>.
- (2) Lai, Q.; Cai, T.; Tsang, S. C. E.; Chen, X.; Ye, R.; Xu, Z.; Argyle, M. D.; Ding, D.; Chen, Y.; Wang, J.; Russell, A. G.; Wu, Y.; Liu, J.; Fan, M. Chemical Looping Based Ammonia Production—A Promising Pathway for Production of the Noncarbon Fuel. *Science Bulletin* **2022**, *67* (20), 2124–2138. <https://doi.org/10.1016/j.scib.2022.09.013>.
- (3) Burrows, L.; Gao, P.-X.; Bollas, G. M. Thermodynamic Feasibility Analysis of Distributed Chemical Looping Ammonia Synthesis. *Chemical Engineering Journal* **2021**, *426*, 131421. <https://doi.org/10.1016/j.cej.2021.131421>.
- (4) Lee Pereira, R. J.; Argyris, P. A.; Spallina, V. A Comparative Study on Clean Ammonia Production Using Chemical Looping Based Technology. *Applied Energy* **2020**, *280*, 115874. <https://doi.org/10.1016/j.apenergy.2020.115874>.
- (5) Sun, W.; Bartel, C. J.; Arca, E.; Bauers, S. R.; Matthews, B.; Orvañanos, B.; Chen, B.-R.; Toney, M. F.; Schelhas, L. T.; Tumas, W.; Tate, J.; Zakutayev, A.; Lany, S.; Holder, A. M.; Ceder, G. A Map of the Inorganic Ternary Metal Nitrides. *Nat. Mater.* **2019**, *18* (7), 732–739. <https://doi.org/10.1038/s41563-019-0396-2>.
- (6) Guo, J.; Wang, P.; Wu, G.; Wu, A.; Hu, D.; Xiong, Z.; Wang, J.; Yu, P.; Chang, F.; Chen, Z.; Chen, P. Lithium Imide Synergy with 3d Transition-Metal Nitrides Leading to Unprecedented Catalytic Activities for Ammonia Decomposition. *Angew. Chem. Int. Ed.* **2015**, *54* (10), 2950–2954. <https://doi.org/10.1002/anie.201410773>.
- (7) Wang, Q.; Pan, J.; Guo, J.; Hansen, H. A.; Xie, H.; Jiang, L.; Hua, L.; Li, H.; Guan, Y.; Wang, P.; Gao, W.; Liu, L.; Cao, H.; Xiong, Z.; Vegge, T.; Chen, P. Ternary Ruthenium Complex Hydrides for Ammonia Synthesis via the Associative Mechanism. *Nat Catal* **2021**, *4* (11), 959–967. <https://doi.org/10.1038/s41929-021-00698-8>.
- (8) Lerch, M.; Janek, J.; Becker, K. D.; Berendts, S.; Boysen, H.; Bredow, T.; Dronskowski, R.; Ebbinghaus, S. G.; Kilo, M.; Lumey, M. W.; Martin, M.; Reimann, C.; Schweda, E.; Valov, I.; Wiemhöfer, H. D. Oxide Nitrides: From Oxides to Solids with Mobile Nitrogen Ions. *Progress in Solid State Chemistry* **2009**, *37* (2–3), 81–131. <https://doi.org/10.1016/j.progsolidstchem.2009.11.004>.
- (9) Barton, J. L. Electrification of the Chemical Industry. *Science* **2020**, *368* (6496), 1181–1182. <https://doi.org/10.1126/science.abb8061>.